

# Pollen-based climatic reconstructions for the interglacial analogues of MIS 1 (MIS 19, 11 and 5) in the Southwestern Mediterranean: insights from ODP Site 976

Dael Sassoon<sup>\*1,4</sup>, Nathalie Combourieu-Nebout<sup>1</sup>, Odile Peyron<sup>2</sup>, Adele Bertini<sup>3</sup>, Francesco Toti<sup>3</sup>, Vincent Lebreton<sup>1</sup>, Marie-Hélène Moncel<sup>1</sup>

*\*corresponding author:*

*Dr Dael Sassoon (dael.sassoon@gmail.com)*

## **Affiliations:**

1: UMR 7194, Histoire Naturelle de l'Homme Préhistorique, CNRS-MNHN, Institut de Paléontologie Humaine, Paris, France

2: Institut des Sciences de l'Évolution de Montpellier, UMR CNRS 5554 ISEM, Université de Montpellier, France

3: Dipartimento di Scienze della Terra, Università di Firenze, Italy

4: Geosciences Barcelona (GEO3BCN), CSIC, Lluís Solè i Sabarès s/n, 08028 Barcelona, Spain

## **Abstract**

Pleistocene interglacials, specifically MIS 19, 11 and 5, have been suggested as analogues of MIS 1 due to similar solar forcing patterns, greenhouse gas concentrations and sea levels. There has been substantial debate regarding which of these is the most suitable analogue and so far there has been no consensus, although what really emerges from recent work is the high variation in regional climate during these periods. One of the limiting factors in our understanding of these potential analogues is the fact that very few long-sequences cover the entire duration of these interglacials at high resolution.

In this study, a multi-method approach is used to produce climatic reconstructions for MIS 19, 11, 5 and 1, using pollen data derived from a single long marine core from ODP Site 976. This represents the first study which attempts to use pollen-based climatic reconstructions to compare MIS 1 with its analogues, representing a necessary contribution to the debate with a focus on the relationships between vegetation and climate in the southwestern Mediterranean.

Three methods of quantitative climate reconstruction have been adopted: the more widely used methods Modern Analogues Technique (MAT) and Weighted Average Partial Least Squares regression (WA-PLS), and a more recent machine-learning method known as Boosted Regression Trees (BRT). The reconstructions show consistent changes in temperature and precipitation during MIS 19, 11, 5 and 1, which correlate well with climatic changes observed in other regional and global proxies, and highlight distinct climatic characteristics of each interglacial period in the southwestern Mediterranean. MIS 19 exhibits high variability and colder temperatures compared to subsequent interglacials and the MIS 1. Conversely, MIS 11 displays warmer temperatures and greater stability, which makes it a useful analogue to understand prolonged interglacials, crucial considering the anthropogenic impacts on the duration of warm climate during the Holocene. MIS 5 exhibits overall warmer conditions, and its higher temperature coupled with fluctuations in solar forcing makes it a less suitable MIS 1 analogue.

Although past interglacials do not offer direct predictions for the Holocene's future, they provide essential insights into Earth's responses to various forcing factors, serving as crucial benchmarks for understanding the Mediterranean's sensitivity to global changes.

## **1. Introduction**

The interglacials of the Pleistocene, particularly those of the past 1 Ma (1 million years) and specifically MIS 19 (ca. 795–755 ka BP), MIS 11 (ca. 424–365 ka BP) and MIS 5 (ca. 127–78 ka BP), have been source of increasing attention over the past two decades because several of them have been suggested as analogues of the Holocene (e.g. Loutre and Berger, 2003; McManus *et al.*, 2003; Tzedakis, 2010; Candy *et al.*, 2014; Yin and Berger, 2015; Giaccio *et al.*, 2015; Varvus *et al.*, 2018). Studying past interglacials can provide a framework to better evaluate the natural timing and duration of the Holocene, and examining the amplitudes and rates of climatic variability can give an indication of how the current interglacial may have been without anthropogenic interference, and how it could evolve under the presence of humans (Loutre and Berger, 2003; Candy *et al.*, 2014; Giaccio *et al.*, 2015). Furthermore, studying past interglacials may help understand abrupt climate change and the impact of these events on ecosystems and human populations (Loutre and Berger, 2003; Nomade *et al.*, 2019).

57 The selection of the interglacials MIS 19, 11 and 5 is mainly based on their similarities with MIS 1 in terms  
58 of astronomical configurations and greenhouse gas (GHG) concentrations (Yin and Berger, 2015). These  
59 interglacials are characterised by low eccentricity and similar precession patterns to MIS 1, small variation in  
60 insolation amplitudes, and elevated GHGs. However, the search for the best analogue has been source of constant  
61 debate (Candy *et al.*, 2014). Chiefly, the arguments have revolved around (1) the best alignment of the insolation  
62 patterns between each interglacial and MIS 1, and (2) the structure and duration of these interglacials compared  
63 with the Holocene (Candy *et al.*, 2014; Past Interglacials Working Group of PAGES, 2016).

64 MIS 5, specifically substage 5e (ca. 128–116 ka BP)—~~known as equivalent to~~ the Eemian (Kukla *et al.*,  
65 1997)—has been ~~previously the first interglacial~~ considered as a modern analogue due to the high temperatures  
66 over most of the Northern Hemisphere (NH) and reduced ice sheets (Yin and Berger, 2015). However, the  
67 appropriateness of this interglacial was put in question by Loutre and Berger (2003) due to its disproportionately  
68 high-amplitude changes in insolation and shorter-lasting high CO<sub>2</sub> concentrations compared to the Holocene.

69 Rather, Loutre and Berger (2003) considered MIS 11 to be closer to MIS 1. Specifically, the climatic optimum  
70 of MIS 11c (ca. 427–400 ka BP) has long been recognised as an analogue of the Holocene, owing to similar sea  
71 levels, elevated temperatures, reduced astronomical forcing and high atmospheric CO<sub>2</sub> concentrations (McManus  
72 *et al.*, 2003; Desprat *et al.*, 2005; Hes *et al.*, 2022). This prolonged and stable period has received further attention  
73 because it occurs after one of the harshest glacial conditions of the past 1 Ma (Berger and Loutre, 2003; Raymo  
74 and Mitrovica, 2012; Oliveira *et al.*, 2018), which had important implications on the rise of early hominin  
75 populations including the spread of Neanderthals and their traditions across Europe and the Mediterranean  
76 (Moncel *et al.*, 2016; Blain *et al.*, 2021; Sassoon *et al.*, 2023). The suitability of MIS 11c as an analogue has been  
77 supported by several studies (e.g. Berger and Loutre, 2002, 2003; McManus *et al.*, 2003; Olson and Hearty, 2009;  
78 Raymo and Mitrovica, 2012). Candy *et al.* (2014) pointed out that this interglacial matches the pattern of solar  
79 insolation of the Holocene more closely than any other interglacial of the past 500 ka. However, ~~recent other~~  
80 studies have questioned its reliability as analogue due to the unique antiphasing between precession and insolation  
81 and obliquity—two precession peaks occurring during one obliquity cycle (Ruddiman, 2007; Tzedakis, 2010;  
82 Nomade *et al.* 2019; Tzedakis *et al.*, 2022).

83 Other authors argue that MIS 19 has greater resemblance to the Holocene, owing to a closer phasing of  
84 obliquity and precession whereby the maximum obliquity is in phase with the minimum precession at the onset  
85 of both interglacials (Tzedakis, 2010). This has been supported by several records in the North Atlantic and  
86 Mediterranean (Pol *et al.*, 2010; Tzedakis *et al.*, 2012; Sanchez Goñi *et al.*, 2016a; Giaccio *et al.*, 2015; Nomade  
87 *et al.*, 2019). This feature, along with similar duration of the climatic optimum, similar mid-June insolation and  
88 comparably elevated CO<sub>2</sub> concentrations, has highlighted the viability of MIS 19 as a modern analogue. However,  
89 Tzedakis (2010) demonstrated important differences between the trends of GHG concentrations during MIS 19  
90 and MIS 1, and the climatic structure of MIS 19. Furthermore, it was found that MIS 19c was generally colder  
91 than MIS 5e and MIS 11c (Jouzel *et al.*, 2007), and therefore possibly less climatically comparable to the Holocene  
92 especially in the Northern Hemisphere.

93 So far, there has been no consensus on which of these interglacials is the best MIS 1 analogue, and what really  
94 emerges from the literature is the high variation in regional climate during MIS 19, 11 and 5. For instance,  
95 the appropriateness of MIS 11 as an analogue was supported by McManus *et al.* (2003) in the North Atlantic and  
96 by Wang *et al.* (2023) in China, but it was found to be questionable in the Nordic Seas in the study by Bauch *et al.*  
97 (2000). This heterogeneity and lack of long cores makes it extremely important to compare these analogues  
98 with MIS 1 at a regional scale, using high-resolution records with timeframes that encapsulate the entire  
99 interglacials.

100 One region which can help shed some light on this debate is the Mediterranean, due to its high sensitivity to  
101 climate change (Lionello and Scarascia, 2018). It is also an area which has been historically affected by  
102 anthropogenic pressures, and is likely to be impacted by future warming and drought (Guiot and Cramer, 2016;  
103 MedECC 2020; IPCC, 2022), making it imperative to understand the drivers of environmental and climate change  
104 across the basin so that we can develop a better framework to predict the trajectory of our current interglacial  
105 (Combourieu-Nebout *et al.*, 2015). Moreover, several long cores are available for the Mediterranean region, such  
106 as the terrestrial records from Tenaghi Philippon (Pross *et al.*, 2015; Koutsodendris *et al.*, 2023), Lake Ohrid  
107 (Sadori *et al.*, 2016; Wagner *et al.*, 2019; Donders *et al.*, 2021), Padul (Ortiz *et al.* 2010; Camuera *et al.*, 2018) and  
108 marine records from the Iberian Margin (e.g. Sanchez Goñi *et al.*, 2016a,b). Some of these long pollen sequences  
109 allowed to quantitatively reconstruct past climate changes during MIS 11 (Kousis *et al.*, 2018), MIS 5 (Sinopoli  
110 *et al.*, 2019) and MIS 1 (Peyron *et al.*, 2011, Camuera *et al.* 2021).

111 Recent palynological studies from ODP Site 976 in the Alboran Sea, southwestern Mediterranean, have  
112 yielded high-resolution pollen records for MIS 1 (Combourieu-Nebout *et al.*, 2009, 2013; Dormoy *et al.*, 2009),  
113 MIS 5 (Masson-Delmotte *et al.*, 2005), MIS 11 (Sassoon *et al.*, 2023) and MIS 19 (Toti *et al.*, 2020), providing a  
114 unique opportunity to investigate the regional suitability of these interglacials as analogues of MIS 1 using proxies  
115 from a single core. This study aims to provide quantitative estimates of past climate changes for each interglacial  
116 by implementing a robust multi-method approach (Peyron *et al.*, 2017; Salonen *et al.*, 2019; Robles *et al.*, 2023),

117 using pollen data derived from the long marine core of ODP Site 976. This approach enables a comparison of  
118 Holocene-MIS 1 analogues and represents a necessary contribution to the debate on the links between vegetation  
119 and climate in the Mediterranean.

120 The objectives of this study are to:

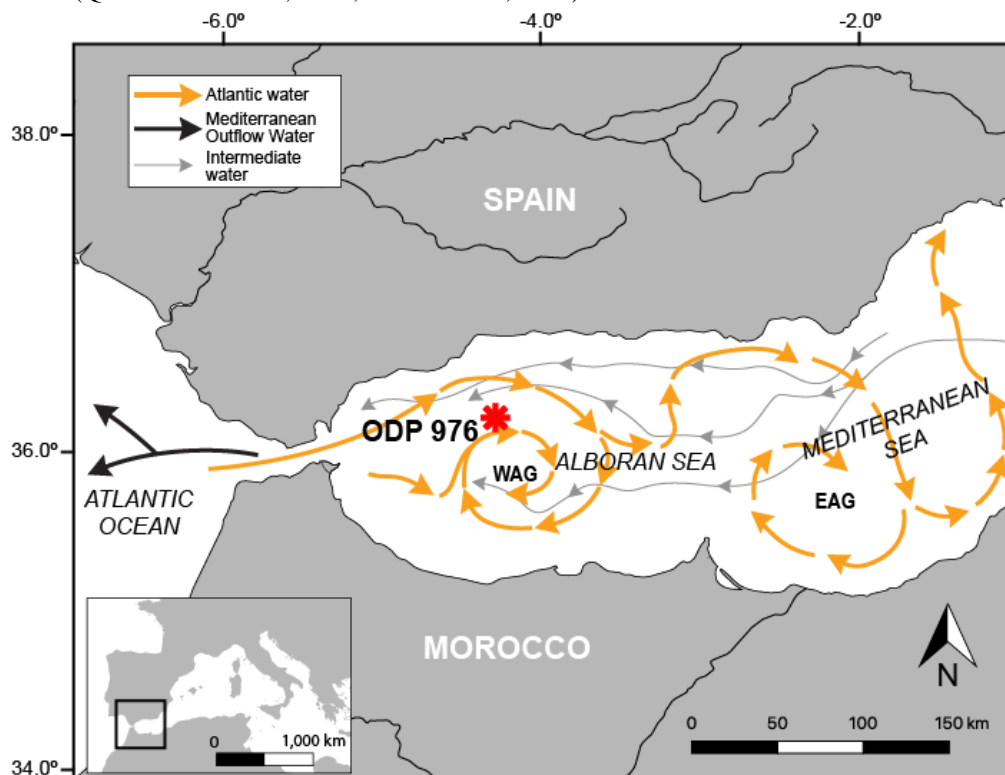
- 121 1. Reconstruct temperature and precipitation parameters during MIS 19, MIS 11, MIS 5 and MIS 1 using  
122 a pollen-based multi-method approach
- 123 2. Assess the reliability of multiple quantitative reconstruction methods
- 124 3. Compare climatic variability during the interglacials with local and global proxies
- 125 4. Evaluate the suitability of the interglacials MIS 19, MIS 11 and MIS 5 as analogues of MIS 1 the Holocene  
126 in the Southwestern Mediterranean.

## 128 2. Site description

129 This study used pollen records derived from the marine core of the Ocean Drilling Program (ODP) Site 976 in the  
130 Western Alboran Sea (36°12.3'N 4°18.8'W), collected in 1999 during leg 161 (Shipboard Scientific Party, 1996).  
131 This site (Fig. 1) is located about 110 km off the coast of the Strait of Gibraltar at a depth of 1108 m. (Combourieu-  
132 Nebout *et al.*, 1999, 2009; Gonzalez-Donoso *et al.*, 2000). Due to its susceptibility to polar, tropical, and Atlantic  
133 influences, the Alboran Sea is extremely sensitive to climate changes on centennial and millennial scales, making  
134 it an ideal location to study climatic variability and interglacial comparisons Alonso *et al.*, 1999; Combourieu-  
135 Nebout *et al.*, 1999, 2002, 2009; Fletcher and Sanchez Goñi, 2008; Dormoy *et al.*, 2009; Toti *et al.*, 2020; Bulian  
136 *et al.*, 2022).

137 The Alboran Sea measures 150 km in width and 350 km in length, forming a narrow extensional basin (Alonso  
138 *et al.*, 1999) between the Mediterranean Sea to the east and the Atlantic Ocean to the west (Bulian *et al.*, 2022).  
139 The northern coast of the basin borders with Spain while it borders with Morocco to the south. Circulation in the  
140 Alboran Sea is influenced by the exchange of waters at the Strait of Gibraltar whereby low-salinity waters from  
141 the Atlantic. The Alboran Sea is dominated by water circulation which is predominantly a result of the exchange  
142 of waters at the Strait of Gibraltar whereby low salinity waters from the Atlantic enter the basin and high-salinity  
143 waters from the Mediterranean outflow into the ocean (Bulian *et al.*, 2022). This results in the Eastern Alboran  
144 Gyres (EAG) and the Western Alboran Gyres (WAG) (Bulian *et al.*, 2022), two anti-cyclonic gyres (~~fig~~Fig. 1).

145 This part of the Mediterranean is affected by the Southern Azores cyclone resulting in long, dry summers with  
146 mean temperatures typically exceeding 20°C. In contrast, winters are mild and rainy, with temperatures ranging  
147 10°C on the coast and -7°C at higher elevations resulting in an altitudinal gradient; annual precipitation is usually  
148 400–1400 mm (Quézel and Médail, 2003; Grieser *et al.*, 2006).



149  
150 **Figure 1 - Map showing the location of ODP Site 976 and the present-day surface and water circulation in**  
151 **the Alboran Sea (modified from Combourieu-Nebout *et al.*, 1999).**

152  
153 Vegetation cover is a function of an altitudinal gradient owing to the presence of the Moroccan Rif and Betic  
154 Cordillera (Quézel and Medail, 2003). The coast is dominated mainly by steppe with *Lygeum*, *Artemisia* and  
155 Mediterranean taxa (e.g. *Olea*, *Phillyrea*, *Pistacia*, and *Quercus ilex*). Humid-temperate oak forest with *Quercus*  
156 *deciduous* and Ericaceae dominates the mid-altitudes. Higher elevations are mainly characterised by cold-  
157 temperate coniferous forests with *Pinus* and *Abies*. Although once more spread in the Mediterranean, *Cedrus* is  
158 only found now at higher elevations in Morocco (Ozenda, 1975; [Barbero et al., 1981](#); [Benabid, 1982](#); Rivas  
159 Martinez, 1982; [Barbero et al., 1981](#); [Benabid, 1982](#)).

### 161 **3. Methods**

#### 162 3.1 Fossil pollen datasets

163 The fossil pollen datasets used to run the pollen-based quantitative climatic reconstructions are all obtained from  
164 the ODP Site 976 marine record from the studies listed below. All records excluded *Pinus*, due to its  
165 overrepresentation in marine samples (Heusser and Balsam, 1977; Naughton et al., 2007). The ages used in this  
166 study are in calendar ka (cal ka).

- 167 - The pollen record for MIS 19 (Toti et al., 2020) comprises 102 samples. The chronology was based on the  
168 initial age models from de Kaenel et al. (1999) and Grafenstein et al. (1999). Samples were taken every  
169 10 cm, yielding an average temporal resolution of 450 years between samples.
- 170 - The pollen record for MIS 11 has a total of 141 samples (Sassoon et al., 2023). The chronology for the  
171 fossil pollen record is based on von Grafenstein et al. (1999). Age interpolation revealed a lowermost age  
172 of 433.868 ka BP at 118.8 m and an uppermost age of 356.456 ka BP at 98.85 m. The pollen record for  
173 MIS 11 has an almost consistent resolution of 10 cm, achieving average temporal resolutions of ca. 128  
174 years between samples.
- 175 — The MIS 5 record has 105 samples (Combourieu-Nebout et al., 2002; Masson-Delmotte et al., 2005). The  
176 chronology for this record was based on the age model by Combourieu-Nebout et al. (2002) but has been  
177 extended to 130 ka BP by correlation with deep sea core MD95-2042 (Shackleton et al., 2003) and  
178 NorthGRIP  $\delta^{18}\text{O}$  record (NorthGRIP, 2004). Samples were taken at an average resolution of 10 cm,  
179 yielding an average temporal resolution of 500 years between samples.
- 180 - The record for MIS 1 was based on the uppermost 10m of the ODP Site 976 core, with a total of 136  
181 samples (Combourieu-Nebout et al., 2009). The chronology, [based on calibrations by Bard et al. \(1998\),](#)  
182 [Stuiver and Reimer \(1993\) and Stuiver et al. \(1998\)](#), is built on ten  $^{14}\text{C}$  AMS radiocarbon ages, specifically  
183 measured on monospecific samples of *Globigerina bulloides* and *Neogloboquadrina pachyderma*, which  
184 revealed a lowermost age of 25 cal ka. The pollen analysis involved sampling at 10 cm intervals, with a  
185 higher resolution of 1–5 cm for the Bølling/Allerød and the early Holocene, yielding a resolution  
186 which varies from ~20–40 years during the abrupt events to 200–500 years elsewhere.

187 [Due to the use of different age models derived from various proxies, especially when comparing our records with](#)  
188 [other studies, as well as the use of different calibration methods, some records may appear misaligned in the](#)  
189 [figures in regard to age.](#)

#### 190 3.2 Pollen-based climate reconstructions methods

191 Three methods of climate reconstruction have been used to derive quantitatively changes in temperature and  
192 precipitation parameters for the ODP Site 976 pollen records: Modern Analogues Technique (MAT; Guiot, 1990),  
193 Weighted Average Partial Least Squares regression (WA-PLS; Ter Braak and Juggins, 1993) and Boosted  
194 Regression Trees (BRT; Salonen et al., 2014).

195 [The MAT and WA-PLS techniques have been effectively used for climate reconstructions across various](#)  
196 [Mediterranean areas and time periods based on terrestrial and marine pollen records \(e.g., Cheddadi et al., 1998;](#)  
197 [Joannin et al., 2012; Mauri et al., 2015; Herzsuh et al., 2023\).](#) These results are often supported by other  
198 [independent proxies, enhancing the reliability of these reconstructions. For instance, biomarker analysis from](#)  
199 [Tenaghi Philippon \(Ardenghi et al., 2019\) or Lake Matese \(Robles et al., 2023\) has provided insight into](#)  
200 [temperature and moisture variability that aligns with pollen-based climate reconstructions. Similarly, Lake Ohrid's](#)  
201 [pollen record corroborates shifts in centennial-scale vegetation dynamics and climate variability during MIS 11](#)  
202 [\(Kousis et al., 2018\) and MIS 5 \(Sinopoli et al., 2019; Koutsodendris et al., 2019, demonstrating convergence](#)  
203 [with independent climatic proxies. Further evidence from Lago di Pergusa in central Sicily highlights vegetation](#)  
204 [and climate shifts over the last 7,000 years, with pollen data supporting findings from other proxies from the](#)  
205 [Mediterranean \(Sadori et al., 2013\). The multi-proxy approach implemented in these studies shows the reliability](#)  
206 [MAT and WA-PLS as robust methods for reconstructing past climate conditions.](#)

207 [MAT and WA-PLS have been previously used for climate reconstruction focusing on different time periods](#)  
208 [in the Mediterranean region on both terrestrial and marine pollen records \(e.g. Cheddadi et al., 1998; Davis et al.,](#)  
209 [2003; Pross et al., 2009; Peyron et al., 2011, 2013, 2017; Joannin et al., 2012; Kotthoff et al., 2008; Dormoy et](#)  
210 [al., 2011\).](#)

212 *et al.*, 2009; Sanchez Goñi *et al.*, 2012; Desprat *et al.*, 2013; Sadori *et al.*, 2013; Mauri *et al.*, 2015; Kousis *et al.*,  
213 2018; Ardenghi *et al.*, 2019; Sinopoli *et al.*, 2019; Koutsodendris *et al.*, 2019; Robles *et al.*, 2023; Herzsuh *et*  
214 *al.*, 2023). The results are often well supported by other Mediterranean records and independent proxies such as  
215 alkenones and other biomarkers,  $\delta^{18}\text{O}$  isotopes and sea surface temperature reconstructions, showing the reliability  
216 of these methods.

217 The MAT uses technique involves applying information from the present-day environment to quantitatively  
218 reconstruct past climate derived from fossil assemblages (Chevalier *et al.*, 2020). MAT functions by determining  
219 the degree of dissimilarity between past pollen assemblages and modern pollen data. By using squared-chord  
220 distance calculations, MAT selects a number of modern pollen data considered as analogues for each fossil pollen  
221 assemblage to infer past climatic values (Guiot, 1990).

222 In contrast to the MAT which is an “assemblages approach”, the WA-PLS method is a true transfer function  
223 meaning that it requires statistical calibration between the climate parameters and modern pollen assemblages  
224 (Chevalier *et al.*, 2020). It is a regression method which supposes the unimodal relationship between pollen  
225 percentages and climate parameters.

226 In comparison to the other methods, BRT is a machine learning method developed for ecology (De'ath, 2007;  
227 Elith *et al.*, 2008) and has recently been adopted for palaeoecology and palaeoclimatic reconstructions (Salonen  
228 *et al.*, 2014). It uses random binary splitting and cross-validation to predict the relationship between climatic  
229 variables and pollen assemblages (Chevalier *et al.*, 2020). In BRTs, great numbers of simple regression-tree  
230 models are combined to produce a final model optimised for prediction, using cross-validation for model building.  
231 This approach is promising for Mediterranean terrestrial records (Robles *et al.*, 2023; d'Oliveira *et al.*, 2023;  
232 Robles *et al.*, 2023) but has never been tested on marine pollen records or indeed records of the Mid-Pleistocene.

233 All three methods were calibrated using an updated version of the high-quality and taxonomically consistent  
234 modern pollen dataset (Peyron *et al.*, 2013; Dugerdil *et al.*, 2021) containing 3,267 samples from European and  
235 Mediterranean regions. *Pinus* has been omitted because its overrepresentation in the Mediterranean pollen  
236 spectrum could mask climatically-related signals from other taxa (Sinopoli *et al.*, 2019).

237 In this study, we reconstructed the following climatic parameters: (1) mean annual temperature (TANN); (2)  
238 mean temperatures of the coldest month (Twin) and (3) warmest month (Tsum); (4) mean annual precipitation  
239 (PANN); (5) summer precipitation (Psum); (6) winter precipitation (Pwin). The entire dataset includes the  
240 parameters for growing degree days above 5°C (GDD5), the ratio of actual over potential evapotranspiration  
241 (AET/PET), and further seasonal parameters including autumn and spring temperature and precipitation (Taut and  
242 Tspr, Paut and Pspr, respectively). The studies by Combourieu-Nebout *et al.* (2009) and Dormoy *et al.* (2009),  
243 which implement pollen-based reconstructions for MIS 1 using pollen data from ODP Site 976, represent a crucial  
244 foundation for the present paper. While providing guidance, however, these previous studies only applied the  
245 MAT method, therefore the application of new methods is necessary to enable the comparison with the results for  
246 the other Holocene analogues.

247 Quantitative reconstruction methods and reliability tests were carried out with the software R using the  
248 package ‘*rioja*’ (Juggins, 2020). The reliability of pollen-inferred climate reconstruction methods was estimated  
249 through bootstrapping cross-validation by calculating the correlation coefficient values between the variables ( $R^2$ ),  
250 and using the Root Mean Square Error (RMSE) criterion. Higher  $R^2$  and lower RMSE indicate greater validity of  
251 the reconstructed parameters. Loess smoothing of 0.2 was applied to the raw data in the plots to view the overall  
252 trends of the parameters.

## 254 **4. Results and discussion**

### 256 **4.1 Multi-method approach: reliability and differences between the methods**

257 The temperature and precipitation reconstructions for the three methods yielded coherent results for the  
258 interglacials and interstadials investigated, aligning reasonably with trends observed in other regional climatic  
259 proxies (section 4.2).

260 A comparison of the methods across the four interglacials, based on the  $R^2$  and RMSE values, reveals  
261 discrepancies in the performance trends. To exemplify these differences between methods, the  $R^2$  and RMSE  
262 results for TANN and PANN are shown in table 1. Overall, the models reconstruct TANN more consistently than  
263 PANN, based on the significant difference between the RMSE values for these parameters across all MIS periods.  
264 BRT consistently demonstrates robust performance, with high  $R^2$  values ranging from 0.918 to 0.920 for TANN  
265 and 0.822 to 0.826 for PANN, alongside low RMSE values compared to the other methods. The MAT method,  
266 akin to BRT, shows strong performance with high  $R^2$  values ranging from 0.865 to 0.866 for TANN and slightly  
267 lower values of 0.711 to 0.713 for PANN, alongside comparatively low RMSE values. However, in comparison  
268 to BRT, the MAT method tends to have slightly lower  $R^2$  and higher RMSE, and there is a greater degree of  
269 fluctuation for the parameters reconstructed which is interpreted as greater sensitivity to changes in the pollen  
270 assemblages. In contrast, WA-PLS exhibits lower  $R^2$  values (ranging from 0.445 to 0.683) and higher RMSE  
271 values (ranging from 4.271 to 232.650) across both TANN and PANN parameters, indicating potentially poorer

272 model performance compared to BRT and MAT. Notably, BRT and MAT methods demonstrate greater  
 273 consistency in performance across interglacials and parameters compared to WA-PLS, suggesting their superior  
 274 efficacy in reconstructing climatic parameters across different temporal periods.

275 The observed trends in performance of the methods for TANN and PANN are applicable across all parameters  
 276 reconstructed (see supplementary data); BRT and MAT consistently exhibit strong performance characterized by  
 277 high  $R^2$  values and low RMSE scores for all reconstructed parameter, while the WA-PLS method has lower  $R^2$   
 278 values and higher RMSE scores across the board, suggesting a tendency toward less accurate reconstructions.  
 279 These results were previously reported in other studies in regions outside the Mediterranean which compare the  
 280 reliability of these methods, and which found that MAT and BRT are more reliable than WA-PLS (Dugerdil et  
 281 al., 2021; d'Oliveira et al., 2023).

282  
 283 **Table 1 –  $R^2$  and RMSE results from the methods BRT, WA-PLS and MAT for selected parameters (TANN and PANN) for the interglacials analysed in this study.**

		<u>MIS 1</u>		<u>MIS 5</u>		<u>MIS 11</u>		<u>MIS 19</u>	
		$R^2$	RMSE	$R^2$	RMSE	$R^2$	RMSE	$R^2$	RMSE
<b>BRT</b>	<b>TANN</b>	0.918	2.965	0.919	2.960	0.920	2.962	0.919	2.947
	<b>PANN</b>	0.826	175.89 2	0.822	176.922	0.825	176.590	0.823	176.822
<b>WA-PLS</b>	<b>TANN</b>	0.683	4.271	0.683	4.275	0.683	4.277	0.683	4.275
	<b>PANN</b>	0.453	232.51 8	0.453	232.646	0.453	232.552	0.445	232.650
<b>MAT</b>	<b>TANN</b>	0.865	3.067	0.866	3.063	0.865	3.072	0.865	3.067
	<b>PANN</b>	0.713	184.26 1	0.712	184.385	0.711	187.333	0.711	183.010

284  
 285

#### 286 4.2 Climatic reconstructions for each interglacial

##### 287 4.2.1 MIS 20–19 (803–748 ka BP)

288 The reconstructions for MIS 20–19 show large-amplitude changes in temperature and precipitation (Fig. 2, Tab.  
 289 2). During the period reconstructed for the MIS 20 glacial between 803–786 ka BP, results indicate a cold and dry  
 290 climate, linked to the occurrence of steppic and semi-desertic taxa such as *Artemisia*, *Amaranthaceae* and  
 291 *Ephedra*, ~~which are adapted to cold climates~~ (Toti *et al.*, 2020). Throughout MIS 20, TANN fluctuates around 4.7  
 292 °C, with PANN averaging approximately 460 mm~~⁄yr~~, although there is a contrast between the periods 803–800  
 293 ka BP and 799–787 ka BP (Fig. 2, Tab. 2). In the former period, PANN is around 600 mm~~⁄yr~~ and Pwin around  
 294 200 mm~~⁄yr~~, while in the latter period PANN decreases to below 400 mm~~⁄yr~~ and Pwin to below 50mm~~⁄yr~~ (Fig.  
 295 S2). The transition to harsher conditions during the late MIS 20 (around 799 ka BP) was associated with colder  
 296 conditions, as evidenced by palynological and foraminiferal records (Toti *et al.*, 2020). This corresponds to a  
 297 shutdown of the Atlantic Meridional Overturning Circulation (AMOC) during that time (Cacho *et al.*, 2000;  
 298 Moreno *et al.*, 2004). Maiorano *et al.* (2016) observed this in the Montalbano Jonico section (southern Italy) and  
 299 referred to it as a Heinrich-type event (Med-HTIX) in analogy to those of the last termination (TI), and similarly  
 300 the warm-cold episodes during TIX have been named the Bølling-Allerød-like (Med-BATIX) and Younger-  
 301 Dryas-like (Med-YDTIX) events (Maiorano *et al.*, 2016).

302 From ~~788786–774–773~~ ka BP, the reconstructions for TANN indicate a rise from 2–7 °C during the glacial to  
 303 6–13 °C, indicating the transition to MIS 19 (Fig. 2). This period is equivalent to the climatic optimum MIS 19c.  
 304 This trend is also indicated by PANN, which increases from 350–500 mm during the glacial to between 600–800  
 305 mm across the three methods during the climatic optimum, indicating warmer and wetter conditions compared to  
 306 MIS 20 (Toti *et al.*, 2020). This climatic amelioration is interrupted by a short-lived event to cooler and drier  
 307 conditions and a change in seasonality around 785 ka BP. This event has been observed in other pollen records  
 308 including Montalbano Jonico (Bertini *et al.*, 2015) and speleothem records like Sulmona (Regattieri *et al.*, 2019).

309 In the Alboran Sea, a peak in warmth and humidity is observed around 778 ka BP throughout the three  
 310 methods, although some differences in the methods are observed, where WA-PLS and BRT suggest a more  
 311 gradual temperature and precipitation increase than MAT, which indicates greater amplitude fluctuations (Fig. 2).  
 312 TANN averages between 5 and 10°C and PANN is around 500–700 mm~~⁄yr~~, with Pwin values of around 150–300  
 313 mm~~⁄yr~~ and Twin around 0°C, suggesting temperate summers and mild winters during MIS 19c (Fig. 2, Fig. S2).  
 314 These reconstructions correlate well (Fig. 2) with the progressive increase in CH<sub>4</sub> and CO<sub>2</sub> observed in the EPICA  
 315

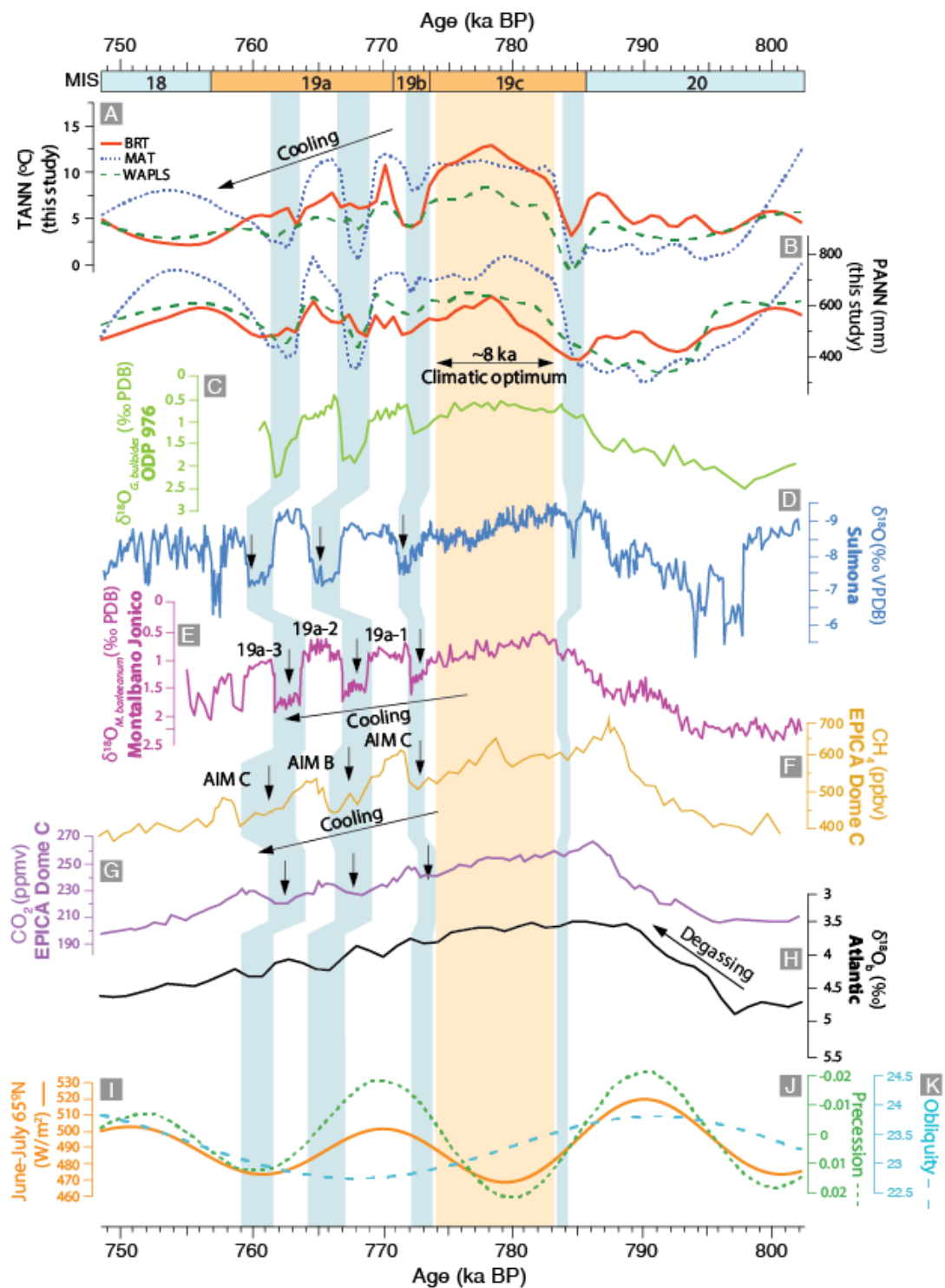
316 ice cores (Jouzel *et al.*, 2007; Nehrbass-Ahles *et al.*, 2020), and decline in Atlantic  $\delta^{18}\text{O}$  (e.g. Voelker *et al.*, 2010;  
 317 [Oliveira \*et al.\*, 2016](#)[Sanchez Goñi \*et al.\*, 2016a](#)).

318 There is a decisive fall in temperature centred between 773–771 ka BP, along with a slight decrease in  
 319 precipitation (Tab. 2), consistent with a return to colder and drier conditions during MIS 19b-a (Toti *et al.*, 2020).  
 320 Twin fluctuates from  $-9^{\circ}\text{C}$  to  $7^{\circ}\text{C}$ , indicating substantial variability in winter temperatures, while Tsum ranges  
 321 from  $13^{\circ}\text{C}$  to  $22^{\circ}\text{C}$ , suggesting fluctuations in summer warmth (Fig. S2). TANN varies between  $0^{\circ}\text{C}$  and  $14^{\circ}\text{C}$ ,  
 322 indicating overall climatic changes throughout the year. PANN ranges from 370 mm to 750 mm, reflecting  
 323 fluctuations in annual precipitation levels. This is followed by three large-amplitude fluctuations during MIS 19a  
 324 (Fig. 2, Tab. 2), with extreme peaks at 770 and 765 ka BP, separated by two significant events of climatic  
 325 deterioration at 768 and 764 ka BP, which are linked to the high frequency alternation between forested and open  
 326 vegetation observed in the pollen record. This shows good agreement with oscillations in the benthic  $\delta^{18}\text{O}$  record  
 327 of Montalbano Jonico from Nomade *et al.* (2019), who labelled these 19a-1, 19a-2 and 19a-3. These fluctuations  
 328 also correlate well with those observed in the benthic  $\delta^{18}\text{O}$  record from Sulmona (Giaccio *et al.*, 2015; Regattieri  
 329 *et al.*, 2019), Atlantic  $\delta^{18}\text{O}$  (e.g. Voelker *et al.*, 2010; [Sanchez Goñi \*et al.\*, 2016a](#)[Oliveira \*et al.\*, 2016](#)) as well as  
 330 the  $\text{CH}_4$  (Loulergue *et al.*, 2008) and  $\text{CO}_2$  observed in the EPICA ice cores (Jouzel *et al.*, 2007; Nehrbass-Ahles  
 331 *et al.*, 2020). These climatic oscillations may have been caused by a shift in the position of the ITCZ causing  
 332 northward pressure on the Mediterranean leading to more arid summers and enhanced winter precipitation (Toti  
 333 *et al.*, 2020).  
 334

**Table 2 – Summary of results of the pollen-based climatic reconstructions for MIS 20–19**

Interval	Age (ka BP)	Summary
<b>MIS 19a and 19b</b>	773–756	Decisive fall in temperature centred between 773–771 ka BP. Slight decrease in precipitation but to a lesser extent and consistent with a return to colder and drier conditions. Three large-amplitude fluctuations with extreme peaks at 770 and 765 ka BP, separated by two significant events of climatic deterioration at 768 and 764 ka BP. Continued large-amplitude changes in temperature and precipitation.
<b>MIS 19c climatic optimum</b>	786–773	TANN shows a rise from $2\text{--}7^{\circ}\text{C}$ during the glacial to $6\text{--}13^{\circ}\text{C}$ . PANN increases from a range of 350–500 mm during the glacial to between 600–800 mm. MAT suggests the largest changes in both temperature and precipitation. Peak in warmth and humidity observed synchronously around 778 ka BP.
<b>MIS 20/19 transition</b>	803–786	MAT suggests the largest changes in both temperature and precipitation during this transition. Shift from glacial conditions (MIS 20) to interglacial conditions (MIS 19).

335



337 Figure 2 – Comparison of the pollen-based quantitative reconstructions from ODP976 for MIS 19, (A)  
 338 TANN and (B) PANN (BRT=red solid line; MAT=blue dotted line; WA-PLS=green dashed line), with other  
 339 regional and global proxies: (C)  $\delta^{18}\text{O}_{\text{G, bulloides}}$  record from ODP976 (Toti et al., 2020); (D)  $\delta^{18}\text{O}$  records of  
 340 Sulmona basin sediments (Regattieri et al., 2019); (E)  $\delta^{18}\text{O}_{\text{M. barleeanum}}$  record from Montalbano Jonico  
 341 (Nomade et al., 2019); (F) Methane ( $\text{CH}_4$ ) atmospheric concentrations (Loulergue et al., 2008) and (G)  $\text{CO}_2$   
 342 atmospheric concentrations from Antarctic EPICA Dome C ice cores (Nehrbass-Ahles et al., 2020); (H)  
 343 Atlantic  $\delta^{18}\text{O}$  (Voelker et al., 2010); (I) Summer insolation (Laskar et al., 2004); (J) Precession index and  
 344 (K) Obliquity curve (Berger and Loutre, 1991). Orange band indicates the period encompassing the  
 345 climatic optimum, and the blue bands highlight major millennial-scale climatic events.  
 346



#### 347 4.2.2 MIS 12–11 (434–356 ka BP)

348 Between 434 and 427 ka BP, reconstructions for the end of MIS 12 show a generally cold and dry climate (Fig.  
349 3). Annual temperature reconstructions reveal consistently low values across methods, with the coldest period  
350 occurring before 430 ka BP (Tab. 3). During this period, Twin shows temperatures ranging  $-5$ – $0$  °C and Tsum  
351 does not rise above  $17$  °C (Fig. S3). Following a brief warming around 430 ka BP, a rapid return to colder  
352 conditions is observed at 428–426 ka BP across all three methods (Fig. 3). This abrupt shift to colder conditions  
353 coincides with decreased sea surface temperatures (SSTs) and increased  $\delta^{18}\text{O}_{G. bulloides}$  in the record from the same  
354 ODP976 core by Brice (2007), who made the analogy with a Younger Dryas-like (YD-1) event. Other studies refer  
355 to this as the Ht4 Heinrich-type event (Hodell *et al.*, 2008; Rodrigues *et al.*, 2011; Girone *et al.*, 2013; Marino *et*  
356 *al.*, 2018). Vázquez Riveiros *et al.* (2013) noted enhanced Ice Rafted Debris (IRD) coeval with a sudden decrease  
357 in North Atlantic SSTs during this event, indicating significant ice-rafting. Other pollen-based reconstructions,  
358 particularly those from Lake Ohrid which used the MAT method (Kousis *et al.*, 2018), show a short-lived decrease  
359 in temperatures, precipitation, and forest cover prior to the onset of warmer and wetter conditions during  
360 Termination V.

361 From 427 to 405 ka BP, a period with consistently high temperatures and precipitation are observed (Fig. 3,  
362 Tab. 3), consistent with the warmest part of MIS 11, substage MIS 11c (Sassoon *et al.*, 2023). This transition has  
363 also been observed in other records (Fig. 3) in the Mediterranean region (Tzedakis, 2010; Girone *et al.*, 2013;  
364 Kousis *et al.*, 2018; [Ardenghi \*et al.\*, 2019](#); Koutsodendris *et al.*, 2019; [Ardenghi \*et al.\*, 2019](#); Azibeiro *et al.*, 2021),  
365 the North Atlantic off the Iberian coast (Desprat *et al.*, 2005; Oliveira *et al.*, 2018) and continental Europe (Reille  
366 and de Beaulieu, 1995). TANN rises from around  $8$  °C to  $\sim 10$ – $15$  °C, over the timeframe of ca. 2,000 years. BRT  
367 and WA-PLS show Tsum values of around  $18$  °C, while the MAT method estimates warmest-month temperatures  
368 of over  $22$  °C (Fig. S3). This warming is in agreement with the expansion of forest biomass observed in several  
369 other records from across the Mediterranean basin throughout Termination V including Lake Ohrid (Kousis *et al.*,  
370 2018), Tenaghi Philippon (Wijmstra and Smit, 1976; Tzedakis *et al.*, 2006; Pross *et al.* 2015; Ardenghi *et al.*,  
371 2019; Koutsodendris *et al.*, 2023) and Bouchet/Praclaux (Reille and de Beaulieu, 1995). This increase in  
372 temperatures during MIS 11c may be linked to the MIS 11.3 light isotopic event (Oliveira *et al.*, 2018) and the  
373 highest summer insolation recorded for MIS11 in the Northern Hemisphere (Sassoon *et al.*, 2023). The warming  
374 trend is also coeval with the rise in Antarctic air temperatures and Atlantic CO<sub>2</sub> records (Fig. 3) (Jouzel *et al.*,  
375 2007; Loulergue *et al.*, 2008; Nehrbass-Ahles *et al.*, 2020). These results correlate with the highest SSTs, highest  
376 CO<sub>2</sub> and CH<sub>4</sub> concentrations (Jouzel *et al.*, 2007; Nehrbass-Ahles *et al.*, 2020), and reduced  $\delta^{18}\text{O}$  (e.g. Voelker *et*  
377 *al.*, 2010; Oliveira *et al.*, 2018).

378 Precipitation also increases during the climatic optimum, suggesting warm and humid conditions (Fig. 3, Tab.  
379 3). Annual precipitation results from BRT and WA-PLS show a rise from  $500$  mm $\cdot$ yr<sup>-1</sup> during the glacial to  $600$   
380 mm $\cdot$ yr<sup>-1</sup> for MIS 11c in the period between 429–427 ka BP, while MAT suggests a larger amplitude of change from  
381 around  $380$  mm $\cdot$ yr<sup>-1</sup> to  $600$  mm $\cdot$ yr<sup>-1</sup>. These results are consistent with pollen-based quantitative reconstructions of  
382 Kousis *et al.* (2018) at Lake Ohrid, which suggest a shift to more a humid and warmer climate at the beginning of  
383 MIS 11c. However, the reconstructions for precipitation at Lake Ohrid are comparatively higher than the results  
384 for ODP 976, evidenced by a rise in PANN to  $800$ – $1000$  mm $\cdot$ yr<sup>-1</sup> at Lake Ohrid (Kousis *et al.*, 2018). At Tenaghi  
385 Philippon, precipitation reconstructions derived from calcium/iron (log(Ca/Fe)) ratio by Koutsodendris *et al*  
386 (2023) show that MIS 11c was one of the wettest interglacials at this site with a significant difference between the  
387 climatic optimum and the rest of MIS 11. This is a significant finding because this corroborates the hypothesis  
388 put forward by several authors (Kandiano *et al.*, 2012; Kousis *et al.*, 2018; Sassoon *et al.*, 2023) who suggested,  
389 on the basis of pollen assemblages, that during MIS 11c, the climate in the southwestern Mediterranean was  
390 warmer and drier than Lake Ohrid and Tenaghi Philippon in the Balkan Peninsula. Although this might be an  
391 effect of a difference in altitude between the sites (which might also explain the difference in annual temperature)  
392 and the nature of the substrates observed (marine vs. terrestrial), it might be indicative of an easterly humidity  
393 gradient within the wider region owed to the formation of a bipolar see-saw pattern in precipitation between the  
394 western and eastern Mediterranean possibly caused by a weakening of the AMOC during the deglaciation (Kousis  
395 *et al.*, 2018).

396 During the MIS 11c optimum, a noteworthy fluctuation occurs around 408 ka BP, mainly indicated in our  
397 reconstructions by a decrease in PANN (Fig. 3). This is related to a moderate-intensity contraction in temperate  
398 and Mediterranean forests (Sassoon *et al.*, 2023). Oliveira *et al.* (2016) and Kousis *et al.* (2018) have linked this  
399 forest contraction with the “Older Holstenian Oscillation” (OHO), also found in other records from Europe (West,  
400 1956; Kelly, 1964; Turner, 1970; Kukla, 2003; Koutsodendris *et al.*, 2011, 2012, 2023; Tye *et al.*, 2016). Our  
401 reconstructions indicate a reduction in TANN by about  $1$ – $2$ °C, and in PANN by  $50$  mm $\cdot$ yr<sup>-1</sup> on average across the  
402 three methods. This appears to be less intense than the changes inferred for Lake Ohrid (Kousis *et al.*, 2018) or  
403 Tenaghi Philippon (Ardenghi *et al.*, 2019), which suggest a higher amplitude of change in both precipitation and  
404 temperature in the Balkans.

405 Between 400 and 356 ka BP, the substages MIS 11a and 11b exhibit reduced climate variability. Around  
406 400–390 ka BP, a synchronous decline across the reconstructions for temperature and precipitation is interpreted

407 as a cooler and drier phase, recognized as MIS 11b, connected to a decrease in summer insolation. The  
 408 reconstructions show a decline in temperature and precipitation parameters centred around 398 ka BP (Fig. 3).  
 409 Similarly, reconstructions for Lake Ohrid demonstrate reductions in TANN and PANN (Kousis *et al.*, 2018),  
 410 indicating a synchronous cooling across the Mediterranean Basin on land and the sea. Around 390–367 ka BP,  
 411 recognised as substage MIS 11a, a return to warmer and more humid conditions, though relatively less temperate  
 412 as the conditions during MIS 11c, are observed. Temperature reconstructions vary depending on methods, with  
 413 WA-PLS and BRT indicating less variation than MAT suggests. PANN and Pwin also increase compared to  
 414 previous levels at the end of MIS 11b, showing high variability during MIS 11a (Fig. 3, Fig. S3). Overall, however,  
 415 these trends correlate with patterns observed in palaeoclimatic records from the North Atlantic and Mediterranean  
 416 and seem to reflect summer insolation (Candy *et al.*, 2014, 2024).

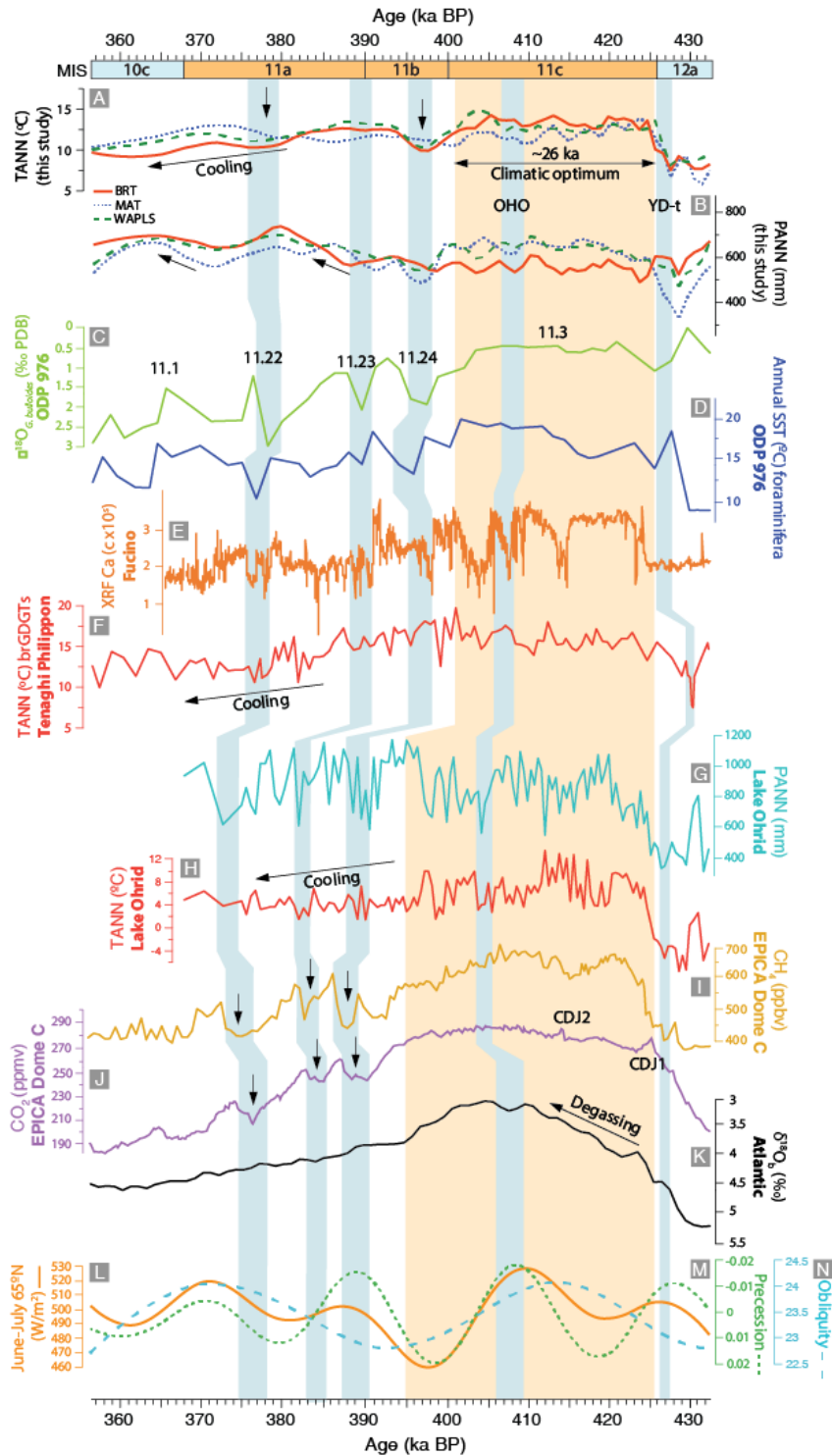
417 The fluctuations during MIS 11a and 11b can be correlated with the light isotopic events 11.24, 11.23 and  
 418 11.22 (Fig.3), observed in  $\delta^{18}\text{O}$  records (Brice, 2007; Desprat *et al.*, 2005; Oliveira *et al.*, 2018). Particularly, the  
 419 drop in precipitation and temperature around 397 ka BP, reflective of the rise in steppe taxa in ODP 976, is  
 420 synchronous with light isotopic event 11.24, also observed at IODP Site U1385 (Oliveira *et al.*, 2018), MD01-  
 421 2447 (Desprat *et al.*, 2005, 2007), at Lake Ohrid (Kousis *et al.*, 2018), and at Tenaghi Philippon (Ardenghi *et al.*,  
 422 2019). The alkenone-based SST record from MD03-2699 show reductions to  $\sim 10^\circ\text{C}$  (Rodrigues *et al.*, 2011). This  
 423 trend can also be compared with falls in  $\text{CO}_2$  and  $\text{CH}_4$  concentrations in the Antarctic EPICA records, which  
 424 exemplify the sensitivity of the Mediterranean to global-scale climate change.

425 From 367 ka BP onwards, the temperature and precipitation reconstructions across all methods collectively  
 426 suggest a transition to a significantly colder and drier climate, consistent with the beginning of the glacial inception  
 427 of MIS 10.  
 428

**Table 3 - Summary of results of the pollen-based climatic reconstructions for MIS 12–11**

Interval	Age (ka BP)	Summary
MIS 11a and b	400–367	Decline in TANN to around $10^\circ\text{C}$ . Twin falls to a minimum of $0^\circ\text{C}$ at 398 ka BP. Tsum shows consistent decline to $\sim 20^\circ\text{C}$ at 397 ka BP. Precipitation parameters for MIS 11b, display a fall in precipitation around 380 ka BP. MAT and BRT suggest a progressive rise in precipitation from 400 ka BP culminating at 395 ka BP.
MIS 11c climatic optimum	427–400	Consistently high temperatures and precipitation. TANN ranges between $10$ and $15^\circ\text{C}$ , indicating relative climatic stability. Three distinctive temperature peaks observed, with the third around 405 ka BP.
MIS 12/11 transition	<del>433</del> 434–427	Lowest annual temperatures ( $\sim 5^\circ\text{C}$ ) before 430 ka BP. Brief temperature peak around 430 ka BP, followed by rapid return to cold conditions at 428 ka BP. Decline in precipitation until 430 ka BP, PANN ranging 400–600 mm. Transition to warmer, more humid climate around 428 ka BP with temperatures over $22^\circ\text{C}$ and annual precipitation rising to 600 mm.

429  
 430  
 431  
 432



433  
 434 **Figure 3 – Comparison of the pollen-based quantitative reconstructions from ODP976 for MIS 11, (A)**  
 435 **TANN and (B) PANN (BRT=red solid line; MAT=blue dotted line; WA-PLS=green dashed line), with other**  
 436 **regional and global proxies: (C)  $\delta^{18}\text{O}_{\text{G. bulloides}}$  and (D) annual SSTs from function transfer of foraminiferal**  
 437 **assemblages from ODP976 (Brice, 2007); (E) XRF (Calcium) counts per second (cps) record from the**  
 438 **Fucino Basin (Giaccio et al., 2019; Monaco et al., 2021); (F) molecular biomarkers (brGDGT)-derived**  
 439 **TANN from Tenaghi Philippon (Ardenghi et al., 2019); (G,H) PANN and (G,H) TANN from Lake Ohrid**  
 440 **derived through the MAT method (Kousis et al., 2018); (I) Methane ( $\text{CH}_4$ ) atmospheric concentrations**  
 441 **(Louergue et al., 2008) and (J)  $\text{CO}_2$  atmospheric concentrations from Antarctic EPICA Dome C ice cores**  
 442 **(Nehrbass-Ahles et al., 2020); (K) Atlantic  $\delta^{18}\text{O}$  (Voelker et al., 2010); (L) Summer insolation (Laskar et**  
 443 **al., 2004); (M) Precession index and (N) Obliquity curve (Berger and Loutre, 1991). Orange band**

444 **indicates the period encompassing the climatic optimum, and the blue bands highlight major millennial-**  
445 **scale climatic events.**

446

#### 447 *4.2.3 MIS 6–5 (133–80 ka BP)*

448 The climatic reconstructions for the period between 133 and 128 ka BP, equivalent to the end of the MIS 6 glacial  
449 period, also referred to as the penultimate glacial, indicate cold and dry conditions, though some differences  
450 between methods are observed (Fig. 4). Generally, the three methods show low values of TANN (range of 10–  
451 13°C) and Twin (range of -5°C to 3°C) for the glacial period (Fig. 4), but there appears to be disagreement in the  
452 reconstruction of Tsum. While BRT and WA-PLS suggest an average Tsum of 20°C, which is already surprisingly  
453 high, MAT indicates higher values (Fig. S4), which might be owed to the tendency of this method to overestimate  
454 parameters as it is more sensitive than the other two methods and has been shown in other studies to have a wider  
455 spread of estimates during glacial periods (Brewer *et al.*, 2008; Sinopoli *et al.*, 2019). On the other hand,  
456 precipitation reconstructions seem to be relatively in agreement with each other, suggesting dry conditions with  
457 PANN under 600mm. The results for this time period are also observed in other records and pollen-based  
458 reconstructions from southern Europe and the Iberian margin (e.g. Sanchez Goñi *et al.*, 1999; Desprat *et al.*, 2005;  
459 Brewer *et al.*, 2008; Sinopoli *et al.*, 2019; Leroy *et al.*, 2023).

460 The transition from MIS 6 to MIS 5 is characterised by a rise in temperature and precipitation indicative of a  
461 gradually warmer and more humid climate. An increase in TANN is visible in all the three methods, from between  
462 10–12 °C during the glacial to 12–15 °C at the beginning of MIS 5e, equivalent to the early Eemian (Fig. 4). This  
463 reflects the shift from steppic taxa to *Quercus* and other temperate vegetation (Fig. S1) as was also recorded in  
464 the marine records of MD952042 (Sanchez Goñi *et al.*, 1999) and MD01-2447 (Desprat *et al.*, 2007) from the  
465 Iberian Margin. This progressive rise is paralleled by the rise in CO<sub>2</sub> and CH<sub>4</sub> from Antarctica, and the decrease  
466 in δ<sup>18</sup>O (Desprat *et al.*, 2005; Voelker *et al.*, 2010; Oliveira *et al.*, 2018). However, this transition towards climatic  
467 amelioration is interrupted by a short-lived event of abrupt cooling and drying, observed already in MIS 19 and  
468 11. These events have previously been observed throughout the interglacials MIS 19, 11 and 5 in records from  
469 the Iberian Margin (Sanchez Goñi *et al.*, 1999; Desprat *et al.*, 2007) and were considered to be events analogue  
470 to Younger Dryas events or Henrich-type events associated with the weakening of the AMOC during the  
471 deglaciation period. While these abrupt cooling and drying events during transitions to interglacials (MIS 19, 11,  
472 and 5) are well-documented in Mediterranean records, such as those from the Iberian Margin, similar YD/H1-like  
473 events are not always present in terrestrial records from mainland Europe such as Tenaghi Philippon or Lake  
474 Ohrid. This may be due to the fact that marine records capture more regional signals compared to terrestrial  
475 records, and the greater sensitivity of sites like the Alboran Sea to such climatic shifts.

476 While there are some differences between the methods in terms of the specific timing of the peak climatic  
477 optimum during the Eemian (something that is itself under particular debate in the literature (e.g. Cheddadi *et*  
478 *al.* 1998; Sanchez Goñi *et al.*, 1999), the reconstructions show that the highest temperatures (>15 °C) and humidity  
479 (≥600 mm) occurred between 127–118 ka BP (Fig. 4, Tab. 4). This is coeval with the lightest isotopic δ<sup>18</sup>O  
480 signature from the Iberian margin (Desprat *et al.*, 2007) and highest sea-surface temperatures recorded in cores  
481 ODP 977 in the Alboran sea (Martrat *et al.*, 2004). During this climatic optimum, Tsum and Twin values peak  
482 with values higher than MIS 19 and 11 averaging >23 °C and 10 °C, respectively, indicating increased temperature  
483 during both winter and summer months (Fig. S4). These parameters indicate a more humid and warmer climate  
484 during the optimum of the Eemian than the present day, which corroborates the findings of several other studies  
485 in Europe (Guiot *et al.*, 1989; Cheddadi *et al.* 1998; Sanchez Goñi *et al.*, 1999; Desprat *et al.*, 2007; Brewer *et al.*,  
486 2008; Leroy *et al.*, 2023). For example, reconstructions from Lake Ohrid, La Grande Pile, Les Echets and Le  
487 Bouchet also show a thermal maximum around this time, between 127 and 118 ka, followed by cooling around  
488 117 ka (Brewer *et al.*, 2008; Sinopoli *et al.*, 2019).

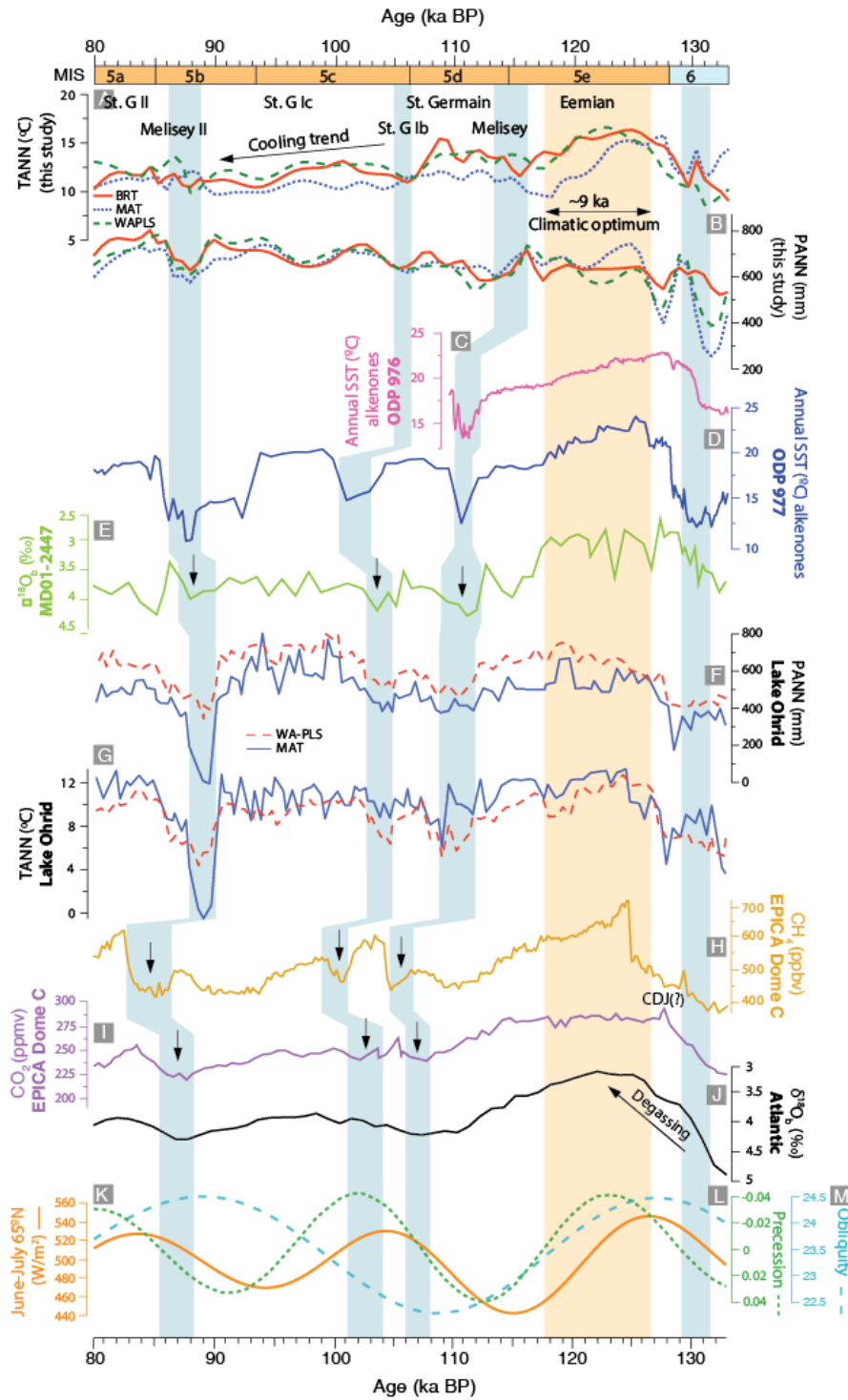
489 Our results also match the findings by Brewer *et al.* (2008), who identified a difference between northern and  
490 southern Europe, whereby records from higher latitudes experiences a sharp drop in temperatures and precipitation  
491 following the optimum whereas the climate remained more stable conditions over a longer period in the south.  
492 Our reconstructions for ODP 976, similarly to those from Lake Ohrid (Sinopoli *et al.*, 2019) and Lago di  
493 Monticchio (Allen *et al.*, 1999; Brewer *et al.*, 2008), exhibit a gradual and continuous cooling trend without a  
494 sudden decrease in temperatures and precipitation following the Eemian optimum, suggesting an intermediate  
495 climate signal more similar to southern European sites than northern ones, and possibly corroborating the idea of  
496 a weak latitudinal gradient during this period. However, our results for Psum and Pwin show that there was still  
497 strong seasonality during the Eemian climate optimum at least in the Western Mediterranean, reflected more by  
498 precipitation parameters than temperature (Fig. S4). During this period, our reconstructions show that, while the  
499 climate was overall wetter than the glacial of MIS 6 (as well as the latter parts of the Eemian), the climatic optimum  
500 was characterised by very dry summers and contrastingly wetter winters. This might be linked with a strong  
501 Mediterranean climate during this time around the Alboran Sea, as previously suggested by Sanchez Goñi *et al.*  
502 (1999) for the Iberian Margin.

503 The tail end of the optimum is characterised by a decrease in temperature and a rise in precipitation, visible  
504 across all three methods, in agreement with other European records (Guiot *et al.*, 1989; Brewer *et al.*, 2008;  
505 Sinopoli *et al.*, 2019). Throughout the rest of the interglacial, several fluctuations are observed between cool and  
506 warm periods, also observed in other southern-European records, with counterparts in Atlantic  $\delta^{18}\text{O}$  records  
507 (Sanchez Goñi *et al.*, 1999; Desprat *et al.*, 2007; Sinopoli *et al.*, 2019). Specifically, these occurred around 115  
508 ka BP (Melisey I), 105 ka BP (St. Germain Ib) and around 87 ka BP (Melisey II), events which are characterised  
509 by colonisation by *Cedrus* and steppic vegetation; these are alternated with temperate phases St. Germain Ia and  
510 Ic, and St Germain II, during which heathlands and deciduous and Mediterranean forests expanded again (Sanchez  
511 Goñi *et al.*, 1999). These events correlate well with the first Dansgaard-Oeschger events (Dansgaard *et al.*, 1993),  
512 DO-25, 24 and 23 described by Masson-Delmotte *et al.* (2005). During this period of variability, our parameters  
513 suggest a progressive rise in precipitation and a slow decline in temperature throughout MIS 5c and the rest of the  
514 interglacial, consistent with climatic reconstructions from the Mediterranean such as Lake Ohrid (Sinopoli *et al.*,  
515 2019) and Lago di Monticchio (Brewer *et al.*, 2008; Sinopoli *et al.*, 2019), as well as records from the Iberian  
516 margin (Sanchez Goñi *et al.*, 1999; Desprat *et al.*, 2007, 2013) and eastern Mediterranean (Leroy *et al.*, 2023),  
517 showing similar trends throughout the Mediterranean. During MIS 5b, a notable drop in PANN is observed around  
518 89–86 ka BP, alongside a moderate rise in TANN. During substage 5a, both parameters decrease further,  
519 consistent with glacial inception of MIS 4 (Fig. 4).  
520

**Table 4 - Summary of results of the pollen-based climatic reconstructions for MIS 6–5**

Interval	Age (ka BP)	Summary
MIS 5a and b cooling	98–80	Drop in precipitation but a smaller rise in temperature around 89–86 ka BP. Parameters show a consistent decline in temperature during MIS 5a consistent with glacial inception moving towards MIS 4.
MIS 5c and d warm events	116–98	Progressive rise in precipitation and a slow decline in temperature during the rest of the interglacial.
Eemian (5e)	128–116	<u>Highest temperatures (~15 °C) and humidity (&gt;600 mm) observed between 127–118 ka BP. Highest temperatures (~15 °C) and humidity (&gt;600 mm) observed between 127–118 ka BP.</u>
MIS 6/5 transition	133–128	Rise in temperature visible in all three methods. Temperature increases from 10–12 °C during the glacial to 12–15 °C at the onset of MIS 5, <u>interrupted briefly by a cooling event during the MIS 6-5 transition.-</u>

521



522  
 523 **Figure 4 – Comparison of the pollen-based quantitative reconstructions from ODP976 for MIS 5, (A)**  
 524 **TANN and (B) PANN (BRT=red solid line; MAT=blue dotted line; WA-PLS=green dashed line), with**  
 525 **other regional and global proxies: (C) Alkenone SSTs from ODP976 (Martrat et al., 2014); (D) Alkenone**  
 526 **SSTs from ODP977 (Martrat et al., 2004); (E) Benthic  $\delta^{18}O$  from MD01-2447 (Desprat et al., 2007); (F)**  
 527 **PANN and (G) TANN from Lake Ohrid derived through MAT and WAPLS (Sinopoli et al., 2019); (H)**  
 528 **Methane ( $CH_4$ ) atmospheric concentrations (Loulergue et al., 2008) and (I)  $CO_2$  atmospheric**  
 529 **concentrations from Antarctic EPICA Dome C ice cores (Nehrbass-Ahles et al., 2020); (J) Atlantic  $\delta^{18}O$**   
 530 **(Voelker et al., 2010); (K) Summer insolation (Laskar et al., 2004); (L) Precession index and (M)**  
 531 **Obliquity curve (Berger and Loutre, 1991). Orange band indicates the period encompassing the climatic**  
 532 **optimum, and the blue bands highlight major millennial-scale climatic events.**  
 533

#### 534 4.2.4 MIS 2–MIS1 (21 ka BP–present day)

535

##### 536 Last Glacial Maximum to HE-1

537 During the Last Glacial Maximum (LGM), around 21–17.5 ka BP, MAT and WA-PLS suggest peculiarly high  
538 TANN and Twin values, ranging between 12–15 °C and 0–10°C, respectively (Fig. 5, Tab. 5). MAT also suggests  
539 drastically higher Tsum values during this period when compared with BRT and WA-PLS. This may once again  
540 be due to the tendency of MAT to overestimate parameters during glacial periods, and is also linked to the inferior  
541 reliability of WA-PLS when compared to the newer method BRT. Combourieu-Nebout *et al.* (2009) also noticed  
542 that their MAT reconstruction for the end of the LGM were higher than expected and closer to present-day levels,  
543 as it appears in the reconstruction methods of this current study. This discrepancy to the possible lack of good  
544 present-day analogues for the cedar/heath pollen association which is dominant in the pollen record at the end of  
545 the LGM (Combourieu-Nebout *et al.*, 2009). In contrast, BRT suggests relatively lower annual and seasonal  
546 temperatures than the other two methods for the LGM period, which is more in line with previous interpretations  
547 made by Combourieu-Nebout *et al.* (2009) on the basis the ODP Site 976 pollen record during this period. In their  
548 study, TANN reconstructions suggested anomalies around -5°C and Twin between -10°C and -15°C. Overall,  
549 precipitation during this period appears to be consistently low across all three methods, with PANN values  
550 remaining below 600 mm~~yr~~, indicating a dry climate in agreement with the previous study on the ODP 976 core  
551 by Combourieu-Nebout *et al.* (2009), as well as the PANN reconstruction for the Padul record (Fig. 5) which  
552 shows a period of low precipitation patterns between 20 and 16 ka BP consistent depleted  $\delta_{DC31}$  values (Camuera  
553 *et al* 2018, 2019, 2022; García-Alix *et al* 2021) and with the study by Davis *et al.* (2024) which shows an overall  
554 decline in mean annual precipitation during the LGM in southern Spai, especially during winter.

555 Between 17 and 15 ka BP, a drastic fall in temperature and precipitation is observed (Fig. 5). This change ~~has~~  
556 ~~been previously attributed to the Oldest Dryas event in the south western Mediterranean, is~~ consistent with  
557 Heinrich Event 1 observed in several other marine and terrestrial records in the Mediterranean (Pons and Reille,  
558 1988; Watts *et al.*, 1996; Combourieu-Nebout *et al.*, 1998, 2002; Allen *et al.*, 2002; Peñalba *et al.*, 1997; Turon  
559 *et al.*, 2003; Naughton *et al.*, 2007; Fletcher and Sanchez Goñi, 2008; Bordon *et al.*, 2009) and has been interpreted  
560 as increased dryness over the Alboran Sea (Combourieu *et al.*, 2009). Our climatic reconstructions suggest  
561 minimum temperatures with Twin values of -5–0°C across all methods, and annual and seasonal precipitation  
562 values similar to the late Pleniglacial with a minimum of ~300 mm shown by the MAT method. This event has a  
563 counterpart in marine records for alkenone-derived SSTs from ODP Site 976 (Martrat *et al.*, 2014) and other  
564 proxies from other Mediterranean sites (Kallel *et al.*, 1997; Rohling *et al.*, 1998; Cacho *et al.*, 2001; Combourieu-  
565 Nebout *et al.*, 2002; Perez Folgado *et al.*, 2003; Camuera *et al.*, 2021). Recent studies from the new Padul record  
566 found a similar pattern in their PANN and TANN reconstructions (Camuera *et al.*, 2022; Rodrigo-Gámiz *et al.*,  
567 2022), suggesting comparable conditions over the Western Mediterranean during this period. This has also been  
568 corroborated by Ludwig *et al.*, (2018) through model simulations of PANN and TANN over the Iberian Peninsula,  
569 which indicated a drastic decline in both parameters during HE-1.

570

##### 571 Lateglacial, beginning of MIS 1

572 A rise in temperature and precipitation is observed between 14.7 and 12.5 ka BP, shown consistently by the three  
573 reconstruction methods (Fig. 5, Tab. 5). Although this is not reflected as strongly by the precipitation parameters,  
574 temperature reconstructions achieved particularly with BRT and WA-PLS show two distinctive periods of  
575 increased warmth centred around 14 and 13 ka BP, attributed respectively to the Bølling and Allerød (B-A) warm  
576 interstadials (Zonneveld, 1996; Combourieu-Nebout *et al.*, 2009; Dormoy *et al.*, 2009; Camuera *et al* 2019, 2021;  
577 Rodrigo-Gamiz *et al.*, 2022). During these periods, Twin values ranging 0–6°C and TANN values of 12–14°C  
578 (Fig. 5, Fig. S5). Precipitation reconstructions suggest similar seasonality to the present-day in the Mediterranean,  
579 with wet winters and dry summers as evidenced by the increase in Pwin but relatively consistent Psum values  
580 (Fig. S5). In comparison with the values reconstructed for the Holocene, temperatures during the B-A remain  
581 slightly subdued (Fig. 5).

582 Between 12.5 and 11.7 ka BP, all three methods indicate a return to colder and drier conditions compared to  
583 the B-A interstadial, related to the Younger Dryas event (YD or H). Twin values during the YD range from  
584 approximately -2°C to 3°C, and TANN values range from 10°C to 13°C. Precipitation is also low across all three  
585 methods, especially in PANN and Pwin, which decline from 700mm and 300m during the B-A to 500mm and  
586 250mm, respectively, during the YD. These results are similar to those reconstructed by Combourieu-Nebout *et*  
587 *al.* (2009) but are slightly higher than the values reconstructed by Dormoy *et al.* (2009). A comparably colder and  
588 more arid climate compared to the B-A in this region was also observed by Camuera *et al.* (2021, 2022) and by  
589 Rodrigo-Gamiz *et al.* (2022), although their values were slightly higher for both parameters perhaps indicating a  
590 slight difference on land within the Iberian Peninsula compared to the conditions in the Alboran Sea at this time.

591 Overall, however, our results show similar timings, trends and amplitudes to what has so far been observed in  
592 regional records from the Mediterranean and Iberian Margin, and global proxies such as CH<sub>4</sub> records from  
593 Antarctica (Jouzel *et al.*, 2007; Nehrbass-Ahles *et al.*, 2020).

594  
595  
596  
597  
598  
599  
600  
601  
602  
603  
604  
605  
606  
607  
608  
609  
610  
611  
612  
613  
614  
615  
616  
617  
618  
619  
620  
621  
622  
623  
624  
625  
626  
627  
628  
629  
630  
631  
632  
633  
634  
635  
636  
637  
638  
639  
640  
641  
642  
643  
644  
645  
646  
647  
648  
649  
650  
651  
652  
653

## Holocene

The transition from the YD to the Holocene at 11.7 ka BP is marked by an increase in temperature and precipitation parameters across all three methods (Fig. 5). TANN reaches similar levels to the present-day, and PANN reaches values above 600mm~~yr~~. Seasonal temperature parameters T<sub>win</sub> and T<sub>sum</sub> show consistently high values with warmer summers and slightly cooler winters. There is a large difference between P<sub>sum</sub> and P<sub>win</sub>, indicating seasonal variation in wetness which may be related to the onset of present-day altitudinal vegetation belts and Mediterranean climate (Combourieu-Nebout *et al.*, 2009). This amelioration is coeval with the increase in SST values from ODP 976 which show warming in marine environments as well as on land at the beginning of the Holocene (Combourieu-Nebout *et al.*, 2002, 2009). This is also shown by alkenone and foraminiferal-based SST records in the nearby core MD 95-2042 (Cacho *et al.*, 2001; Perez Folgado *et al.*, 2003) and the  $\delta^{13}\text{C}$  and  $\delta^{18}\text{O}$  depletion in the MD 90-917 core in the Adriatic Sea (Siani *et al.*, 2013).

Maximum temperatures and precipitation in our reconstructions mark the optimum climatic conditions of the Holocene between 9 and 7 ka BP, consistent with other studies in the Mediterranean (Bar-Matthews *et al.*, 1998; Rossignol-Strick, 1999; Kotthoff *et al.*, 2008; Ramos-Román *et al.* 2018, Marriner *et al.*, 2022), as well as in central Europe (Magny *et al.*, 2002; Martin *et al.*, 2020; Cartapanis *et al.*, 2022; d'Oliveira *et al.*, 2023). As shown by our P<sub>win</sub> and P<sub>sum</sub> values, seasonality is strong during this period—winter precipitation increases significantly (300 to 400 mm~~yr~~) while summer precipitation reaches a minimum (around 50 mm~~yr~~) suggesting strong seasonal contrasts. In the ~~early-Early~~ Holocene, T<sub>win</sub> values range from approximately -0.85 °C to 5.81 °C, while T<sub>sum</sub> values range from 19.15 °C to 23.59 °C. These findings match the reconstructions by Dormoy *et al.* (2009) and Jalut *et al.* (2009) who suggested that in the Western and Central Mediterranean, the climatic optimum of the Holocene was characterised by hot and dry summers and wet and cool winters. This has also been corroborated by more recent climatic reconstructions for Padul (Ramos-Román *et al.*, 2018; Rodrigo-Gamiz *et al.*, 2022). This contrasts with results from Northern and Eastern Europe (Herzshuh *et al.*, 2023), where high year-round moisture and wet summers prevailed (Rossignol-Strick, 1999; Bar-Matthews *et al.*, 1998), consistent with the east-west precipitation gradient observed during the climatic optima of Holocene analogues.

The optimum is interrupted by a short-lived cooling event around 8.4–8.2 ka BP, observed in many other global records (Von Grafenstein *et al.*, 1998; Mayewski *et al.*, 2004; Alley and Agustsdottir, 2005; Pross *et al.*, 2009; Marriner *et al.*, 2022). The reduction in our reconstructed parameters during the 8.2 ka event, particularly the reduction in precipitation although not as much in temperature, can be explained by a reduction in North Atlantic Deep Water (NADW) formation due to increased meltwater from the Laurentide lakes into the North Atlantic (Barber *et al.*, 1999; Ellison *et al.*, 2006).

The reconstructions for PANN indicate a generally decreasing trend for the last 7 ka with good consensus between methods (Fig. 6, Table 6). Meanwhile, TANN shows different amplitudes of change; while BRT and WAPLS indicate an overall upwards trend in temperatures between 6–2 ka BP, MAT suggests a comparatively more drastic decline. Short-term fluctuations previously identified by Combourieu-Nebout *et al.* (2009) and Dormoy *et al.* (2009) are also observed in our record around 6–5, 4.3 and 3.7 ka BP, which roughly correlate with Bond events in the North Atlantic (Bond *et al.*, 1997, 2001).

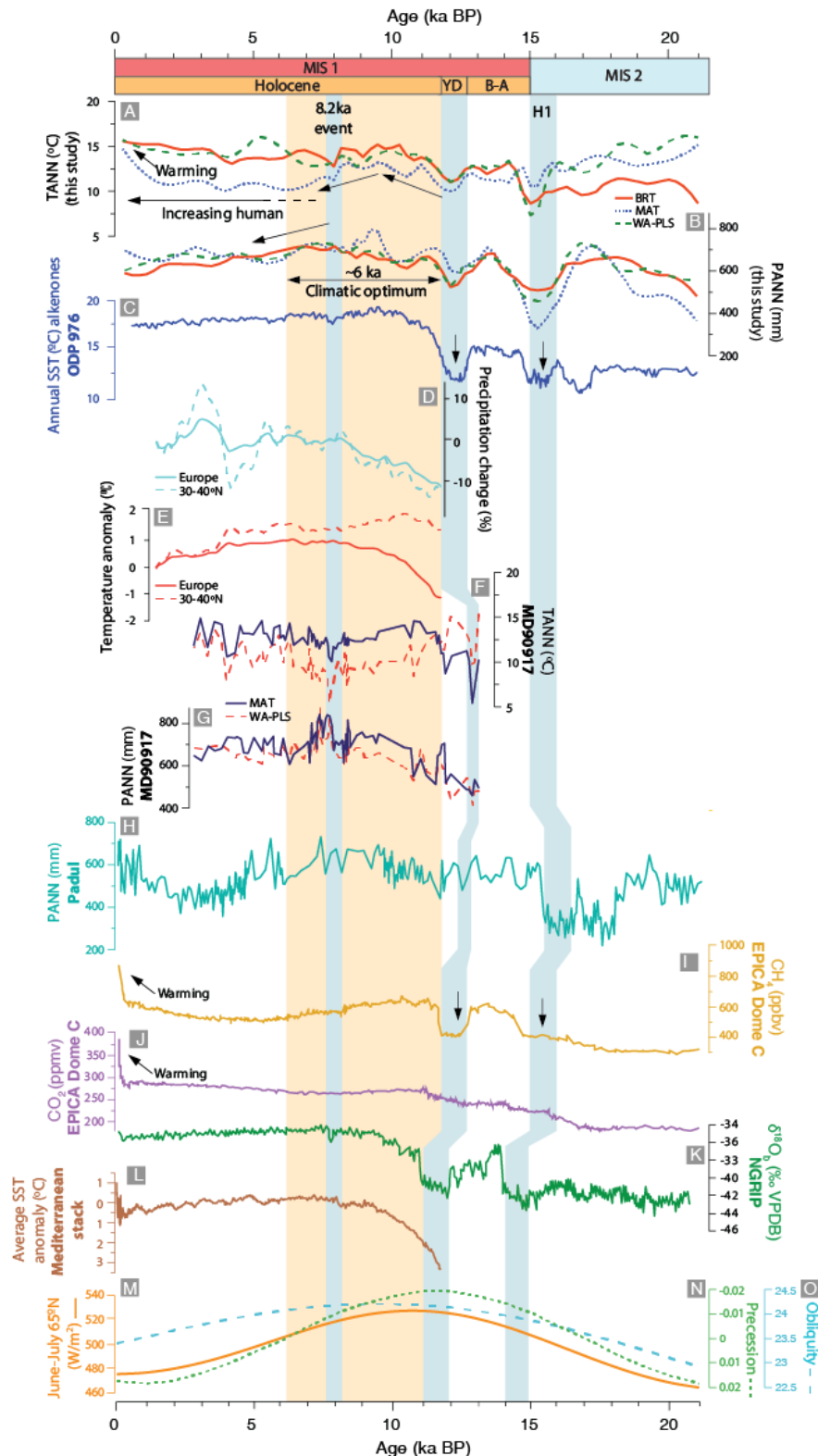
Variability between the results obtained through the different transfer function methods could be attributed to a lack of top samples in our record, which may limit constraints for this period. Differences between our reconstructed records and other Late Holocene pollen-based reconstructions may also reflect site-specific factors. As noted by Combourieu-Nebout *et al.* (2009) and Sassoon *et al.* (2023), the southwestern Mediterranean often shows a less pronounced response to terrestrial drying compared to other Mediterranean regions more influenced by continental conditions. Therefore, our pollen assemblages likely reflect relatively stable local conditions, contributing to the apparent differences in Late Holocene trends between our site and others.

However, the climatic reconstructions from 7 ka onwards must be interpreted cautiously due to the increasing anthropogenic impact during this period and particularly during the last 2 ka. The decline in temperature and precipitation parameters, rather than being a result of progressive cooling, might in fact be an artificial result of increase in semi-desert taxa such as *Artemisia* and reduction in temperate and Mediterranean forest cover (Fig. S1) related to anthropogenic impact in the form of clearing (Combourieu-Nebout *et al.*, 2009). However, although there is an overall warming trend in the last few millennia that could be affected by human activity, the lack of strong pollen signals from anthropogenic taxa (e.g., *Cerealia*-type, *Rumex*, *Plantago lanceolata*, Brassicaceae) suggests that climatic reconstructions are minimally influenced by human impact. ~~¶~~Several other reconstructions for this period in this region (Camuera *et al.*, 2022; Rodrigo-Gamiz *et al.*, 2022; Liu *et al.*, 2023) and in Western Mediterranean (Di Rita *et al.*, 2022) suggest similar findings. Liu *et al.* (2023) proposed that the consistency of climate reconstructions during this period signifies that the changes observed are a reflection of regional climate rather than human activity in the form of agriculture or landscape modification and therefore should be considered as such. On the other hand, during the past 2 ka all methods indicate a substantial rise in temperatures and further decline in precipitation, most likely reflecting at this point the increasing human influence on overall vegetation composition, especially during the ~~p~~Post-Industrial Era (Ruddiman *et al.*, 2016).



**Table 5 - Summary of results of the pollen-based climatic reconstructions for MIS 2–1**

Interval	Age (ka BP)	Summary
<b>Middle-Late Holocene</b>	6.4-present	BRT and WA-PLS indicate an overall upwards trend in temperatures. MAT suggests a comparatively more drastic decline.
<b>Early-Middle Holocene climatic optimum</b>	11.7-6.4	Consistent rise in temperature and precipitation by all three reconstructions. Climatic optimum observed between 11 and 7 ka BP All methods show a temperature rise above 13 °C, peak in precipitation reaching >700 mm. Interrupted by a noteworthy cold and dry event around 8.2 ka BP.
<b>Younger Dryas</b>	12.5-11.7	Return to colder and drier conditions Twin values during YD range from approximately -2°C to 3°C, and TANN values range from 10°C to 13°C. Precipitation is low across all three methods.
<b>Bølling-Allerød</b>	15-12.5	Temperature reconstructions show two distinctive periods of increased warmth. Attributed to Bølling and Allerød warm interstadials. Twin values ranging 0–6°C and TANN values of 12–14°C.
<b>H1-<del>Oldest</del> Dryas</b>	16-15	Drastic fall in temperature and precipitation observed, related to Oldest Dryas (H1) Climatic reconstructions suggest minimum temperatures with Twin values of -5–0°C. Annual and seasonal precipitation values similar to late Pleniglacial (~300 mm shown by MAT method).
<b>MIS 2/1 transition</b>	21.2-15	MAT and WA-PLS show high TANN ranging between 12–15 °C. PANN indicates a large range of 500–800 mm across the three methods. Significant drop in temperature and precipitation during H1; annual temperatures fall to 10–12 °C Precipitation falls below 600 mm (minimum ~300 mm shown by MAT).



656 Figure 5 – Comparison of the pollen-based quantitative reconstructions from ODP976 for MIS 1, (A)  
 657 TANN and (B) PANN (BRT=red solid line; MAT=blue dotted line; WA-PLS=green dashed line), with other  
 658 regional and global proxies: (C) Alkenone SSTs from ODP976 (Martrat et al., 2014); (D) Precipitation  
 659 change (%PANN) and (E) Temperature anomaly (TANN) for Europe derived from WAPLS (Herzschuh  
 660 et al., 2023); (F) PANN and (G) TANN obtained through quantitative pollen-based reconstructions using  
 661 MAT and WAPLS (Combourieu-Nebout et al., 2013); (H) Pollen-based quantitative reconstruction of  
 662 PANN from Padul derived using WAPLS (Camuera et al., 2023); (I) Methane (CH<sub>4</sub>) atmospheric  
 663 concentrations (Loulergue et al., 2008) and (J) CO<sub>2</sub> atmospheric concentrations from Antarctic EPICA

664 Dome C ice cores (Nehrbass-Ahles et al., 2020); (K) NGRIP ice  $\delta^{18}\text{O}$  (North Greenland Ice Core Project  
665 Members, 2004); (L) Average SST anomaly from Mediterranean stack (Marriner et al., 2022); (M) Summer  
666 insolation (Laskar et al., 2004); (N) Precession index and (O) Obliquity curve (Berger and Loutre, 1991).  
667 Orange band indicates the period encompassing the climatic optimum, and the blue bands highlight major  
668 millennial-scale climatic events.

669

#### 670 4.3 Interglacial analogues of the Holocene in the southwestern Mediterranean

671 The climate reconstructions show changes in temperature and precipitation in the Alboran Sea during MIS 19, 11,  
672 5 and the Holocene (Fig. 6), which correlate with climatic changes observed in other regional and global proxies  
673 indicating that overall the reconstructed parameters are reasonable and reliable. Our reconstructions enable a  
674 valuable comparison of the structure and amplitude of millennial-scale climate variation during these periods in  
675 the southwestern Mediterranean.

676 Before delving into a discussion about how MIS 19, 11 and 5 compare climatically and their suitability as  
677 interglacial analogues of the Holocene, the implications of anthropogenic impact over the past 7 ka must be  
678 considered. The extent to which humans have altered the current interglacial and therefore what is considered  
679 'natural' climate change has been subject of substantial debate over the past couple decades (Ruddiman, 2003,  
680 2007; Ruddiman *et al.*, 2016). This is particularly with regard to the origin of the  $\text{CO}_2$  increase by 20 ppmv, as  
681 well as the rise in  $\text{CH}_4$ , during the late Holocene (Yin and Berger, 2015), believed to be a result of the clearing of  
682 forests and agricultures over the past 7 ka BP. Ruddiman (2003, 2007) hypothesised, under what is known as the  
683 early Anthropogenic hypothesis, that the rise in GHGs between 7 ka BP and the Industrial Era is not caused by  
684 natural sources but rather by human intervention in the form of forest clearance, livestock domestication and  
685 flooding of rice paddies (Ruddiman, 2003, 2007; Broecker and Stocker, 2006). The increase in GHGs resulting  
686 from preindustrial farming was enough to cause anomalous warming and prolonged the duration of the  
687 interglacial, whereas based on solar precession the Holocene would be expected to be nearing the end of its natural  
688 course (Yin and Berger *et al.*, 2015). This hypothesis has significant implications on the reliability of comparisons  
689 between MIS 1 and the interglacial analogues, and leads to ~~significantly~~ different conclusions about the natural  
690 trajectory of the Holocene (Tzedakis, 2010). ~~Some authors question the extent of anthropogenic impact on climate~~  
691 ~~during the pre-Industrial period altogether, making the debate over the early Anthropogenic hypothesis somewhat~~  
692 ~~irrelevant.~~ Yin and Berger (2015) highlight that, regardless of the validity of the hypothesis, the 20 ppmv rise in  
693  $\text{CO}_2$  levels during the Late Holocene is modest compared to the dramatic 120 ppmv increase recorded in the 20th  
694 and 21st centuries. This smaller, gradual increase in greenhouse gases during the Late Holocene suggests it was  
695 "natural enough" to serve as a baseline for comparison with earlier interglacial periods.

696 ~~As shown in Figure 6, the MAT method suggests a noticeable warming trend beginning around 2,000 years~~  
697 ~~ago, while both the BRT and WA-PLS methods indicate a slower, more gradual warming over the last 4,000~~  
698 ~~years. This gradual warming trend aligns with the slow rise in greenhouse gases documented in  $\text{CH}_4$  and  $\text{CO}_2$~~   
699 ~~records from EPICA, which show that the highest levels of these gases have only been reached in recent centuries~~  
700 ~~with the onset of the Industrial Era (Jouzel et al., 2007; Pol, 2010; Nehrbass-Ahles et al., 2020). Although human~~  
701 ~~influence on climate is now well-established, the relatively minor contributions of pre-Industrial human activities~~  
702 ~~to GHG levels suggest that the late Holocene remains a suitable reference point for comparing Holocene and~~  
703 ~~Pleistocene interglacials.~~

704 Yin and Berger (2015) state that whether the hypothesis is right or wrong, the increase in  $\text{CO}_2$  by 20 ppmv  
705 during the late Holocene is significantly smaller than the 120 ppmv released during the 20th and 21st centuries,  
706 and therefore the late Holocene can be considered natural enough to enable comparisons with other interglacials.

707 ~~As shown in Figure 6, the MAT method suggests the latest warming trend has occurred over the last 2,000~~  
708 ~~years or so, while BRT and WA-PLS indicate a slower gradual warming over the past 4,000 years. This gradual~~  
709 ~~increase coincides with the gradual increase in GHGs evidenced by the  $\text{CH}_4$  and  $\text{CO}_2$  EPICA records, and these~~  
710 ~~also indicate that it is only in the most recent centuries that peak values are recorded, i.e. since the Industrial Era~~  
711 ~~(Jouzel et al., 2007; Pol, 2010; Nehrbass-Ahles et al., 2020). While the importance of human forcing on climate~~  
712 ~~is recognised, the idea that pre-Industrial activity represented a small enough contribution to GHG emissions is~~  
713 ~~still entertained to allow comparisons between the Holocene and Pleistocene interglacials.~~

714

715

716

717

718

719

720

721

722

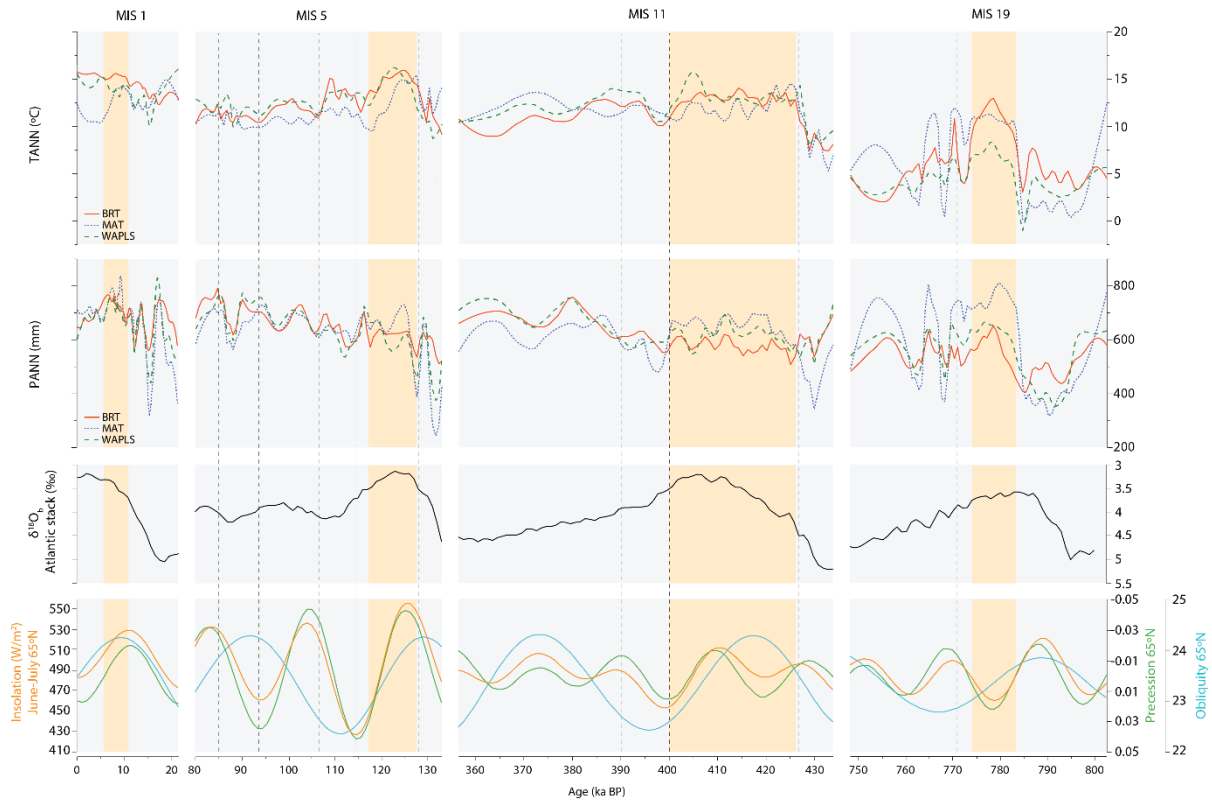


**Figure 6 - Comparison of the quantitative pollen-based reconstructions (TANN and PANN) from ODP976 for MIS 19, 11, 5 and 1, compared with the Atlantic  $\delta^{18}\text{O}$  stack by Voelker et al. (2010) and solar orbital patterns: Summer insolation (Laskar et al., 2004), Precession index and Obliquity curve (Berger and Loutre, 1991). Orange bars indicate the period encompassing the climatic optimum in each interglacial.**

The reconstructions for MIS 19 (Fig. 6) display the highest degree of variability throughout the interglacial, with high-amplitude fluctuations across all three methods between warm and colder substages. Generally, the models show a colder climate than the other interglacials (Fig. 6). These match the findings of other authors and it has been widely recognised that MIS 19 is colder than the interglacials after Termination V (Jouzel *et al.*, 2007; Candy *et al.*, 2014, 2024). When comparing to the EPICA records of MIS 19 to those of the other interglacials, the former shows lower concentrations of GHGs (Pol, 2010; Nehrbass-Ahles *et al.*, 2020), supporting our findings of lower temperatures during this period. A colder climate than present during the climatic optimum of MIS 19c has been observed by Jouzel *et al.* (2007), who stated that this period was characterized by less pronounced warmth than interglacials MIS 5e, 7e, 9c, and 11c. Moreover, a main distinction between MIS 19 and the Holocene is that following the peak of MIS 19, temperatures decline relatively quickly, while during Holocene there is a short-lived decline in temperature, followed by a renewed increase and stabilisation during the Late Holocene (Candy *et al.*, 2014). In general, while the solar forcing of MIS 19 might be more similar to MIS 1, the climatic structure of MIS 19 has little resemblance to MIS 1 when considering the duration of the sustained warmth during the pre-Industrial Holocene, at least in the region around the Alboran Sea.

MIS 11 differs from MIS 19 in the magnitude of temperature variations. It is also much longer than both MIS 19 and MIS 5, and indeed the Holocene, due to its unique antiphasing between insolation and obliquity (Ruddiman *et al.*, 2007; Tzedakis, 2010; Nomade *et al.* 2019; Tzedakis, 2010; Tzedakis *et al.*, 2022). While MIS 11 exhibits warmer temperatures compared to MIS 19, it still shows some degree of variability as observed with its high- and moderate-intensity climatic variability events and climatic fluctuations during the optimum, ~~like the OHO~~. Overall, however, it is significantly more stable than MIS 19. According to Candy *et al.* (2014), if the early Anthropogenic hypothesis is not accepted, MIS 11c is a closer climatic analogue, which means that the current interglacial may last for over 50 ka (Loutre and Berger, 2003; McManus *et al.*, 2003; Candy *et al.*, 2014). If instead this hypothesis is accepted then MIS 19 and MIS 1 become more similar, meaning that the current interglacial would be close to its end if weren't for anthropogenic forcing (Candy *et al.*, 2014; Tzedakis, 2010). The key particularity of accepting MIS 11 as an analogue is that it is the only interglacial with a combination of elevated GHG concentrations and an extended duration. Considering that human activity is affecting the length of the Holocene (Tzedakis *et al.*, 2012; IPCC 2022), this makes MIS 11c an important analogue for how the earth's climatic system functions under extended interglacial conditions (Candy *et al.*, 2014, 2024).

757 Similarly to MIS 11, MIS 5 is characterised by elevated greenhouse gas levels and high sea levels, although  
758 this interglacial has been criticised as an analogue by previous authors due to its high-amplitude fluctuations in  
759 solar forcing. The reconstructions for MIS 5, particularly for MIS 5e (the Eemian), suggest a significantly warmer  
760 climate regime compared with the other interglacial analogues. In terms of duration, MIS 5e is slightly shorter  
761 than MIS 19, but similarly to MIS 11 it exhibits more stable climatic conditions as also corroborated by the lower  
762 variation in SSTs in records from the Western Mediterranean (Martrat *et al.*, 2004). A warmer climate than other  
763 interglacial analogues and the Holocene (specifically, warmer than pre-Industrial levels) has been previously  
764 observed for the Eemian, for example at Padul (Camuera *et al.*, 2019), La Grande Pile (Guiot *et al.* 1989; Brewer  
765 *et al.*, 2008) and in the North Atlantic (Zhuravleva, 2018). On a global average, MIS 5e has been found to be the  
766 warmest interglacial of the past 800 kyr (Tzedakis *et al.*, 2022). When considering the factors together, i.e.  
767 significantly higher temperatures, short duration, and high-amplitude fluctuations in solar forcing, in the case of  
768 our reconstructions MIS 5 appears to be the least suitable analogue when compared with MIS 19 and 11.

769 Our high-resolution climatic reconstructions have demonstrated that in terms of magnitude of warmth,  
770 structure, stability and duration the interglacial analogues of the Holocene are, fundamentally, unique. Although  
771 they all are reoccurring events and share similar patterns such as the abrupt shifts from glacial to interglacial, the  
772 occurrence of climatic optimums soon after the transition, and cold events and Younger-Dryas-like events, the  
773 associated climate feedbacks in each interglacial produce very different climatic histories that are difficult to  
774 compare with the Holocene. As Candy *et al.* (2014) point out, there is no reason to expect that the climate of MIS  
775 1 should naturally follow the pattern of MIS 11 or 19 or indeed MIS 5, despite the close similarities in insolation  
776 forcing, greenhouse gas concentration and temperatures. The study of past interglacials does not offer a direct  
777 blueprint for predicting the future evolution of the Holocene. However, these interglacial analogues are valuable  
778 for exploring the responses of the Earth's processes under different forcing factors which closely resemble the  
779 climate system during the Holocene. What emerges from the climatic reconstructions from ODP Site 976 and the  
780 close comparisons with global and regional records is that this site is extremely sensitive to global changes which  
781 in turn can be used to infer that the southwestern Mediterranean will be highly susceptible to future climate change  
782 and anthropogenic forcing.

## 783 **5. Conclusion**

784 This study has provided ~~valuable~~ insights into the climatic variations during MIS 19, 11, 5 and 1, within the  
785 southwestern Mediterranean region. Through pollen-based climatic reconstructions, we have established  
786 correlations between temperature and precipitation changes in our study area with those observed in other regional  
787 and global proxies, confirming the reliability of our findings. These reconstructions facilitate a comprehensive  
788 comparison of millennial-scale climate variations during these interglacials, shedding light on their unique  
789 climatic structures and amplitudes.

791 The reconstructions highlight a temperature increase from MIS 19 to the Holocene and distinct climatic  
792 characteristics of each interglacial period. MIS 19 exhibits high variability and colder temperatures compared to  
793 subsequent interglacials and the Holocene. Conversely, MIS 11 displays warmer temperatures and greater  
794 stability, offering an insight into interglacials of prolonged duration, crucial when considering that the  
795 anthropogenically-driven warming of the post-Industrial era might be artificially prolonging the current  
796 interglacial. Reconstructions for MIS 5 suggested overall warmer conditions, especially during the Eemian, but  
797 this higher temperature coupled with high-amplitude fluctuations in solar forcing makes it a less suitable Holocene  
798 analogue.

799 While past interglacials do not provide a straightforward blueprint for predicting the future evolution of MIS  
800 1, they offer invaluable insights into Earth's responses to different forcing factors during periods with similar  
801 climatic conditions to the Holocene. The pollen-based climatic reconstructions for MIS 19, 11 and 5 serve as  
802 crucial benchmarks for understanding the sensitivity of the southwestern Mediterranean to global changes, and  
803 underscore the importance of mitigating climate change in this region.

## 804 **Competing interests**

805 At least one of the (co-)authors is a member of the editorial board of *Climate of the Past*.

## 806 **Acknowledgments**

807 We sincerely appreciate the financial support from the ANR project Neandroots (Agence Nationale de la  
808 Recherche, project No. ANR-19-CE27-0011-01), the Muséum national d'Histoire naturelle (MNHN), and the  
809 Centre National de la Recherche Scientifique (CNRS). **ap** Thanks to the ISEM, the Institut des Sciences de  
810 l'Évolution de Montpellier, UMR CNRS 5554 ISEM (Université de Montpellier) for hosting D. Sassoon on  
811 multiple occasions for training on transfer functions. Special thanks to Léa d'Oliveira for the assistance with the  
812 transfer function models and for her help troubleshooting the scripts. This is an ISEM contribution number  
813 ~~XXX~~-(tbe)-2024-285.

814

817 **Supplementary data**

818 Supplementary data to this article can be found online at <https://data.mendeley.com/datasets/m4kzgwk6b9/1>

819

820 **References**

821 [Allen, J. R. M., Watts, W. A., McGee, E., and Huntley, B. Holocene environmental variability – the record from](#)  
822 [Lago Grande di Monticchio, Italy, \*Quatern. Int.\*, 88, 69–80, 2002.](#)

823 [Allen, J.R.M., Huntley, B., Brandt, U., Brauer, A., Hubberten, H., Keller, J., Kraml, M., Mackensen, A., Mingram,](#)  
824 [J., Negendank, J.F.W., Nowaczyk, N.R., Oberhansli, H., Watts, W.A., Wulf, S., Zolitschka, B. Rapid](#)  
825 [environmental changes in southern Europe during the last glacial period. \*Nature\* 400, 740e743. \[https://\]\(https://doi.org/10.1038/23432\)](#)  
826 [doi.org/10.1038/23432, 1999.](#)

827 [Alley, R.B., Agustsdottir, A.M. The 8k event: cause and consequences of a major Holocene abrupt climate change.](#)  
828 [\*Quat Sci Rev.\* 24, 1123–1149, 2005.](#)

829 [Alonso, B., Ercilla, G., Martínez-Ruiz, F., Baraza, J., and Galimont, A. Pliocene-Pleistocene sedimentary facies](#)  
830 [at Site 976: Depositional history in the northwestern Alboran Sea. \*Proc Integr Ocean Drill Program\*,](#)  
831 [161\(1994\), 57–68. <https://doi.org/10.2973/odp.proc.sr.161.206>, 1999.](#)

832 [Ardenghi, N., Mulch, A., Koutsodendris, A., Pross, J., Kahmen, A., and Niedermeyer, E. M. Temperature and](#)  
833 [moisture variability in the eastern Mediterranean region during Marine Isotope Stages 11–10 based on](#)  
834 [biomarker analysis of the Tenaghi Philippon peat deposit. \*Quat Sci Rev.\* 225,](#)  
835 [https://doi.org/10.1016/j.quascirev.2019.105977, 2019.](#)

836 [Azibeiro, L. A., Sierro, F. J., Capotondi, L., Lirer, F., Andersen, N., González-Lanchas, A., Alonso-García, M.,](#)  
837 [Flores, J. A., Cortina, A., Grimalt, J. O., Martrat, B., and Cacho, I. Meltwater flux from northern ice-sheets to](#)  
838 [the Mediterranean during MIS 12. \*Quat Sci Rev.\* 268. <https://doi.org/10.1016/j.quascirev.2021.107108>, 2021.](#)

839 [Bar-Matthews, M., Ayalon, A., and Kaufman, A. \*Middle to late Holocene \(6500 yr period\) paleoclimate in the\*](#)  
840 [Eastern Mediterranean region from stable isotopic composition of speleothems from Soreq Cave, Israel, in:](#)  
841 [Environment and society in times of climate change, edited by: Issar, A. and Brown, N., Kluwer Academic,](#)  
842 [Dordrecht, 203–214, 1998.](#)

843 [Barber, D.C., Dyke, A., Hillaire-Marcel, C., Jennings, A.E., Andrews, J.T., Kerwin, M.W., Bilodeau, G.,](#)  
844 [McNeely, R., Southon, J., Morehead, M.D., and Gagnon, J.M. Forcing of the cold event of 8,200 years ago by](#)  
845 [catastrophic drainage of Laurentide lakes. \*Nature\*, 400\(6742\), pp.344-348, 1999.](#)

846 [Barbero, M., Quézel, P., Rivas-Martínez, S. Contribution à l'étude des groupements forestiers et préforestiers du](#)  
847 [Maroc. \*Phytocoenologia\* 9, pp.311–412, 1981.](#)

848 [Bard, E.: Geochemical and geophysical implications of the radiocarbon calibration, \*Geochim. Cosmochim. Ac.\*,](#)  
849 [62, 2025–2038, 1998.](#)

850 [Bauch, H.A., Erlenkeuser, H., Helmke, J.P., Struck, U. A paleoclimatic evaluation of marine oxygen isotope stage](#)  
851 [11 in the high-northern Atlantic \(Nordic seas\). \*Glob. Planet. Change\*, 24, 27e39,](#)  
852 [https://doi.org/10.1016/S0921-8181\(99\)00067-3, 2000.](#)

853 [Benabid, A. Bref aperçu sur la zonation altitudinale de la végétation climatique du Maroc. \*Ecol. Medit.\*, 8\(1–2\),](#)  
854 [pp.301–315, 1982.](#)

855 [Berger, A., and Loutre, M.F. \*Climate 400,000 years ago, a key to the future?\* In: A.W. Droxler, R.Z. Past](#)  
856 [Interglacials Working Group of Pages, Interglacials of the last 800,000 years. \*R. of Geop.\*, 54, pp.162-219,](#)  
857 [2003.](#)

858 [Berger, A., and Loutre, M.F. An exceptionally Long Interglacial Ahead? \*Science\* 297, 1287–1288,](#)  
859 [doi:10.1226/science.1076120, 2002.](#)

860 [Bertini, A., Toti, F., Marino, M., Ciaranfi, N. Vegetation and climate across the early-middle Pleistocene transition](#)  
861 [at the Montalbano Jonico section \(southern Italy\). \*Quat Int.\* 383, 74-88, 2015.](#)

862 [Blain, H. A., Fagoaga, A., Ruiz-Sánchez, F. J., García-Medrano, P., Ollé, A., and Jiménez-Arenas, J. M. Coping](#)  
863 [with arid environments: A critical threshold for human expansion in Europe at the Marine Isotope Stage 12/11](#)  
864 [transition? The case of the Iberian Peninsula. \*J. Hum. Evol.\* 153. <https://doi.org/10.1016/j.jhevol.2021.102950>,](#)  
865 [2021.](#)

866 [Bond, G., Kromer, B., Beer, J., Muscheler, R., Evans, M.N., Showers, W., Hoffmann, S., Lotti-Bond, R., Hajdas,](#)  
867 [I., and Bonani, G. Persistent solar influence on North Atlantic climate during the Holocene. \*Science\* 278, 1257-](#)  
868 [1266, 2001.](#)

869 [Bond, G., Showers, W., Cheseby, M., Lotti, R., Almasi, P., de Menocal, P., Priore, P., Cullen, H., Hajdas, I., and](#)  
870 [Bonani, G. A pervasive millennial-scale cycle in the North Atlantic Holocene and glacial climates. \*Science\*](#)  
871 [294, 2130-2136, 1997.](#)

872 [Bordon, A., Peyron, O., Lézine, A.-M., Brewer, S., and Fouache, E. Pollen-inferred Late-Glacial and Holocene](#)  
873 [climate in southern Balkans \(Lake Maliq\), \*Quatern. Int.\*, 200, 19–30, 2009.](#)

874 [Brewer, S., Guiot, J., Sánchez-Goni, M.F., and Klotz, S. The climate in Europe during the Eemian: a multi-method](#)  
875 [approach using pollen data. \*Quat Sci Rev.\* 27\(25-26\), pp.2303-2315, 2008.](#)

876 [Brice, R. \*Variabilité Climatique en Mer d'Alboran au cours de la Teminaison V \(MIS 12/11\)\*. Unpublished thesis,](#)  
877 [University of Bordeaux, 2007.](#)

878 [Broecker, W. S., and Stocker, T. L.: The Holocene CO<sub>2</sub> rise. Anthropogenic or natural? \*Eos, Trans. Am. Geophys.\*](#)  
879 [Union, 87\(3\), 27. doi:10.1029/2006EO030002, 2006.](#)

880 [Bulian, F., Kouwenhoven, T. J., Jiménez-Espejo, F. J., Krijgsman, W., Andersen, N., and Sierro, F. J. Impact of](#)  
881 [the Mediterranean-Atlantic connectivity and the late Miocene carbon shift on deep-sea communities in the](#)  
882 [Western Alboran Basin. \*Palaeogeogr. Palaeoclimatol. Palaeoecol.\*, 589,](#)  
883 <https://doi.org/10.1016/j.palaeo.2022.110841>, 2022.

884 [Cacho, I., Grimalt, J. O., Canals, M., Sbaiffi, L., Shackleton, N., Schönfeld, J., and Zahn, R. Variability of the](#)  
885 [western Mediterranean Sea surface temperature during the last 25,000 years and its connection with the](#)  
886 [northern hemisphere climatic changes. \*Paleoceanography\*, 16, 40–52, 2001.](#)

887 [Cacho, I., Grimalt, J.O., Sierro, F.J., Shackleton, N., Canals, M. Evidence for enhanced Mediterranean](#)  
888 [thermohaline circulation during rapid climatic coolings. \*Earth Planet Sci Lett\*, 183, 417–429, 2000.](#)

889 [Camuera, J., Jiménez-Moreno, G., Ramos-Román, M.J., García-Alix, A., Toney, J.L., Anderson, R.S., Jiménez-](#)  
890 [Espejo, F., Bright, J., Webster, C., Yanes, Y., and Carrión, J.S. Vegetation and climate changes during the last](#)  
891 [two glacial-interglacial cycles in the western Mediterranean: a new long pollen record from Padul \(southern](#)  
892 [Iberian Peninsula\). \*Quat Sci Rev\*, 205, pp.86-105, 2019.](#)

893 [Camuera, J., Jiménez-Moreno, G., Ramos-Román, M.J., García-Alix, A., Toney, J.L., Anderson, R.S., Jiménez-](#)  
894 [Espejo, F., Kaufman, D., Bright, J., Webster, C., and Yanes, Y. Orbital-scale environmental and climatic](#)  
895 [changes recorded in a new ~ 200,000-year-long multiproxy sedimentary record from Padul, southern Iberian](#)  
896 [Peninsula. \*Quat Sci Rev\*, 198, pp.91-114, 2018.](#)

897 [Camuera, J., Jiménez-Moreno, G., Ramos-Román, M.J., García-Alix, A., Jiménez-Espejo, F.J., Toney, J.L., and](#)  
898 [Anderson, R.S. Chronological control and centennial-scale climatic subdivisions of the Last Glacial](#)  
899 [Termination in the western Mediterranean region. \*Quat Sci Rev\*, 255, p.106814, 2021.](#)

900 [Camuera, J., Ramos-Román, M.J., Jiménez-Moreno, G., García-Alix, A., Ilvonen, L., Ruha, L., Gil-Romera, G.,](#)  
901 [González-Sampériz, P., and Seppä, H. Past 200 kyr hydroclimate variability in the western Mediterranean and](#)  
902 [its connection to the African Humid Periods. \*Sci. Rep.\*, 12\(1\), p.9050, 2022.](#)

903 [Candy, I., Schreve, D. C., Sherriff, J., and Tye, G. J. Marine Isotope Stage 11: Palaeoclimates, palaeoenvironments](#)  
904 [and its role as an analogue for the current interglacial. \*Earth-Sci Rev\*, 128, 18–51,](#)  
905 <https://doi.org/10.1016/j.earscirev.2013.09.006>, 2014.

906 [Candy, I., Oliveira, D., Parkes, D., Sherriff, J., and Thornalley, D. Marine Isotope Stage 11c in Europe: Recent](#)  
907 [advances in marine–terrestrial correlations and their implications for interglacial stratigraphy—a review.](#)  
908 [Boreas, 2024.](#)

909 [Cartapanis, O., Jonkers, L., Moffa-Sanchez, P., Jaccard, S.L., and de Vernal, A. Complex spatio-temporal](#)  
910 [structure of the Holocene Thermal Maximum. \*Nat. Commun.\*, 13\(1\), p.5662, 2022.](#)

911 [Cheddadi, R., Lamb, H.F., Guiot, J., and van der Kaars, S. Holocene climatic change in Morocco: a quantitative](#)  
912 [reconstruction from pollen data. \*Climate dynamics\*, 14, 883-890, 1998.](#)

913 [Chevalier, M., Davis, B. A. S., Heiri, O., Seppä, H., Chase, B. M., Gajewski, K., Lacourse, T., Telford, R. J.,](#)  
914 [Finsinger, W., Guiot, J., Kühl, N., Maezumi, S. Y., Tipton, J. R., Carter, V. A., Brussel, T., Phelps, L. N.,](#)  
915 [Dawson, A., Zanon, M., Vallé, F., ... Kupriyanov, D. Pollen-based climate reconstruction techniques for late](#)  
916 [Quaternary studies. \*Earth-Sci Rev\*, 210, 103384. https://doi.org/10.1016/j.earscirev.2020.103384, 2020.](#)

917 [Combourieu-Nebout, N., Bertini, A., Russo-Ermolli, E., Peyron, O., Klotz, S., Montade, V., Fauquette, S., Allen,](#)  
918 [J., Fusco, F., Goring, S., Huntley, B., Joannin, S., Lebreton, V., Magri, D., Martinetto, E., Orain, R., and](#)  
919 [Sadori, L. Climate changes in the central Mediterranean and Italian vegetation dynamics since the Pliocene.](#)  
920 [Rev. Palaeobot. Palynol. 218, 127-147, 2015.](#)

921 [Combourieu-Nebout, N., Londeix, L., Baudin, F., Turon, J.-L., von Grafenstein, R., and Zahn, R. \*Quaternary\*](#)  
922 [marine and continental paleoenvironments in the western Mediterranean \(Site 976, Alboran Sea\):](#)  
923 [palynological evidence, in: Proc. ODP Sci. Results, 161: College Station, TX \(Ocean Drilling Program\), edited](#)  
924 [by: Zahn, R., Comas, M. C., and Klaus, A., pp.457–468, 1999.](#)

925 [Combourieu-Nebout, N., Paterne, M., Turon, J. L. and Siani, G. A high-resolution record of the last deglaciation](#)  
926 [in the Central Mediterranean Sea: Palaeovegetation and Palaeohydrological evolution, \*Quat Sci Rev\*, 17, 303–](#)  
927 [317, 1998.](#)

928 [Combourieu-Nebout, N., Peyron, O., Bout-Roumazeille, V., Goring, S., Dormoy, I., Joannin, S., Sadori, L., Siani,](#)  
929 [G., and Magny, M. Holocene vegetation and climate changes in central Mediterranean inferred from a high-](#)  
930 [resolution marine pollen record \(Adriatic Sea\). \*Clim. Past\* 9, 2023–2042, 2013.](#)

931 [Combourieu-Nebout, N., Peyron, O., Dormoy, I., Desprat, S., Beaudouin, C., Kotthoff, U., and Marret, F. Rapid](#)  
932 [climatic variability in the west Mediterranean during the last 25,000 years from high resolution pollen data.](#)  
933 [Clim. Past, 5\(3\), 503–521. https://doi.org/10.5194/cp-5-503-2009, 2009.](#)

934 [Combourieu-Nebout, N., Turon, J. L., Zahn, R., Capotondi, L., Londeix, L., and Pahnke, K. Enhanced aridity and](#)  
935 [atmospheric high-pressure stability over the western Mediterranean during the North Atlantic cold events of](#)

936 [the past 50 k.y. \*Geology\*, 30\(10\), 863–866. \[https://doi.org/10.1130/0091-7613\\(2002\\)030<0863:EAAAHP>2.0.CO;2\]\(https://doi.org/10.1130/0091-7613\(2002\)030<0863:EAAAHP>2.0.CO;2\), 2002.](#)

937

938 [d'Oliveira, L., Dugerdil, L., Ménot, G., Evin, A., Muller, S.D., Ansanay-Alex, S., Azuara, J., Bonnet, C., Bremond, L., Shah, M., and Peyron, O. Reconstructing 15,000 years of southern France temperatures from coupled pollen and molecular \(brGDGT\) markers \(Canroute, Massif Central\). \*Clim. Past\* 19, 2127–2156. <https://doi.org/10.5194/cp-19-2127-2023>, 2023.](#)

939

940

941

942 [Davis, B. A., Fasel, M., Kaplan, J. O., Russo, E., & Burke, A. The climate and vegetation of Europe, northern Africa, and the Middle East during the Last Glacial Maximum \(21 000 yr BP\) based on pollen data. \*Clim. Past\*, 20\(9\), 1939-1988, 2024.](#)

943

944

945 [Dansgaard, W., Johnsen, S.J., Clausen, H.B., Dahl-Jensen, D., Gundestrup, N.S., Hammer, C.U., Hvidberg, C.S., Steffensen, J.P., Sveinbjörnsdóttir, A.E., Jouzel, J., Bond, G. Evidence for general instability of past climate from a 250-kyr ice-core record. \*Nature\* 364, 218-220, 1993.](#)

946

947

948 [De'ath, G. Boosted trees for ecological modeling and prediction. \*Ecology\* 88, 243-251. \[https://doi.org/10.1890/0012-9658\\(2007\\)88\\[243:BTfEMA\\]2.0.CO;2\]\(https://doi.org/10.1890/0012-9658\(2007\)88\[243:BTfEMA\]2.0.CO;2\), 2007.](#)

949

950 [Desprat, S., Combourieu-Nebout, N., Essallami, L., Sicre, M.A., Dormoy, I., Peyron, O., Siani, G., Bout Roumazeilles, V., Turon, J.L. Deglacial and Holocene vegetation and climatic changes at the southernmost tip of the Central Mediterranean from a direct land–sea correlation. \*Clim. Past\* 9, 767-787, 2013.](#)

951

952

953 [Desprat, S., Sánchez Goñi, M. F., Naughton, F., Turon, J. L., Duprat, J., Malaizé, B., Cortijo, E., Peypouquet, J. P. Climate variability of the last five isotopic interglacials: Direct land-sea-ice correlation from the multiproxy analysis of North-Western Iberian margin deep-sea cores. \*Developments in Quaternary Science\*, 7\(C\), pp.375-386. \[https://doi.org/10.1016/S1571-0866\\(07\\)80050-9\]\(https://doi.org/10.1016/S1571-0866\(07\)80050-9\), 2007.](#)

954

955

956

957 [Desprat, S., Sánchez Goñi, M. F., Turon, J. L., McManus, J. F., Loutre, M. F., Duprat, J., Malaizé, B., Peyron, O., Peypouquet, J. P. Is vegetation responsible for glacial inception during periods of muted insolation changes? \*Quat Sci Rev\*, 24\(12-13\), pp.1361-1374. <https://doi.org/10.1016/j.quascirev.2005.01.005>, 2005.](#)

958

959

960 [Di Rita, F., Ghilardi, M., Fagel, N., Vacchi, M., Warichet, F., Delanghe, D., Sicurani, J., Martinet, L., Robresco, S. Natural and anthropogenic dynamics of the coastal environment in northwestern Corsica \(western Mediterranean\) over the past six millennia. \*Quat Sci Rev\*, 278, p.107372, 2022.](#)

961

962

963 [Donders, T., Panagiotopoulos, K., Koutsodendris, A., Bertini, A., Mercuri, A.M., Masi, A., Combourieu-Nebout, N., Joannin, S., Kouli, K., Kousis, I., Peyron, O. 1.36 million years of Mediterranean forest refugium dynamics in response to glacial–interglacial cycle strength. \*PNAS\*, 118\(34\), p.e2026111118, 2021.](#)

964

965

966 [Dormoy, I., Peyron, O., Combourieu-Nebout, N., Goring, S., Kotthoff, U., Magny, M., Pross, J. Terrestrial climate variability and seasonality changes in the Mediterranean region between 15,000 and 4,000 years BP deduced from marine pollen records. \*Clim. Past\* 5, 615-632. <https://doi.org/10.5194/cp-5-615-2009>, 2009.](#)

967

968

969 [Dugerdil, L., Joannin, S., Peyron, O., Jouffroy-Bapicot, I., Vannièrre, B., Boldgiv, B., Unkelbach, J., Behling, H., Ménot, G. Climate reconstructions based on GDGT and pollen surface datasets from Mongolia and Baikal area: calibrations and applicability to extremely cold–dry environments over the Late Holocene. \*Clim. Past\*, 17\(3\), pp.1199-1226, 2021.](#)

970

971

972

973 [Ellison, C.R., Chapman, M.R., Hall, I.R. Surface and deep ocean interactions during the cold climate event 8,200 years ago. \*Science\*, 312\(5782\), pp.1929-1932, 2006.](#)

974

975 [Elith, J., Leathwick, J. R., Hastie, T. A working guide to boosted regression trees. \*J. Anim. Ecol.\*, 77\(4\), 802-813, 2008.](#)

976

977 [Fletcher W., Sanchez Goñi M.F. Orbital- and sub-orbital-scale climate impacts on vegetation of the western Mediterranean basin over the last 48,000 yr. \*Quat. Res.\*, 70\(3\), 451-464, 2008.](#)

978

979 [García-Alix, A., Camuera, J., Ramos-Román, M.J., Toney, J.L., Sachse, D., Schefuß, E., Jiménez-Moreno, G., Jiménez-Espejo, F.J., López-Avilés, A., Anderson, R.S., Yanes, Y. Paleohydrological dynamics in the Western Mediterranean during the last glacial cycle. \*Glob. Planet. Change\*, 202, p.103527, 2021.](#)

980

981

982 [Giaccio, B., Regattieri, E., Zanchetta, G., Nomade, S., Renne, P.R., Sprain, C.J., Drysdale, R.N., Tzedakis, P.C., Messina, P., Scardia, G., Sposato, A. Duration and dynamics of the best orbital analogue to the present interglacial. \*Geology\*, 43\(7\), 603-606, 2015.](#)

983

984

985 [Giaccio, B., Leicher, N., Mannella, G., Monaco, L., Regattieri, E., Wagner, B., Zanchetta, G., Gaeta, M., Marra, F., Nomade, S., Palladino, D.M., Pereira, A., Scheidt, S., Sottili, G., Wonik, T., Wulf, S., Zeeden, C., Ariztegui, D., Cavinato, G.P., Dean, J.R., Florindo, F., Leng, M.J., Macri, P., Niespolo, E., Renne, P.R., Rolf, C., Sadori, L., Thomas, C. & Tzedakis, P.C. Extending the tephra and palaeoenvironmental record of the Central Mediterranean back to 430 ka: A new core from Fucino Basin, central Italy. \*Quaternary Science Reviews\*, vol. 225, 106003, 2019.](#)

986

987

988

989

990

991 [Girone, A., Maiorano, P., Marino, M., Kucera, M. Calcareous plankton response to orbital and millennial-scale climate changes across the Middle Pleistocene in the western Mediterranean. \*Palaeogeogr. Palaeoclimatol. Palaeoecol.\*, 392, 105-116. <https://doi.org/10.1016/j.palaeo.2013.09.005>, 2013.](#)

992

993

994 [Gonzalez-Donoso, J.M., Serrano, F., Linares, D. Sea surface temperature during the Quaternary at ODP Sites 976 and 975 \(western Mediterranean\). \*Palaeogeogr. Palaeoclimatol. Palaeoecol.\* 162, 17-44, 2000.](#)

995



996 [Grafenstein, U., Erlenkeuser, H., Brauer, A., Jouzel, J., Johnsen, S.J. A mid-European decadal isotope-climate](#)  
 997 [record from 15,500 to 5000 years BP. \*Science\*, 284\(5420\), 1654-1657, 1999.](#)  
 998 [Grieser, J., Giommes, R., Bernardi, M. New LocClim – the Local Climate Estimator of FAO, \*Geophysical\*](#)  
 999 [research abstracts](#), 8, 08305, 2006.  
 1000 [Guiot, J., Cramer, W. Climate Change: The 2015 Paris Agreement Thresholds and Mediterranean Basin](#)  
 1001 [Ecosystems. \*Science\*, 354, 465-468, 2016.](#)  
 1002 [Guiot, J. Methodology of the last climatic reconstruction in France from pollen data. \*Palaeogeogr.\*](#)  
 1003 [Palaeoclimatol. Palaeoecol.](#) 80, 49-69, 1990.  
 1004 [Guiot, J., Pons, A., de Beaulieu, J.-L., Reille, M. A 140,000 year continental climate reconstruction from two](#)  
 1005 [European pollen records. \*Nature\* 338, 309-313, 1989.](#)  
 1006 [Herzschuh, U., Böhmer, T., Chevalier, M., Hébert, R., Dallmeyer, A., Li, C., Cao, X., Peyron, O., Nazarova, L.,](#)  
 1007 [Novenko, E.Y., Park, J. Regional pollen-based Holocene temperature and precipitation patterns depart from](#)  
 1008 [the Northern Hemisphere mean trends. \*Clim. Past\*, 19\(7\), 1481-1506, 2023.](#)  
 1009 [Hes, G., Sanchez-Goñi, M.F., and Bouttes, N. Impact of terrestrial biosphere on the atmospheric](#)  
 1010 [CO2-concentration across Termination V. \*Clim. Past\*, 18\(6\), 1429–1451, 2022. \[https://doi.org/10.5194/cp-18-\]\(https://doi.org/10.5194/cp-18-1429-2022\)](#)  
 1011 [1429-2022](#)  
 1012 [Heusser, L. E. and Balsam, W. L. Pollen distribution in the north-east Pacific Ocean. \*Quat. Res.\* 7, 45–62, 1977.](#)  
 1013 [Hodell, D. A., Channeil, J. E. T., Curtis, J. H., Romero, O. E., and Röhl, U. Onset of “Hudson Strait” Heinrich](#)  
 1014 [events in the eastern North Atlantic at the end of the middle Pleistocene transition \(~640 ka\)?](#)  
 1015 [Palaeoceanography 23\(4\), 1–16, 2008. <https://doi.org/10.1029/2008PA001591>](#)  
 1016 [Huntley, B. Europe. \*Vegetation history\* \(ed. by B. Huntley and T. Webb III\), pp. 341–383. Kluwer Academic](#)  
 1017 [Publishers, Dordrecht, 1988.](#)  
 1018 [IPCC. \*Climate Change: Impacts, Adaptation and Vulnerability\*. Accessible at:](#)  
 1019 <https://www.ipcc.ch/report/ar6/wg2/>, 2022.  
 1020 [Jalut, G., Dedoubat, J. J., Fontugne, M., and Otto, T. Holocene circum-Mediterranean vegetation changes: Climate](#)  
 1021 [forcing and human impact. \*Quatern. Int.\* 200, 4–18, 2009.](#)  
 1022 [Joannin, S., Brugiapaglia, E., De Beaulieu, J.L., Bernardo, L., Magny, M., Peyron, O., Goring, S., and Vannièrè,](#)  
 1023 [B. Pollen-based reconstruction of Holocene vegetation and climate in southern Italy: the case of Lago](#)  
 1024 [Trifoglietti. \*Clim. Past\* 8\(6\), 1973-1996, 2012.](#)  
 1025 [Jouzel, J., Masson-Delmotte, V., Cattani, O., Dreyfus, G., Falourd, S., Hoffmann, G., Minster, B., Nouet, J.,](#)  
 1026 [Barnola, J.M., Chappellaz, J., Fischer, H., Gallet, J.C., Johnsen, S., Leuenberger, M., Loulergue, L., Luethi,](#)  
 1027 [D., Oerter, H., Parrenin, F., Raisbeck, G., Raynaud, D., Schilt, A., Schwander, J., Selmo, E., Souchez, R.,](#)  
 1028 [Spahni, R., Stauffer, B., Steffensen, J.P., Stenni, B., Stocker, T.F., Tison, J.L., Werner, M., Wolff, E.W. Orbital](#)  
 1029 [and millennial Antarctic climate variability over the past 800,000 years. \*Science\* 317\(5839\), 793-796, 2007.](#)  
 1030 [Juggins, S. Package “rioja” – Analysis of Quaternary Science Data. \*The Comprehensive R Archive Network\*, 2020.](#)  
 1031 [Kaenel, E., Siesser, W.G., Murat, A. Pleistocene calcareous nannofossil biostratigraphy and the western](#)  
 1032 [Mediterranean sapropels, Sites 974 to 977 and 979. In: Zhan, R., Comas, M.C., Klaus, A. \(Eds.\), \*Proc. ODP\*](#)  
 1033 [Sci. Results. 161. College Station, Texas, 15–183, 1999.](#)  
 1034 [Kallel, N., Paterne, M., Labeyrie, L., Duplessy, J.-C., and Arnold, M. Temperature and salinity records of the](#)  
 1035 [Tyrrhenian Sea during the last 18,000 years. \*Palaeogeogr. Palaeoclimatol. Palaeoecol.\* 135, 97–108, 1997.](#)  
 1036 [Kandiano, E.S., Bauch, H.A., Fahl, K., Helmke, J.P., Röhl, U., Pérez-Folgado, M., and Cacho, I. The meridional](#)  
 1037 [temperature gradient in the eastern North Atlantic during MIS 11 and its link to the ocean–atmosphere system.](#)  
 1038 [Palaeogeogr. Palaeoclimatol. Palaeoecol.](#) 333, 24–39, 2012.  
 1039 [Kelly, M.R. The Middle Pleistocene of North Birmingham. \*Philos. Trans. R. Soc. Lond.\* B247, 533–592, 1964.](#)  
 1040 [Kotthoff, U., Pross, J., Müller, U.C., Peyron, O., Schmiedl, G., Schulz, H., and Bordon, A. Climate dynamics in](#)  
 1041 [the borderlands of the Aegean Sea during formation of sapropel S1 deduced from a marine pollen record.](#)  
 1042 [Quat. Sci. Rev. 27, 832–845, 2008. <https://doi.org/10.1016/j.quascirev.2007.12.001>](#)  
 1043 [Kousis, I., Koutsodendris, A., Peyron, O., Leicher, N., Francke, A., Wagner, B., Giaccio, B., Knipping, M., and](#)  
 1044 [Pross, J. Centennial-scale vegetation dynamics and climate variability in SE Europe during Marine Isotope](#)  
 1045 [Stage 11 based on a pollen record from Lake Ohrid. \*Quat. Sci. Rev.\* 190, 20–38, 2018.](#)  
 1046 [https://doi.org/10.1016/j.quascirev.2018.04.014](#)  
 1047 [Koutsodendris, A., Brauer, A., Pälke, H., Müller, U.C., Dulski, P., Lotter, A.F., and Pross, J. Sub-decadal to](#)  
 1048 [decadal-scale climate cyclicity during the Holsteinian interglacial \(MIS 11\) evidenced in annually laminated](#)  
 1049 [sediments. \*Clim. Past\* 7, 987–999, 2011.](#)  
 1050 [Koutsodendris, A., Pross, J., Müller, U. C., Brauer, A., Fletcher, W. J., Köhl, N., Kirilova, E., Verhagen, F. T. M.,](#)  
 1051 [Lücke, A., and Lotter, A. F. A short-term climate oscillation during the Holsteinian interglacial \(MIS 11c\): An](#)  
 1052 [analogy to the 8.2ka climatic event? \*Glob. Planet. Change\* 92–93, 224–235, 2012.](#)  
 1053 [https://doi.org/10.1016/j.gloplacha.2012.05.011](#)

1054 [Koutsodendris, A., Kousis, I., Peyron, O., Wagner, B., and Pross, J. The Marine Isotope Stage 12 pollen record](#)  
1055 [from Lake Ohrid \(SE Europe\): Investigating short-term climate change under extreme glacial conditions. \*Quat.\*](#)  
1056 [\*Sci. Rev.\* 221, 105873, 2019.](#)

1057 [Koutsodendris, A., Dakos, V., Fletcher, W.J., Knipping, M., Kotthoff, U., Milner, A.M., Müller, U.C., Kaboth-](#)  
1058 [Bahr, S., Kern, O.A., Kolb, L., and Vakhrameeva, P. Atmospheric CO<sub>2</sub> forcing on Mediterranean biomes](#)  
1059 [during the past 500 kyrs. \*Nat. Commun.\* 14\(1\), 1664, 2023.](#)

1060 [Kukla, G. Continental records of MIS 11. \*Washington DC American Geophysical Union Geophysical Monograph\*](#)  
1061 [Series 137, 207-211, 2003.](#)

1062 [Kukla, G., McManus, J. F., Rousseau, D.-D., and Chuine, I. How long and how stable was the last interglacial?](#)  
1063 [\*Quat. Sci. Rev.\* 16, 605–612, 1997.](#)

1064 [Leroy, S.A.G., Henry, P., Peyron, O., Rostek, F., Kende, J., Bard, E., and Tachikawa, K. Palynology,](#)  
1065 [palaeoclimate and chronology from the Saalian Glacial to Saint-Germain II interstadial from two long cores](#)  
1066 [at the limit between the Mediterranean and Euxinian regions. \*Quat. Sci. Rev.\* 311, 108145, 2023.](#)

1067 [Lionello, P., Scarascia, L. The relation between climate change in the Mediterranean region and global warming.](#)  
1068 [\*Reg. Environ. Chang.\* 18, 1481–1493, 2018.](#)

1069 [Liu, M., Shen, Y., González-Sampériz, P., Gil-Romera, G., Ter Braak, C.J., Prentice, I.C. and Harrison, S.P.](#)  
1070 [Holocene climates of the Iberian Peninsula: pollen-based reconstructions of changes in the west-east gradient](#)  
1071 [of temperature and moisture. \*Clim. Past\* 19, 803–834, 2023. <https://doi.org/10.5194/cp-19-803-2023>](#)

1072 [Loulergue, L., Schilt, A., Spahni, R., Masson-Delmotte, V., Blunier, T., Lemieux, B., Barnola, J.M., Raynaud,](#)  
1073 [D., Stocker, T.F., Chappellaz, J. Orbital and millennial-scale features of atmospheric CH<sub>4</sub> over the past](#)  
1074 [800,000 years. \*Nature\* 453, 383-386, 2008.](#)

1075 [Loutre, M.F., Berger, A. Marine Isotope Stage 11 as an analogue for the present interglacial. \*Glob. Planet. Change\*](#)  
1076 [36, 209-217, 2003. \[https://doi.org/10.1016/S0921-8181\\(02\\)00186-8\]\(https://doi.org/10.1016/S0921-8181\(02\)00186-8\)](#)

1077 [Ludwig, P., Shao, Y., Kehl, M. and Weniger, G.C. The Last Glacial Maximum and Heinrich event I on the Iberian](#)  
1078 [Peninsula: A regional climate modelling study for understanding human settlement patterns. \*Glob. Planet.\*](#)  
1079 [Change 170, 34-47, 2018.](#)

1080 [Magny, M., Miramont, C. and Sivan, O. Assessment of the impact of climate and anthropogenic factors on](#)  
1081 [Holocene Mediterranean vegetation in Europe on the basis of palaeohydrological records. \*Palaeogeogr.\*](#)  
1082 [Palaeoclimatol. Palaeoecol. 186\(1-2\), 47-59, 2002.](#)

1083 [Maiorano, P., Bertini, A., Capolongo, D., Eramo, G., Gallicchio, S., Girone, A., Pinto, D., Toti, F., Ventruti, G.,](#)  
1084 [Marino, M. Climate signatures through the marine isotope stage 19 in the Montalbano Jonico section \(southern](#)  
1085 [Italy\): a land-sea perspective. \*Palaeogeogr. Palaeoclimatol. Palaeoecol.\* 461, 341-361, 2016.](#)

1086 [Marino, M., Girone, A., Maiorano, P., Di Renzo, R., Piscitelli, A., and Flores, J. A. Calcareous plankton and the](#)  
1087 [mid-Brunhes climate variability in the Alboran Sea \(ODP Site 977\). \*Palaeogeogr. Palaeoclimatol.\*](#)  
1088 [Palaeoecol. 508, 91–106, 2018. <https://doi.org/10.1016/j.palaeo.2018.07.023>](#)

1089 [Marriner, N., Kaniewski, D., Pourkerman, M. and Devillers, B. Anthropocene tipping point reverses long-term](#)  
1090 [Holocene cooling of the Mediterranean Sea: A meta-analysis of the basin's Sea Surface Temperature records.](#)  
1091 [\*Earth-Sci Rev\* 227, 103986, 2022.](#)

1092 [Martrat, B., Grimalt, J.O., Lopez-Martinez, C., Cacho, I., Sierro, F.J., Flores, J.A., Zahn, R., Canals, M., Curtis,](#)  
1093 [J.H. and Hodell, D.A. Abrupt temperature changes in the Western Mediterranean over the past 250,000 years.](#)  
1094 [\*Science\* 306\(5702\), 1762-1765, 2004.](#)

1095 [Martin, C., Menot, G., Thouveny, N., Peyron, O., Andrieu-Ponel, V., Montade, V., Davtian, N., Reille, M. and](#)  
1096 [Bard, E. Early Holocene thermal maximum recorded by branched tetraethers and pollen in Western Europe](#)  
1097 [\(Massif Central, France\). \*Quat. Sci. Rev.\* 228, 106109, 2020.](#)

1098 [Martrat, B., Jimenez-Amat, P., Zahn, R. and Grimalt, J.O. Similarities and dissimilarities between the last two](#)  
1099 [deglaciations and interglaciations in the North Atlantic region. \*Quat. Sci. Rev.\* 99, 122-134, 2014.](#)

1100 [Masson-Delmotte, V., Landais, A., Combourieu-Nebout, N., von Grafenstein, U., Jouzel, J., Caillon, N.,](#)  
1101 [Chappellaz, J., Dahl-Jensen, D., Johnsen, S.J. and Stenni, B. Variabilité climatique rapide pendant les périodes](#)  
1102 [chaudes et froides aux pôles et en Europe. \*Comptes rendus. Géoscience\* 337\(10-11\), 935-946, 2005.](#)

1103 [Mauri, A., Davis, B., Collins, P. M., and Kaplan, J. The climate of Europe during the Holocene: A gridded pollen-](#)  
1104 [based reconstruction and its multi-proxy evaluation. \*Quat. Sci. Rev.\* 112, 109–127, 2015.](#)

1105 [Mayewski, P.A., Rohling, E.E., Stager, J.C., Karlen, W., Maasch, K.A., Meeker, L.D., Meyerson, E.A., Gasse,](#)  
1106 [F., van Kreveld, S., Holmgren, K., Lee-Thorp, J., Rosqvist, G., Rack, F., Staubwasser, M., Schneider, R.R.,](#)  
1107 [Steig, E.J. Holocene climate variability. \*Quat. Res.\* 62, 243-255, 2004.](#)

1108 [McManus, J.F., Oppo, D.W., Cullen, J.L. and Healey, S. Marine isotope stage 11 \(MIS 11\): analog for Holocene](#)  
1109 [and future climate? \*Washington DC American Geophysical Union Geophysical Monograph Series\* 137, 69-](#)  
1110 [85, 2003.](#)

1111 [MedECC. Climate and Environmental Change in the Mediterranean Basin – Current Situation and Risks for the](#)  
1112 [Future. In: \*Climate and Environmental Change in the Mediterranean Basin – Current Situation and Risks for\*](#)

1113 [the Future. First Mediterranean Assessment Report](#), edited by W. Cramer, J. Guiot and K. Marini, 60.  
1114 [Marseille: Union for the Mediterranean, 2020.](#)  
1115 [Monaco, L., Palladino, D.M., Gaeta, M., Marra, F., Sottili, G., Leicher, N., Mannella, G., Nomade, S., Pereira,](#)  
1116 [A., Regattieri, E., Wagner, B., Zanchetta, G., Albert, P.G., Arienzo, I., D'Antonio, M., Petrosino, P., Manning,](#)  
1117 [C.J. & Giaccio, B. Mediterranean tephrostratigraphy and peri-Tyrrhenian explosive activity reevaluated in light](#)  
1118 [of the 430-365 ka record from Fucino Basin \(central Italy\). \*Earth-Science Reviews\*, vol. 220, 103706, 2021.](#)  
1119 [Moncel, M. H., Arzarello, M., and Peretto, C. The Holsiteinian period in Europe \(MIS 11-9\). \*Quat. Int.\* 409, 1–8,](#)  
1120 [2016.](#)  
1121 [Moreno, A., Cacho, I., Canals, M., Grimalt, J.O., Sanchez Vidal, A. Millennial-scale variability in the productivity](#)  
1122 [signal from the Alboran Sea record, western Mediterranean Sea. \*Palaeogeogr. Palaeoclimatol. Palaeoecol.\*](#)  
1123 [211\(3-4\), 205-219, 2004.](#)  
1124 [Naughton, F., Sánchez Goñi, M. F., Desprat, S., Turon, J. L., Duprat, J., Malaizé, B., Joli, C., Cortijo, E., Drago,](#)  
1125 [T., and Freitas, M. C. Present-day and past \(last 25,000 years\) marine pollen signal off western Iberia. \*Mar.\*](#)  
1126 [\*Micropaleontol.\* 62, 91–114, 2007.](#)  
1127 [Nehrbass-Ahles, C., Shin, J., Schmitt, J., Bereiter, B., Joos, F., Schilt, A., Schmidely, L., Silva, L., Teste, G.,](#)  
1128 [Grilli, R. and Chappellaz, J. Abrupt CO2 release to the atmosphere under glacial and early interglacial climate](#)  
1129 [conditions. \*Science\* 369\(6506\), 1000-1005, 2020.](#)  
1130 [Nomade, S., Bassinot, F., Marino, M., Simon, Q., Dewilde, F., Maiorano, P., Isguder, G., Blamart, D., Girone,](#)  
1131 [A., Scao, V., Pereira, A., Toti, F., Bertini, A., Combourieu-Nebout, N., Peral, M., Bourles, D.L., Petrosino, P.,](#)  
1132 [Galicchio, S., Ciaranfi, N. High-resolution foraminifer stable isotope record of MIS 19 at Montalbano Jonico,](#)  
1133 [southern Italy: a window into Mediterranean climatic variability during a low-eccentricity interglacial. \*Quat.\*](#)  
1134 [\*Sci. Rev.\* 205, 106-125, 2019.](#)  
1135 [NorthGRIP Members. High-resolution record of Northern Hemisphere climate extending into the last interglacial](#)  
1136 [period. \*Nature\*, 431: 147–151, 2004.](#)  
1137 [Oliveira, D., Desprat, S., Yin, Q., Naughton, F., Trigo, R., Rodrigues, T., Abrantes, F. and Sánchez Goñi, M.F.](#)  
1138 [Unraveling the forcings controlling the vegetation and climate of the best orbital analogues for the present](#)  
1139 [interglacial in SW Europe. \*Climate Dynamics\*, 51, pp.667-686, 2018.](#)  
1140 [Olson, S.L., Hearty, P.J.A. A sustained 121m sea level highstand during MIS 11 \(400 ka\): direct fossil and](#)  
1141 [sedimentary evidence from Bermuda. \*Quat Sci Rev\* 28, 271–285, 2009.](#)  
1142 [Ortiz, Trinidad. Torres, Antonio Delgado, J.F. Llamas, Vicente Soler, Maruja Valle, Ramón Julià, Laura Moreno,](#)  
1143 [Arantxa Díaz-Bautista. Palaeoenvironmental changes in the Padul Basin \(Granada, Spain\) over the last 1Ma](#)  
1144 [based on the biomarker content, \*Palaeogeogr. Palaeoclimatol. Palaeoecol.\*, 298, 286-299, ISSN 0031-0182,](#)  
1145 [2010. <https://doi.org/10.1016/j.palaeo.2010.10.003>.](#)  
1146 [Ozenda, P. Sur les étages de végétation dans les montagnes du bassin méditerranéen. \*Documents de Cartographie\*](#)  
1147 [\*Ecologique\*, 16, pp.1–32, 1975.](#)  
1148 [Past Interglacials Working Group of PAGES. Interglacials of the last 800,000 years. \*Reviews of Geophysics\*, 54\(1\),](#)  
1149 [162-219, 2016.](#)  
1150 [Peñalba, M.C., Maurice, A., Guiot, J., Duplessy, J.C., de Beaulieu, J.L. Termination of the last glaciation in the](#)  
1151 [Iberian Peninsula Inferred from the Pollen Sequence of Quintanar de la Sierra. \*Quat. Res.\* 48, 205–214, 1997.](#)  
1152 [Pérez-Folgado, M., Sierro, F.J., Flores, J.A., Grimalt, J.O. and Zahn, R. Paleoclimatic variations in foraminifer](#)  
1153 [assemblages from the Alboran Sea \(Western Mediterranean\) during the last 150 ka in ODP Site 977. \*Mar.\*](#)  
1154 [\*Geol.\*, 212\(1-4\),113-131, 2004.](#)  
1155 [Peyron, O., Combourieu-Nebout, N., Brayshaw, D., Goring, S., Andrieu-Ponel, V., Desprat, S., Fletcher, W.,](#)  
1156 [Gambin, B., Ioakim, C., Joannin, S., Kotthoff, U., Kouli, K., Montade, V., Pross, J., Sadori, L., Magny, M.](#)  
1157 [Precipitation changes in the Mediterranean basin during the Holocene from terrestrial and marine pollen](#)  
1158 [records: a model-data comparison. \*Clim. Past\*, 13, 249-265, <https://doi.org/10.5194/cp-13-249-2017>, 2017.](#)  
1159 [Peyron, O., Goring, S., Dormoy, I., Kotthoff, U., Pross, J., De Beaulieu, J.L., Drescher-Schneider, R., Vanniere,](#)  
1160 [B., Magny, M. Holocene seasonality changes in the central Mediterranean region reconstructed from the pollen](#)  
1161 [sequences of Lake Accesa \(Italy\) and Tenaghi Philippon \(Greece\). \*Holocene\* 21, 131-146,](#)  
1162 [<https://doi.org/10.1177/0959683610384162>, 2011.](#)  
1163 [Peyron, O., Magny, M., Goring, S., Joannin, S., De Beaulieu, J.L., Brugiapaglia, E., Sadori, L., Garfi, G., Kouli,](#)  
1164 [K., Ioakim, C. and Combourieu-Nebout, N. Contrasting patterns of climatic changes during the Holocene](#)  
1165 [across the Italian Peninsula reconstructed from pollen data. \*Clim. Past\*, 9\(3\), pp.1233-1252, 2013.](#)  
1166 [Pol, K., Masson Delmotte, V., Johnsen, S., Bigler, M., Cattani, O., Durand, G., Falourd, S., Jouzel, J., Minster,](#)  
1167 [B., Parrenin, F., Ritz, C., Steen Larsen C. H., Stenni, B. New MIS 19 EPICA Dome C high resolution](#)  
1168 [deuterium data: hints for a problematic preservation of climate variability at sub-millennial scale in the “oldest](#)  
1169 [ice”. \*Earth Planet Sci. Lett.\* 298, 95-103, 2010.](#)  
1170 [Pons, A. and Reille, M. The Holocene and Upper Pleistocene pollen record from Padul \(Granada, Spain\): a new](#)  
1171 [study, \*Palaeogeogr. Palaeoclimatol. Palaeoecol.\*, 66, 243–263, 1988.](#)

1172 [Pross, J., Christanis, K., Fischer, T., Fletcher, W.J., Hardiman, M., Kalaitzidis, S., Knipping, M., Kotthoff, U.,](#)  
1173 [Milner, A.M., Muller, U.C. and Schmiedl, G. The 1.35-Ma-long terrestrial climate archive of Tenaghi](#)  
1174 [Philippon, northeastern Greece: Evolution, exploration, and perspectives for future research. \*Newsletters on\*](#)  
1175 [Stratigraphy](#), 48(3), 253-276, 2015.

1176 [Pross, J., Kotthoff, U., Müller, U. C., Peyron, O., Dormoy, I., Schmiedl, G., Kalaitzidis, S., and Smith, A. M.](#)  
1177 [Massive perturbation in terrestrial ecosystems of the Eastern Mediterranean region associated with the 8.2 kyr](#)  
1178 [B.P. climatic event, \*Geology\*, 37, 887–890, 2009.](#)

1179 [Quézel, P. and Médail, F. \*Ecologie et biogéographie des forêts du bassin méditerranéen\*, Elsevier-Lavoisier eds,](#)  
1180 [Paris, France, 571 pp., 2003.](#)

1181 [Ramos-Román, M.J., Jiménez-Moreno, G., Camuera, J., García-Alix, A., Anderson, R.S., Jiménez-Espejo, F.J.](#)  
1182 [and Carrión, J.S. Holocene climate aridification trend and human impact interrupted by millennial-and](#)  
1183 [centennial-scale climate fluctuations from a new sedimentary record from Padul \(Sierra Nevada, southern](#)  
1184 [Iberian Peninsula\). \*Clim. Past\*, 14\(1\), 117-137, 2018.](#)

1185 [Raymo, M.E. and Mitrovica, J.X. Collapse of polar ice sheets during the stage 11 interglacial. \*Nature\*, 483\(7390\),](#)  
1186 [453-456, 2012.](#)

1187 [Regattieri, E., Giaccio, B., Galli, P., Nomade, S., Peronace, E., Messina, P., Sposato, A., Boschi, C., Gemelli, M.](#)  
1188 [A multi-proxy record of MIS 11-12 deglaciation and glacial MIS 12 instability from the Sulmona Basin](#)  
1189 [\(central Italy\). \*Quat Sci Rev\* 132, 12-145, 2016.](#)

1190 [Reille, M., and de Beaulieu, J. L. Long Pleistocene pollen records from the Praclaux crater, south-central France.](#)  
1191 [\*Quat. Res.\*, 44\(2\), 205–215. <https://doi.org/10.1006/qres.1995.1065>, 1995.](#)

1192 [Rivas-Martínez, S. Bioclimatic stages, chorological sectors and series of vegetation in Mediterranean Spain. \*Ecol.\*](#)  
1193 [mediterr.](#), 8(1), 275-288, 1982.

1194 [Robles M., Peyron O., Ménot G., Brugiapaglia E., Wulf S., Appelt O., Blache M., Vannièrè B., Dugerdil L., Paura](#)  
1195 [B., Ansanay-Alex S., Cromartie A., Charlet L., Guédron S., de Beaulieu JL, and Joannin, S. Climate changes](#)  
1196 [during the Lateglacial in South Europe: new insights based on pollen and brGDGTs of Lake Matese in Italy,](#)  
1197 [\*Clim. Past\*, 19, 493–515. <https://doi.org/10.5194/cp-19-493-2023>, 2023.](#)

1198 [Rodrigo-Gámiz, M., García-Alix, A., Jiménez-Moreno, G., Ramos-Román, M.J., Camuera, J., Toney, J.L.,](#)  
1199 [Sachse, D., Anderson, R.S. and Damsté, J.S.S. Paleoclimate reconstruction of the last 36 kyr based on](#)  
1200 [branched glycerol dialkyl glycerol tetraethers in the Padul palaeolake record \(Sierra Nevada, southern Iberian](#)  
1201 [Peninsula\). \*Quat Sci Rev\*, 281, p.107434, 2022.](#)

1202 [Rodrigues, T., Voelker, A.H.L., Grimalt, J.O., Abrantes, F., Naughton, F. Iberian Margin sea surface temperature](#)  
1203 [during MIS 15 to 9 \(580-300 ka\): glacial sub-orbital variability versus interglacial stability. \*Paleoceanography\*](#)  
1204 [26, 1e16, <https://doi.org/10.1029/2010PA001927>, 2011.](#)

1205 [Rohling, E.J., Fenton, M., Jorissen, F.J., Bertrand, P., Ganssen, G., Caulet, J.P. Magnitudes of sea-level lowstands](#)  
1206 [of the past 500,000 years. \*Nature\* 394, 162e165, <https://doi.org/10.1038/28134>, 1998.](#)

1207 [Rossignol-Strick, M. The Holocene climatic optimum and pollen records of sapropel 1 in the Eastern](#)  
1208 [Mediterranean, 9000–6000 BP. \*Quat. Sci. Rev.\* 18, 515–530, 1999.](#)

1209 [Ruddiman, W.F. The anthropogenic greenhouse era began thousands of years ago. \*Climatic change\*, 61\(3\), 261-](#)  
1210 [293, 2003.](#)

1211 [Ruddiman, W.F. The early anthropogenic hypothesis: Challenges and responses. \*Rev Geophys\*, 45\(4\), 2007.](#)

1212 [Ruddiman, W.F., Fuller, D.Q., Kutzbach, J.E., Tzedakis, P.C., Kaplan, J.O., Ellis, E.C., Vavrus, S.J., Roberts,](#)  
1213 [C.N., Fyfe, R., He, F. and Lemmen, C. Late Holocene climate: Natural or anthropogenic? \*Rev Geophys\*, 54\(1\),](#)  
1214 [93-118, 2016.](#)

1215 [Sadori, L., Ortu, E., Peyron, O., Zanchetta, G., Vannièrè, B., Desmet, M. and Magny, M. The last 7 millennia of](#)  
1216 [vegetation and climate changes at Lago di Pergusa \(central Sicily, Italy\). \*Clim. Past\*, 9\(4\), pp.1969-1984, 2013.](#)

1217 [Sadori, L., Koutsodendris, A., Panagiotopoulos, K., Masi, A., Bertini, A., Combourieu-Nebout, N., Francke, A.,](#)  
1218 [Kouli, K., Joannin, S., Mercuri, A.M. and Peyron, O. Pollen-based paleoenvironmental and paleoclimatic](#)  
1219 [change at Lake Ohrid \(south-eastern Europe\) during the past 500 ka. \*Biogeosciences\*, 13\(5\), pp.1423-1437,](#)  
1220 [2016.](#)

1221 [Salonen, J.S., Korpela, M., Williams, J.W., Luoto, M. Machine-learning based reconstructions of primary and](#)  
1222 [secondary climate variables from North American and European fossil pollen data. \*Sci. Rep.\* 9, 1–13,](#)  
1223 [<https://doi.org/10.1038/s41598-019-52293-4>, 2019.](#)

1224 [Salonen, J.S., Luoto, M., Alenius, T., Heikkilä, M., Seppä, H., Telford, R.J. and Birks, H.J.B. Reconstructing](#)  
1225 [palaeoclimatic variables from fossil pollen using boosted regression trees: comparison and synthesis with other](#)  
1226 [quantitative reconstruction methods. \*Quat Sci Rev\*, 88, 69-81, 2014.](#)

1227 [Sánchez Goñi, M. F., Rodrigues, T., Hodell, D.A., Polanco-Martinez, J.M., Alonso-Garcia, M., Hernandez-](#)  
1228 [Almeida, I., Desprat, S. and Ferretti, P., 2016. Tropically-driven climate shifts in southwestern Europe during](#)  
1229 [MIS 19, a low eccentricity interglacial. \*Earth and Planetary Science Letters\*, 448, pp.81-93, 2016a.](#)

1230 [Sánchez Goñi, M. F., Llave, E., Oliveira, D., Naughton, F., Desprat, S., Ducassou, E., Hodell, D. A., and](#)  
1231 [Hernández-Molina, F. J. Climate changes in southwestern Iberia and Mediterranean Outflow variations during](#)

1232 [two contrasting cycles of the last 1 Myrs: MIS 31-MIS 30 and MIS 12-MIS 11. \*Glob. Planet. Change\*, 136,](#)  
 1233 [18–29, <https://doi.org/10.1016/j.gloplacha.2015.11.006>, 2016b.](#)  
 1234 [Sánchez Goñi, M., Eynaud, F., Turon, J. L., and Shackleton, N. J. High resolution palynological record off the](#)  
 1235 [Iberian margin: direct land-sea correlation for the Last Interglacial complex. \*Earth Planet Sci Lett\*, 171\(1\),](#)  
 1236 [123-137, 1999.](#)  
 1237 [Sassoon, D., Lebreton, V., Combourieu-Nebout, N., Peyron, O. and Moncel, M.H. Palaeoenvironmental Changes](#)  
 1238 [in the Southwest Mediterranean \(ODP Site 976, Alboran Sea\) During the MIS 12/11 Transition and the MIS](#)  
 1239 [11 Interglacial. \*Quat Sci Rev\*, 304: 108010.](#)  
 1240 [Shackleton, N.J., Sánchez-Goñi, M.F., Pailler, D. and Lancelot, Y. Marine isotope substage 5e and the Eemian](#)  
 1241 [interglacial. \*Glob. Planet. Change\*, 36\(3\), 151-155, 2003.](#)  
 1242 [Shipboard Scientific Party. Site 976. In: \*Comas, M.C., Zahn, R., Klaus, A., et al. \(Eds.\), Proc. ODP, Init. Repts.,\*](#)  
 1243 [\*vol. 161, Ocean Drilling Program\*, College Station, TX, pp. 179-297, 1996.](#)  
 1244 [Siani, G., Michel, E., De Pol-Holz, R., DeVries, T., Lamy, F., Carel, M., Isguder, G., Dewilde, F. and Laurantou,](#)  
 1245 [A. Carbon isotope records reveal precise timing of enhanced Southern Ocean upwelling during the last](#)  
 1246 [deglaciation. \*Nat. Commun.\*, 4\(1\), p.2758, 2013.](#)  
 1247 [Sinopoli, G., Peyron, O., Masi, A., Holtvoeth, J., Francke, A., Wagner, B. and Sadori, L. Pollen-based temperature](#)  
 1248 [and precipitation changes in the Ohrid Basin \(western Balkans\) between 160 and 70 ka. \*Clim. Past\*, 15\(1\),53-](#)  
 1249 [71, 2019.](#)  
 1250 [Stuiver, M. and Reimer, P. J.: Extended 14C database and revised CALIB radiocarbon calibration program,](#)  
 1251 [Radiocarbon, 35, 215–230, 1993.](#)  
 1252 [Stuiver, M., Reimer, P. J., Bard, E., Beck, W., Burr, G. S., Hughen, K. A., Kromer, B., McCormac, F. G., van der](#)  
 1253 [Plicht, J., and Spurk, M.: INTCAL98 radiocarbon age calibration, 24 000 cal BP, Radiocarbon, 40, 1041–](#)  
 1254 [1083, 1998.](#)  
 1255 [ter Braak, C.J.F., Juggins, S. Weighted averaging partial least squares regression \(WA-PLS\): an improved method](#)  
 1256 [for reconstructing environmental variables from species assemblages. \*Hydrobiologia\* 269–270, 485–502,](#)  
 1257 [https://doi.org/10.1007/BF00028046, 1993.](#)  
 1258 [Toti, F., Bertini, A., Girone, A., Marino, M., Maiorano, P., Bassinot, F., Combourieu-Nebout, N., Nomade, S.,](#)  
 1259 [and Bucciatti, A. Marine and terrestrial climate variability in the western Mediterranean Sea during marine](#)  
 1260 [isotope stages 20 and 19. \*Quat Sci Rev\*, 243, <https://doi.org/10.1016/j.quascirev.2020.106486>, 2020.](#)  
 1261 [Turner, C. The Middle Pleistocene deposits at Marks Tey, Essex. \*Philosophical Transactions of the Royal Society\*](#)  
 1262 [of London, Series B 257, 373–440, 1970.](#)  
 1263 [Turon, J.-L., Lézine, A.-M., and Denèfle, M. Land–sea correlations for the last deglaciation inferred from a pollen](#)  
 1264 [and dinocyst record from the Portuguese margin, \*Quat. Res.\*, 59, 88–96, 2003.](#)  
 1265 [Tye, G.J., Sherriff, J., Candy, I., Coxon, P., Palmer, A., Mcclymont, E.L., Schreve, D.C. The d18O stratigraphy](#)  
 1266 [of the Hoxnian lacustrine sequence at Marks Tey, Essex, UK: implications for the climatic structure of MIS](#)  
 1267 [11 in Britain. \*J. Quat. Sci.\* 31, 75-92, <https://doi.org/10.1002/jqs.2840>, 2016.](#)  
 1268 [Tzedakis, P. C., Hodell, D. A., Nehrbass-Ahles, C., Mitsui, T., and Wolff, E. W. Marine Isotope Stage 11c: An](#)  
 1269 [unusual interglacial. \*Quat Sci Rev\*, 284, 107493, <https://doi.org/10.1016/j.quascirev.2022.107493>, 2022.](#)  
 1270 [Tzedakis, P. C., Hooghiemstra, H., and Pälike, H. The last 1.35 million years at Tenaghi Philippon: revised](#)  
 1271 [chronostratigraphy and long-term vegetation trends. \*Quat Sci Rev\*, 25\(23–24\), 3416–3430,](#)  
 1272 [https://doi.org/10.1016/j.quascirev.2006.09.002, 2006.](#)  
 1273 [Tzedakis, P.C. The MIS 11–MIS 1 analogy, southern European vegetation, atmospheric methane and the " early](#)  
 1274 [anthropogenic hypothesis". \*Clim. Past\*, 6\(2\), 131-144, 2010.](#)  
 1275 [Tzedakis, P.C., Channell, J.E.T., Hodell, D.A., Kleiven, H.F. and Skinner, L.C. Determining the natural length of](#)  
 1276 [the current interglacial. \*Nat Geosci\*, 5\(2\), 138-141, 2012.](#)  
 1277 [Vavrus, S.J., He, F., Kutzbach, J.E. et al. Glacial Inception in Marine Isotope Stage 19: An Orbital Analog for a](#)  
 1278 [Natural Holocene Climate. \*Sci. Rep.\*, 8, 10213, <https://doi.org/10.1038/s41598-018-28419-5>, 2018.](#)  
 1279 [Vázquez Riveiros, N., Waelbroeck, C., Skinner, L., Duplessy, J. C., McManus, J. F., Kandiano, E. S., and Bauch,](#)  
 1280 [H. A. The “MIS 11 paradox” and ocean circulation: Role of millennial scale events. \*Earth Planet Sci Lett\*,](#)  
 1281 [371–372, 258–268, <https://doi.org/10.1016/j.epsl.2013.03.036>, 2013.](#)  
 1282 [Voelker, A. H. L., Rodrigues, T., Billups, K., Oppo, D., McManus, J., Stein, R., Hefter, J., and Grimalt, J. O.](#)  
 1283 [Variations in mid-latitude North Atlantic surface water properties during the mid-Brunhes \(MIS 9-14\) and](#)  
 1284 [their implications for the thermohaline circulation. \*Clim. Past\*, 6\(4\), 531–552, \[https://doi.org/10.5194/cp-6-\]\(https://doi.org/10.5194/cp-6-531-2010\)](#)  
 1285 [531-2010, 2010.](#)  
 1286 [Wang, Y., Yang, X., Wang, Y., Wang, Q., and Edwards, R. L. The structure of marine isotope Stage 11 and its](#)  
 1287 [alignment with the Holocene. \*Palaeogeogr. Palaeoclimatol. Palaeoecol.\*, 609, 111311,](#)  
 1288 [https://doi.org/10.1016/j.palaeo.2022.111311, 2023.](#)  
 1289 [Watts, W. A., Allen, J. R. M., Huntley, B., and Fritz, S. C. Vegetation history and climate of the last 15 000 years](#)  
 1290 [at Laghi di Monticchio, Southern Italy. \*Quaternary Sci. Rev.\*, 15, 113–132, 1996.](#)

1291 [West, R. The Quaternary deposits at Hoxne, Suffolk. \*Philosophical Transactions of the Royal Society London.\*](#)  
1292 [Series B 239, 265–356, 1956.](#)

1293 [Wijmstra, T. A. and Smit, A. Palynology of the middle part \(30–78 metres\) of the 120 m deep section in Northern](#)  
1294 [Greece \(Macedonia\). \*Acta Bot. Neerl.\* 25, 297–312, 1976.](#)

1295 [Yin, Q., and Berger, A. Interglacial analogues of the Holocene and its natural near future. \*Quat Sci Rev.\* 120, 28–](#)  
1296 [46, <https://doi.org/10.1016/j.quascirev.2015.04.008>, 2015.](#)

1297 [Zhuravleva, A. \*Paleoceanographic and climatic teleconnections between the subarctic and subtropical North\*](#)  
1298 [Atlantic during the last interglacial \(MIS 5e\). Doctoral dissertation.](#)  
1299 [https://doi.org/10.13140/RG.2.2.26501.86242, 2018.](#)

1300 [Zonneveld, K.A. Palaeoclimatic reconstruction of the last deglaciation \(18-8 ka BP\) in the Adriatic Sea region; a](#)  
1301 [land-sea correlation based on palynological evidence. \*Palaeogeogr. Palaeoclimatol. Palaeoecol.\*, 122\(1-4\),](#)  
1302 [89-106.](#)

1303

1304 [Allen, J. R. M., Watts, W. A., McGee, E., and Huntley, B.. Holocene environmental variability—the record from](#)  
1305 [Lago Grande di Monticchio, Italy, \*Quatern. Int.\*, 88, 69–80, 2002.](#)

1306 [Allen, J.R.M., Huntley, B., Brandt, U., Brauer, A., Hubberten, H., Keller, J., Kraml, M., Mackensen, A., Mingram,](#)  
1307 [J., Negendank, J.F.W., Nowaczyk, N.R., Oberhansli, H., Watts, W.A., Wulf, S., Zolitschka, B. Rapid](#)  
1308 [environmental changes in southern Europe during the last glacial period. \*Nature\* 400, 740e743. \[https://\]\(https://doi.org/10.1038/23432\)](#)  
1309 [doi.org/10.1038/23432, 1999.](#)

1310 [Alley, R.B., Agustsdottir, A.M. The 8k event: cause and consequences of a major Holocene abrupt climate change.](#)  
1311 [\*Quat Sci Rev.\* 24, 1123–1149, 2005.](#)

1312 [Alonso, B., Ercilla, G., Martínez Ruiz, F., Baraza, J., and Galimont, A. Pliocene Pleistocene sedimentary facies](#)  
1313 [at Site 976: Depositional history in the northwestern Alboran Sea. \*Proc Integr Ocean Drill Program\*,](#)  
1314 [161\(1994\), 57–68. <https://doi.org/10.2973/odp.proc.sr.161.206>, 1999.](#)

1315 [Ardenghi, N., Mulch, A., Koutsodendris, A., Pross, J., Kahmen, A., and Niedermeyer, E. M. Temperature and](#)  
1316 [moisture variability in the eastern Mediterranean region during Marine Isotope Stages 11–10 based on](#)  
1317 [biomarker analysis of the Tenaghi Philippon peat deposit. \*Quat Sci Rev.\*, 225.](#)  
1318 [https://doi.org/10.1016/j.quascirev.2019.105977, 2019.](#)

1319 [Azibeiro, L. A., Sierro, F. J., Capotondi, L., Lirer, F., Andersen, N., González Lanchas, A., Alonso García, M.,](#)  
1320 [Flores, J. A., Cortina, A., Grimalt, J. O., Martrat, B., and Cacho, I. Meltwater flux from northern ice sheets to](#)  
1321 [the Mediterranean during MIS 12. \*Quat Sci Rev.\* 268. <https://doi.org/10.1016/j.quascirev.2021.107108>, 2021.](#)

1322 [Bar Matthews, M., Ayalon, A., and Kaufman, A. Middle to late Holocene \(6500-yr period\) paleoclimate in the](#)  
1323 [Eastern Mediterranean region from stable isotopic composition of speleothems from Soreq Cave, Israel, in:](#)  
1324 [Environment and society in times of climate change, edited by: Issar, A. and Brown, N., Kluwer Academic,](#)  
1325 [Dordrecht, 203–214, 1998.](#)

1326 [Barber, D.C., Dyke, A., Hillaire Marcel, C., Jennings, A.E., Andrews, J.T., Kerwin, M.W., Bilodeau, G.,](#)  
1327 [McNeely, R., Southon, J., Morehead, M.D., and Gagnon, J.M. Forcing of the cold event of 8,200 years ago by](#)  
1328 [catastrophic drainage of Laurentide lakes. \*Nature\*, 400\(6742\), pp.344–348, 1999.](#)

1329 [Barbero, M., Quézel, P., Rivas Martínez, S. Contribution à l'étude des groupements forestiers et préforestiers du](#)  
1330 [Maroc. \*Phytocoenologia\* 9, pp.311–412, 1981.](#)

1331 [Bauch, H.A., Erlenkeuser, H., Helmke, J.P., Struck, U. A paleoclimatic evaluation of marine oxygen isotope stage](#)  
1332 [11 in the high northern Atlantic \(Nordic seas\). \*Glob. Planet. Change\*, 24, 27e39.](#)  
1333 [https://doi.org/10.1016/S0921-8181\(99\)00067-3, 2000.](#)

1334 [Benabid, A. Bref aperçu sur la zonation altitudinale de la végétation climatique du Maroc, \*Ecol. Medit.\*, 8\(1–2\),](#)  
1335 [pp.301–315, 1982.](#)

1336 [Berger, A., and Loutre, M.F. \*Climate 400,000 years ago, a key to the future?\* In: A.W. Droxler, R.Z. Past](#)  
1337 [Interglacials Working Group of Pages, Interglacials of the last 800,000 years. \*R. of Geop.\*, 54, pp.162–219,](#)  
1338 [2003.](#)

1339 [Berger, A., and Loutre, M.F. An exceptionally Long Interglacial Ahead? \*Science\* 297, 1287–1288.](#)  
1340 [doi:10.1226/science.1076120, 2002.](#)

1341 [Bertini, A., Toti, F., Marino, M., Ciaranfi, N. Vegetation and climate across the early-middle Pleistocene transition](#)  
1342 [at the Montalbano Jonico section \(southern Italy\). \*Quat Int.\* 383, 74–88, 2015.](#)

1343 [Blain, H. A., Fagoaga, A., Ruiz Sánchez, F. J., García Medrano, P., Ollé, A., and Jiménez Arenas, J. M. Coping](#)  
1344 [with arid environments: A critical threshold for human expansion in Europe at the Marine Isotope Stage 12/11](#)  
1345 [transition? The case of the Iberian Peninsula. \*J. Hum. Evol.\*, 153. <https://doi.org/10.1016/j.jhevol.2021.102950>,](#)  
1346 [2021.](#)

1347 [Bond, G., Kromer, B., Beer, J., Muscheler, R., Evans, M.N., Showers, W., Hoffmann, S., Lotti Bond, R., Hajdas,](#)  
1348 [I., and Bonani, G. Persistent solar influence on North Atlantic climate during the Holocene. \*Science\* 278, 1257–](#)  
1349 [1266, 2001.](#)

1350 Bond, G., Showers, W., Cheseby, M., Lotti, R., Almasi, P., de Menocal, P., Priore, P., Cullen, H., Hajdas, I., and  
1351 Bonani, G. A pervasive millennial-scale cycle in the North Atlantic Holocene and glacial climates. *Science*  
1352 294, 2130–2136, 1997.

1353 Bordon, A., Peyron, O., Lézine, A. M., Brewer, S., and Fouache, E. Pollen-inferred Late Glacial and Holocene  
1354 climate in southern Balkans (Lake Maliq). *Quatern. Int.*, 200, 19–30, 2009.

1355 Brewer, S., Guiot, J., Sánchez-Gómez, M.F., and Klotz, S. The climate in Europe during the Eemian: a multi-method  
1356 approach using pollen data. *Quat Sci Rev*, 27(25–26), pp.2303–2315, 2008.

1357 Brice, R. *Variabilité Climatique en Mer d'Alboran au cours de la Teminaison V (MIS-12/11)*. Unpublished thesis,  
1358 University of Bordeaux, 2007.

1359 Broecker, W. S., and Stocker, T. L.: The Holocene CO<sub>2</sub> rise. Anthropogenic or natural? *Eos, Trans. Am. Geophys.*  
1360 *Union*, 87(3), 27. doi:10.1029/2006EO030002, 2006.

1361 Bulian, F., Kouwenhoven, T. J., Jiménez-Espejo, F. J., Krijgsman, W., Andersen, N., and Sierro, F. J. Impact of  
1362 the Mediterranean Atlantic connectivity and the late Miocene carbon shift on deep-sea communities in the  
1363 Western Alboran Basin. *Palaeogeogr. Palaeoclimatol. Palaeoecol.*, 589.  
1364 <https://doi.org/10.1016/j.palaeo.2022.110841>, 2022.

1365 Cacho, I., Grimalt, J. O., Canals, M., Saffi, L., Shackleton, N., Schönfeld, J., and Zahn, R. Variability of the  
1366 western Mediterranean Sea surface temperature during the last 25,000 years and its connection with the  
1367 northern hemisphere climatic changes. *Paleoceanography*, 16, 40–52, 2001.

1368 Cacho, I., Grimalt, J.O., Sierro, F.J., Shackleton, N., Canals, M. Evidence for enhanced Mediterranean  
1369 thermohaline circulation during rapid climatic coolings. *Earth Planet Sci Lett*, 183, 417–429, 2000.

1370 Camuera, J., Jiménez-Moreno, G., Ramos-Román, M.J., García-Alix, A., Toney, J.L., Anderson, R.S., Jiménez-  
1371 Espejo, F., Bright, J., Webster, C., Yanes, Y., and Carrión, J.S. Vegetation and climate changes during the last  
1372 two glacial-interglacial cycles in the western Mediterranean: a new long-pollen record from Padul (southern  
1373 Iberian Peninsula). *Quat Sci Rev*, 205, pp.86–105, 2019.

1374 Camuera, J., Jiménez-Moreno, G., Ramos-Román, M.J., García-Alix, A., Toney, J.L., Anderson, R.S., Jiménez-  
1375 Espejo, F., Kaufman, D., Bright, J., Webster, C., and Yanes, Y. Orbital-scale environmental and climatic  
1376 changes recorded in a new ~200,000-year long multiproxy sedimentary record from Padul, southern Iberian  
1377 Peninsula. *Quat Sci Rev*, 198, pp.91–114, 2018.

1378 Camuera, J., Jiménez-Moreno, G., Ramos-Román, M.J., García-Alix, A., Jiménez-Espejo, F.J., Toney, J.L., and  
1379 Anderson, R.S. Chronological control and centennial-scale climatic subdivisions of the Last Glacial  
1380 Termination in the western Mediterranean region. *Quat Sci Rev*, 255, p.106814, 2021.

1381 Camuera, J., Ramos-Román, M.J., Jiménez-Moreno, G., García-Alix, A., Ilvonen, L., Ruha, L., Gil-Romera, G.,  
1382 González-Sampériz, P., and Seppä, H. Past 200 kyr hydroclimate variability in the western Mediterranean and  
1383 its connection to the African Humid Periods. *Sci. Rep.*, 12(1), p.9050, 2022.

1384 Candy, I., Schreve, D. C., Sherriff, J., and Tye, G. J. Marine Isotope Stage 11: Palaeoclimates, palaeoenvironments  
1385 and its role as an analogue for the current interglacial. *Earth Sci Rev*, 128, 18–51.  
1386 <https://doi.org/10.1016/j.earscirev.2013.09.006>, 2014.

1387 Candy, I., Oliveira, D., Parkes, D., Sherriff, J., and Thornalley, D. Marine Isotope Stage 11c in Europe: Recent  
1388 advances in marine-terrestrial correlations and their implications for interglacial stratigraphy—a review.  
1389 *Boreas*, 2024.

1390 Cartapanis, O., Jonkers, L., Moffa-Sánchez, P., Jaccard, S.L., and de Vernal, A. Complex spatio-temporal  
1391 structure of the Holocene Thermal Maximum. *Nat. Commun.*, 13(1), p.5662, 2022.

1392 Cheddadi, R., Lamb, H.F., Guiot, J., and van der Kaars, S. Holocene climatic change in Morocco: a quantitative  
1393 reconstruction from pollen data. *Climate dynamics*, 14, 883–890, 1998.

1394 Chevalier, M., Davis, B. A. S., Heiri, O., Seppä, H., Chase, B. M., Gajewski, K., Lacourse, T., Telford, R. J.,  
1395 Finsinger, W., Guiot, J., Kühl, N., Maezumi, S. Y., Tipton, J. R., Carter, V. A., Brussel, T., Phelps, L. N.,  
1396 Dawson, A., Zanon, M., Vallé, F., ... Kupriyanov, D. Pollen-based climate reconstruction techniques for late  
1397 Quaternary studies. *Earth Sci Rev*, 210, 103384. <https://doi.org/10.1016/j.earscirev.2020.103384>, 2020.

1398 Combourieu-Nebout, N., Bertini, A., Russo-Ermolli, E., Peyron, O., Klotz, S., Montade, V., Fauquette, S., Allen,  
1399 J., Fusco, F., Goring, S., Huntley, B., Joannin, S., Lebreton, V., Magri, D., Martinetto, E., Orain, R., and  
1400 Sadori, L. Climate changes in the central Mediterranean and Italian vegetation dynamics since the Pliocene.  
1401 *Rev. Palaeobot. Palynol.* 218, 127–147, 2015.

1402 Combourieu-Nebout, N., Londeix, L., Baudin, F., Turon, J. L., von Grafenstein, R., and Zahn, R. *Quaternary  
1403 marine and continental palaeoenvironments in the western Mediterranean (Site 976, Alboran Sea):  
1404 palynological evidence*, in: Proc. ODP Sci. Results, 161: College Station, TX (Ocean Drilling Program), edited  
1405 by: Zahn, R., Comas, M. C., and Klaus, A., pp.457–468, 1999.

1406 Combourieu-Nebout, N., Paterne, M., Turon, J. L., and Siani, G. A high-resolution record of the last deglaciation  
1407 in the Central Mediterranean Sea: Palaeovegetation and Palaeohydrological evolution. *Quat Sci Rev*, 17, 303–  
1408 317, 1998.

1409 Combourieu Nebout, N., Peyron, O., Bout Roumazeille, V., Goring, S., Dormoy, I., Joannin, S., Sadori, L., Siani,  
1410 G., and Magny, M. Holocene vegetation and climate changes in central Mediterranean inferred from a high-  
1411 resolution marine pollen record (Adriatic Sea). *Clim. Past* 9, 2023–2042, 2013.

1412 Combourieu Nebout, N., Peyron, O., Dormoy, I., Desprat, S., Beaudouin, C., Kotthoff, U., and Marret, F. Rapid  
1413 climatic variability in the west Mediterranean during the last 25,000 years from high resolution pollen data.  
1414 *Clim. Past*, 5(3), 503–521. <https://doi.org/10.5194/ep-5-503-2009>, 2009.

1415 Combourieu Nebout, N., Turon, J. L., Zahn, R., Capotondi, L., Londeix, L., and Pahnke, K. Enhanced aridity and  
1416 atmospheric high pressure stability over the western Mediterranean during the North Atlantic cold events of  
1417 the past 50 k.y. *Geology*, 30(10), 863–866. [https://doi.org/10.1130/0091-7613\(2002\)030<0863:EAAHP>2.0.CO;2](https://doi.org/10.1130/0091-7613(2002)030<0863:EAAHP>2.0.CO;2), 2002.

1419 d'Oliveira, L., Dugerdil, L., Ménot, G., Evin, A., Muller, S.D., Ansanay Alex, S., Azuara, J., Bonnet, C., Bremond,  
1420 L., Shah, M., and Peyron, O. Reconstructing 15,000 years of southern France temperatures from coupled  
1421 pollen and molecular (brGDGT) markers (Canroute, Massif Central). *Clim. Past* 19, 2127–2156.  
1422 <https://doi.org/10.5194/ep-19-2127-2023>.

1423 Dansgaard, W., Johnsen, S.J., Clausen, H.B., Dahl Jensen, D., Gundestrup, N.S., Hammer, C.U., Hvidberg, C.S.,  
1424 Steffensen, J.P., Sveinbjörnsdottir, A.E., Jouzel, J., Bond, G. Evidence for general instability of past climate  
1425 from a 250 kyr ice core record. *Nature* 364, 218–220, 1993.

1426 Davis, B. A. S., Brewer, S., Stevenson, A. C., Guiot, J. The temperature of Europe during the Holocene  
1427 reconstructed from pollen data. *Quat Sci Rev*, 22, 1701–1716, 2003.

1428 De'ath, G. Boosted trees for ecological modeling and prediction. *Ecology* 88, 243–251.  
1429 [https://doi.org/10.1890/0012-9658\(2007\)88\[243:BTFFEMA\]2.0.CO;2](https://doi.org/10.1890/0012-9658(2007)88[243:BTFFEMA]2.0.CO;2), 2007.

1430 Desprat, S., Combourieu Nebout, N., Essallami, L., Sicre, M.A., Dormoy, I., Peyron, O., Siani, G., Bout  
1431 Roumazeilles, V., Turon, J.L. Deglacial and Holocene vegetation and climatic changes at the southernmost tip  
1432 of the Central Mediterranean from a direct land–sea correlation. *Clim. Past* 9, 767–787, 2013.

1433 Desprat, S., Sánchez Goñi, M. F., Naughton, F., Turon, J. L., Duprat, J., Malaizé, B., Cortijo, E., Peypouquet, J.  
1434 P. Climate variability of the last five isotopic interglacials: Direct land–sea–ice correlation from the multiproxy  
1435 analysis of North–Western Iberian margin deep–sea cores. *Developments in Quaternary Science*, 7(C), pp.375–  
1436 386. [https://doi.org/10.1016/S1571-0866\(07\)80050-9](https://doi.org/10.1016/S1571-0866(07)80050-9), 2007.

1437 Desprat, S., Sánchez Goñi, M. F., Turon, J. L., McManus, J. F., Loutre, M. F., Duprat, J., Malaizé, B., Peyron, O.,  
1438 Peypouquet, J. P. Is vegetation responsible for glacial inception during periods of muted insolation changes?  
1439 *Quat Sci Rev*, 24(12–13), pp.1361–1374. <https://doi.org/10.1016/j.quascirev.2005.01.005>, 2005.

1440 Di Rita, F., Ghilardi, M., Fagel, N., Vacchi, M., Warichet, F., Delanghe, D., Sicurani, J., Martinet, L., Robreseco,  
1441 S. Natural and anthropogenic dynamics of the coastal environment in northwestern Corsica (western  
1442 Mediterranean) over the past six millennia. *Quat Sci Rev*, 278, p.107372, 2022.

1443 Donders, T., Panagiotopoulos, K., Koutsodendris, A., Bertini, A., Mercuri, A.M., Masi, A., Combourieu Nebout,  
1444 N., Joannin, S., Kouli, K., Kousis, I., Peyron, O. 1.36 million years of Mediterranean forest refugium dynamics  
1445 in response to glacial–interglacial cycle strength. *PNAS*, 118(34), p.e2026111118, 2021.

1446 Dormoy, I., Peyron, O., Combourieu Nebout, N., Goring, S., Kotthoff, U., Magny, M., Pross, J. Terrestrial climate  
1447 variability and seasonality changes in the Mediterranean region between 15,000 and 4,000 years BP deduced  
1448 from marine pollen records. *Clim. Past* 5, 615–632. <https://doi.org/10.5194/ep-5-615-2009>, 2009.

1449 Dugerdil, L., Joannin, S., Peyron, O., Jouffroy Bapicot, I., Vannièrre, B., Boldgiv, B., Unkelbach, J., Behling, H.,  
1450 Ménot, G. Climate reconstructions based on GDGT and pollen surface datasets from Mongolia and Baikal  
1451 area: calibrations and applicability to extremely cold–dry environments over the Late Holocene. *Clim. Past*,  
1452 17(3), pp.1199–1226, 2021.

1453 Ellison, C.R., Chapman, M.R., Hall, I.R. Surface and deep ocean interactions during the cold climate event 8,200  
1454 years ago. *Science*, 312(5782), pp.1929–1932, 2006.

1455 Elith, J., Leathwick, J. R., Hastie, T. A working guide to boosted regression trees. *J. Anim. Ecol.*, 77(4), 802–813,  
1456 2008.

1457 Fletcher W., Sanchez Goñi M.F. Orbital and sub-orbital scale climate impacts on vegetation of the western  
1458 Mediterranean basin over the last 48,000 yr. *Quat. Res.*, 70(3), 451–464, 2008.

1459 García Alix, A., Camuera, J., Ramos Román, M.J., Toney, J.L., Sachse, D., Schefuß, E., Jiménez Moreno, G.,  
1460 Jiménez Espejo, F.J., López Avilés, A., Anderson, R.S., Yanes, Y. Paleohydrological dynamics in the  
1461 Western Mediterranean during the last glacial cycle. *Glob. Planet. Change*, 202, p.103527, 2021.

1462 Giaccio, B., Regattieri, E., Zanchetta, G., Nomade, S., Renne, P.R., Sprain, C.J., Drysdale, R.N., Tzedakis, P.C.,  
1463 Messina, P., Scardia, G., Sposato, A. Duration and dynamics of the best orbital analogue to the present  
1464 interglacial. *Geology*, 43(7), 603–606, 2015.

1465 Girone, A., Maiorano, P., Marino, M., Kucera, M. Calcareous plankton response to orbital and millennial scale  
1466 climate changes across the Middle Pleistocene in the western Mediterranean. *Palaeogeogr. Palaeoclimatol.*  
1467 *Palaeoecol.*, 392, 105–116. <https://doi.org/10.1016/j.palaeo.2013.09.005>, 2013.



1468 Gonzalez-Donoso, J.M., Serrano, F., Linares, D. Sea surface temperature during the Quaternary at ODP Sites 976  
1469 and 975 (western Mediterranean). *Palaeogeogr. Palaeoclimatol. Palaeoecol.* 162, 17–44, 2000.

1470 Grafenstein, U., Erlenkeuser, H., Brauer, A., Jouzel, J., Johnsen, S.J. A mid-European decadal isotope climate  
1471 record from 15,500 to 5000 years BP. *Science*, 284(5420), 1654–1657, 1999.

1472 Grieser, J., Giommes, R., Bernardi, M. New LocClim—the Local Climate Estimator of FAO. *Geophysical  
1473 research abstracts*, 8, 08305, 2006.

1474 Guiot, J., Cramer, W. Climate Change: The 2015 Paris Agreement Thresholds and Mediterranean Basin  
1475 Ecosystems. *Science*, 354, 465–468, 2016.

1476 Guiot, J. Methodology of the last climatic reconstruction in France from pollen data. *Palaeogeogr.  
1477 Palaeoclimatol. Palaeoecol.* 80, 49–69, 1990.

1478 Guiot, J., Pons, A., de Beaulieu, J. L., Reille, M. A 140,000 year continental climate reconstruction from two  
1479 European pollen records. *Nature* 338, 309–313, 1989.

1480 Herzschuh, U., Böhmer, T., Chevalier, M., Hébert, R., Dallmeyer, A., Li, C., Cao, X., Peyron, O., Nazarova, L.,  
1481 Novenko, E.Y., Park, J. Regional pollen-based Holocene temperature and precipitation patterns depart from  
1482 the Northern Hemisphere mean trends. *Clim. Past*, 19(7), 1481–1506, 2023.

1483 Hes, G., Sanchez Goñi, M.F., and Bouttes, N. Impact of terrestrial biosphere on the atmospheric  
1484 CO<sub>2</sub> concentration across Termination V. *Clim. Past*, 18(6), 1429–1451, 2022. <https://doi.org/10.5194/ep-18-1429-2022>

1485 Heusser, L. E. and Balsam, W. L. Pollen distribution in the north-east Pacific Ocean. *Quat. Res.* 7, 45–62, 1977.

1486 Hodell, D. A., Channeil, J. E. T., Curtis, J. H., Romero, O. E., and Röhl, U. Onset of “Hudson Strait” Heinrich  
1487 events in the eastern North Atlantic at the end of the middle Pleistocene transition (~640 ka)?  
1488 *Paleoceanography* 23(4), 1–16, 2008. <https://doi.org/10.1029/2008PA001591>

1489 Huntley, B. Europe. *Vegetation history* (ed. by B. Huntley and T. Webb III), pp. 341–383. Kluwer Academic  
1490 Publishers, Dordrecht, 1988.

1491 IPCC. *Climate Change: Impacts, Adaptation and Vulnerability*. Accessible at:  
1492 <https://www.ipcc.ch/report/ar6/wg2/>, 2022.

1493 Jalut, G., Dedoubat, J. J., Fontugne, M., and Otto, T. Holocene circum-Mediterranean vegetation changes: Climate  
1494 forcing and human impact. *Quatern. Int.* 200, 4–18, 2009.

1495 Joannin, S., Brugiapaglia, E., De Beaulieu, J.L., Bernardo, L., Magny, M., Peyron, O., Goring, S., and Vannièrè,  
1496 B. Pollen-based reconstruction of Holocene vegetation and climate in southern Italy: the case of Lago  
1497 Trifoglietti. *Clim. Past* 8(6), 1973–1996, 2012.

1498 Jouzel, J., Masson-Delmotte, V., Cattani, O., Dreyfus, G., Falourd, S., Hoffmann, G., Minster, B., Nouet, J.,  
1499 Barnola, J.M., Chappellaz, J., Fischer, H., Gallet, J.C., Johnsen, S., Leuenberger, M., Loulergue, L., Luethi,  
1500 D., Oerter, H., Parrenin, F., Raisbeck, G., Raynaud, D., Schilt, A., Schwander, J., Selmo, E., Souchez, R.,  
1501 Spahni, R., Stauffer, B., Steffensen, J.P., Stenni, B., Stocker, T.F., Tison, J.L., Werner, M., Wolff, E.W. Orbital  
1502 and millennial Antarctic climate variability over the past 800,000 years. *Science* 317(5839), 793–796, 2007.

1503 Juggins, S. Package “rioja”—Analysis of Quaternary Science Data. *The Comprehensive R Archive Network*, 2020.

1504 Kaenel, E., Siesser, W.G., Murat, A. Pleistocene calcareous nannofossil biostratigraphy and the western  
1505 Mediterranean sapropels, Sites 974 to 977 and 979. In: Zhan, R., Comas, M.C., Klaus, A. (Eds.), *Proc. ODP  
1506 Sci. Results*. 161. College Station, Texas, 15–183, 1999.

1507 Kallel, N., Paterne, M., Labeyrie, L., Duplessy, J. C., and Arnold, M. Temperature and salinity records of the  
1508 Tyrrhenian Sea during the last 18,000 years. *Palaeogeogr. Palaeoclimatol. Palaeoecol.* 135, 97–108, 1997.

1509 Kandiano, E.S., Bauch, H.A., Fahl, K., Helmke, J.P., Röhl, U., Pérez-Folgado, M., and Cacho, I. The meridional  
1510 temperature gradient in the eastern North Atlantic during MIS 11 and its link to the ocean-atmosphere system.  
1511 *Palaeogeogr. Palaeoclimatol. Palaeoecol.* 333, 24–39, 2012.

1512 Kelly, M.R. The Middle Pleistocene of North Birmingham. *Philos. Trans. R. Soc. Lond.* B247, 533–592, 1964.

1513 Kotthoff, U., Pross, J., Müller, U.C., Peyron, O., Schmiedl, G., Schulz, H., and Bordon, A. Climate dynamics in  
1514 the borderlands of the Aegean Sea during formation of sapropel S1 deduced from a marine pollen record.  
1515 *Quat. Sci. Rev.* 27, 832–845, 2008. <https://doi.org/10.1016/j.quascirev.2007.12.001>

1516 Kousis, I., Koutsodendris, A., Peyron, O., Leicher, N., Francke, A., Wagner, B., Giaccio, B., Knipping, M., and  
1517 Pross, J. Centennial-scale vegetation dynamics and climate variability in SE Europe during Marine Isotope  
1518 Stage 11 based on a pollen record from Lake Ohrid. *Quat. Sci. Rev.* 190, 20–38, 2018.  
1519 <https://doi.org/10.1016/j.quascirev.2018.04.014>

1520 Koutsodendris, A., Brauer, A., Pälike, H., Müller, U.C., Dulski, P., Lotter, A.F., and Pross, J. Sub-decadal to  
1521 decadal-scale climate cyclicity during the Holsteinian interglacial (MIS 11) evidenced in annually laminated  
1522 sediments. *Clim. Past* 7, 987–999, 2011.

1523 Koutsodendris, A., Pross, J., Müller, U. C., Brauer, A., Fletcher, W. J., Kühl, N., Kirilova, E., Verhagen, F. T. M.,  
1524 Lücke, A., and Lotter, A. F. A short-term climate oscillation during the Holsteinian interglacial (MIS 11c): An  
1525 analogy to the 8.2ka climatic event? *Glob. Planet. Change* 92–93, 224–235, 2012.  
1526 <https://doi.org/10.1016/j.gloplacha.2012.05.011>

1528 Koutsodendris, A., Kousis, I., Peyron, O., Wagner, B., and Pross, J. The Marine Isotope Stage 12 pollen record  
1529 from Lake Ohrid (SE Europe): Investigating short term climate change under extreme glacial conditions. *Quat.*  
1530 *Sci. Rev.* 221, 105873, 2019.

1531 Koutsodendris, A., Dakos, V., Fletcher, W.J., Knipping, M., Kotthoff, U., Milner, A.M., Müller, U.C., Kaboth-  
1532 Bahr, S., Kern, O.A., Kolb, L., and Vakhrameeva, P. Atmospheric CO<sub>2</sub> forcing on Mediterranean biomes  
1533 during the past 500 kyrs. *Nat. Commun.* 14(1), 1664, 2023.

1534 Kukla, G. Continental records of MIS 11. *Washington DC American Geophysical Union Geophysical Monograph*  
1535 *Series* 137, 207–211, 2003.

1536 Kukla, G., McManus, J. F., Rousseau, D. D., and Chuine, I. How long and how stable was the last interglacial?  
1537 *Quat. Sci. Rev.* 16, 605–612, 1997.

1538 Leroy, S.A.G., Henry, P., Peyron, O., Rostek, F., Kende, J., Bard, E., and Tachikawa, K. Palynology,  
1539 palaeoclimate and chronology from the Saalian Glacial to Saint Germain II interstadial from two long cores  
1540 at the limit between the Mediterranean and Euxinian regions. *Quat. Sci. Rev.* 311, 108145, 2023.

1541 Lionello, P., Scarascia, L. The relation between climate change in the Mediterranean region and global warming-  
1542 *Reg. Environ. Chang.* 18, 1481–1493, 2018.

1543 Liu, M., Shen, Y., González Sampériz, P., Gil Romera, G., Ter Braak, C.J., Prentice, I.C. and Harrison, S.P.  
1544 Holocene climates of the Iberian Peninsula: pollen based reconstructions of changes in the west-east gradient  
1545 of temperature and moisture. *Clim. Past* 19, 803–834, 2023. <https://doi.org/10.5194/cp-19-803-2023>

1546 Loulergue, L., Schilt, A., Spahni, R., Masson-Delmotte, V., Blunier, T., Lemieux, B., Barnola, J.M., Raynaud,  
1547 D., Stocker, T.F., Chappellaz, J. Orbital and millennial scale features of atmospheric CH<sub>4</sub> over the past  
1548 800,000 years. *Nature* 453, 383–386, 2008.

1549 Loutre, M.F., Berger, A. Marine Isotope Stage 11 as an analogue for the present interglacial. *Glob. Planet. Change*  
1550 36, 209–217, 2003. [https://doi.org/10.1016/S0921-8181\(02\)00186-8](https://doi.org/10.1016/S0921-8181(02)00186-8)

1551 Ludwig, P., Shao, Y., Kehl, M. and Weniger, G.C. The Last Glacial Maximum and Heinrich event I on the Iberian  
1552 Peninsula: A regional climate modelling study for understanding human settlement patterns. *Glob. Planet.*  
1553 *Change* 170, 34–47, 2018.

1554 Magny, M., Miramont, C. and Sivan, O. Assessment of the impact of climate and anthropogenic factors on  
1555 Holocene Mediterranean vegetation in Europe on the basis of palaeohydrological records. *Palaeogeogr.*  
1556 *Palaeoclimatol. Palaeoecol.* 186(1–2), 47–59, 2002.

1557 Maiorano, P., Bertini, A., Capolongo, D., Eramo, G., Gallicchio, S., Gironi, A., Pinto, D., Toti, F., Ventrucci, G.,  
1558 Marino, M. Climate signatures through the marine isotope stage 19 in the Montalbano Jonico section (southern  
1559 Italy): a land-sea perspective. *Palaeogeogr. Palaeoclimatol. Palaeoecol.* 461, 341–361, 2016.

1560 Marino, M., Gironi, A., Maiorano, P., Di Renzo, R., Piscitelli, A., and Flores, J. A. Calcareous plankton and the  
1561 mid-Brunhes climate variability in the Alboran Sea (ODP Site 977). *Palaeogeogr. Palaeoclimatol.*  
1562 *Palaeoecol.* 508, 91–106, 2018. <https://doi.org/10.1016/j.palaeo.2018.07.023>

1563 Marriner, N., Kaniewski, D., Pourkerman, M. and Devillers, B. Anthropocene tipping point reverses long-term  
1564 Holocene cooling of the Mediterranean Sea: A meta-analysis of the basin's Sea Surface Temperature records.  
1565 *Earth Sci Rev* 227, 103986, 2022.

1566 Martrat, B., Grimalt, J.O., Lopez Martinez, C., Cacho, I., Sierro, F.J., Flores, J.A., Zahn, R., Canals, M., Curtis,  
1567 J.H. and Hodell, D.A. Abrupt temperature changes in the Western Mediterranean over the past 250,000 years.  
1568 *Science* 306(5702), 1762–1765, 2004.

1569 Martin, C., Menot, G., Thouveny, N., Peyron, O., Andrieu-Ponel, V., Montade, V., Davtian, N., Reille, M. and  
1570 Bard, E. Early Holocene thermal maximum recorded by branched tetraethers and pollen in Western Europe  
1571 (Massif Central, France). *Quat. Sci. Rev.* 228, 106109, 2020.

1572 Martrat, B., Jimenez Amat, P., Zahn, R. and Grimalt, J.O. Similarities and dissimilarities between the last two  
1573 deglaciations and interglaciations in the North Atlantic region. *Quat. Sci. Rev.* 99, 122–134, 2014.

1574 Masson-Delmotte, V., Landais, A., Combourieu-Nebout, N., von Grafenstein, U., Jouzel, J., Caillon, N.,  
1575 Chappellaz, J., Dahl-Jensen, D., Johnsen, S.J. and Stenni, B. Variabilité climatique rapide pendant les périodes  
1576 chaudes et froides aux pôles et en Europe. *Comptes rendus. Géoscience* 337(10–11), 935–946, 2005.

1577 Mauri, A., Davis, B., Collins, P. M., and Kaplan, J. The climate of Europe during the Holocene: A gridded pollen-  
1578 based reconstruction and its multi-proxy evaluation. *Quat. Sci. Rev.* 112, 109–127, 2015.

1579 Mayewski, P.A., Rohling, E.E., Stager, J.C., Karlen, W., Maasch, K.A., Meeker, L.D., Meyerson, E.A., Gasse,  
1580 F., van Kereveld, S., Holmgren, K., Lee-Thorp, J., Rosqvist, G., Raek, F., Staubwasser, M., Schneider, R.R.,  
1581 Steig, E.J. Holocene climate variability. *Quat. Res.* 62, 243–255, 2004.

1582 McManus, J.F., Oppo, D.W., Cullen, J.L. and Healey, S. Marine isotope stage 11 (MIS 11): analog for Holocene  
1583 and future climate? *Washington DC American Geophysical Union Geophysical Monograph Series* 137, 69–  
1584 85, 2003.

1585 MedECC. Climate and Environmental Change in the Mediterranean Basin—Current Situation and Risks for the  
1586 Future. In: *Climate and Environmental Change in the Mediterranean Basin—Current Situation and Risks for*

1587 *the Future. First Mediterranean Assessment Report*, edited by W. Cramer, J. Guiot and K. Marini, 60.  
1588 Marseille: Union for the Mediterranean, 2020.

1589 Moncel, M. H., Arzarello, M., and Peretto, C. The Holsiteinian period in Europe (MIS 11-9). *Quat. Int.* 409, 1–8,  
1590 2016.

1591 Moreno, A., Cacho, I., Canals, M., Grimalt, J.O., Sanchez Vidal, A. Millennial scale variability in the productivity  
1592 signal from the Alboran Sea record, western Mediterranean Sea. *Palaeogeogr. Palaeoclimatol. Palaeoecol.*  
1593 211(3-4), 205–219, 2004.

1594 Naughton, F., Sánchez Goñi, M. F., Desprat, S., Turon, J. L., Duprat, J., Malaizé, B., Joli, C., Cortijo, E., Drago,  
1595 T., and Freitas, M. C. Present day and past (last 25,000 years) marine pollen signal off western Iberia. *Mar.*  
1596 *Micropaleontol.* 62, 91–114, 2007.

1597 Nehrbass Ahles, C., Shin, J., Schmitt, J., Bereiter, B., Joos, F., Schilt, A., Schmidely, L., Silva, L., Teste, G.,  
1598 Grilli, R. and Chappellaz, J. Abrupt CO<sub>2</sub> release to the atmosphere under glacial and early interglacial climate  
1599 conditions. *Science* 369(6506), 1000–1005, 2020.

1600 Nomade, S., Bassinot, F., Marino, M., Simon, Q., Dewilde, F., Maiorano, P., Isguder, G., Blamart, D., Girone,  
1601 A., Seao, V., Pereira, A., Toti, F., Bertini, A., Combourieu Nebout, N., Peral, M., Bourles, D.L., Petrosino, P.,  
1602 Galliechio, S., Ciaranfi, N. High resolution foraminifer stable isotope record of MIS 19 at Montalbano Jonico,  
1603 southern Italy: a window into Mediterranean climatic variability during a low eccentricity interglacial. *Quat.*  
1604 *Sci. Rev.* 205, 106–125, 2019.

1605 NorthGRIP Members. High resolution record of Northern Hemisphere climate extending into the last interglacial  
1606 period. *Nature*, 431: 147–151, 2004.

1607 Oliveira, D., Desprat, S., Rodrigues, T., Naughton, F., Hodell, D., Trigo, R., Rufino, M., Lopes, C., Abrantes, F.,  
1608 and Sánchez Goñi, M. F. The complexity of millennial scale variability in southwestern Europe during MIS  
1609 11. *Quat. Res. (United States)*, 86(3), pp.373–387. <https://doi.org/10.1016/j.yqres.2016.09.002>, 2016.

1610 Olson, S.L., Hearty, P.J.A. A sustained 121m sea level highstand during MIS 11 (400 ka): direct fossil and  
1611 sedimentary evidence from Bermuda. *Quat Sci Rev* 28, 271–285, 2009.

1612 Ortiz, Trinidad. Torres, Antonio Delgado, J.F. Llamas, Vicente Soler, Maruja Valle, Ramón Julià, Laura Moreno,  
1613 Arantxa Díaz Bautista. Palaeoenvironmental changes in the Padul Basin (Granada, Spain) over the last 1Ma  
1614 based on the biomarker content, *Palaeogeogr. Palaeoclimatol. Palaeoecol.*, 298, 286–299, ISSN-0031-0182,  
1615 2010. <https://doi.org/10.1016/j.palaeo.2010.10.003>.

1616 Ozenda, P. Sur les étages de végétation dans les montagnes du bassin méditerranéen. *Documents de Cartographie*  
1617 *Ecologique*, 16, pp.1–32, 1975.

1618 Past Interglacials Working Group of PAGES. Interglacials of the last 800,000 years. *Reviews of Geophysics*, 54(1),  
1619 162–219, 2016.

1620 Peñalba, M.C., Maurice, A., Guiot, J., Duplessy, J.C., de Beaulieu, J.L. Termination of the last glaciation in the  
1621 Iberian Peninsula Inferred from the Pollen Sequence of Quintanar de la Sierra. *Quat. Res.* 48, 205–214, 1997.

1622 Pérez Folgado, M., Sierro, F.J., Flores, J.A., Grimalt, J.O. and Zahn, R. Paleoclimatic variations in foraminifer  
1623 assemblages from the Alboran Sea (Western Mediterranean) during the last 150 ka in ODP Site 977. *Mar.*  
1624 *Geol.*, 212(1-4), 113–131, 2004.

1625 Peyron, O., Combourieu Nebout, N., Brayshaw, D., Goring, S., Andrieu Ponel, V., Desprat, S., Fletcher, W.,  
1626 Gambin, B., Ioakim, C., Joannin, S., Kotthoff, U., Kouli, K., Montade, V., Pross, J., Sadori, L., Magny, M.  
1627 Precipitation changes in the Mediterranean basin during the Holocene from terrestrial and marine pollen  
1628 records: a model data comparison. *Clim. Past*, 13, 249–265, <https://doi.org/10.5194/cp-13-249-2017>, 2017.

1629 Peyron, O., Goring, S., Dormoy, I., Kotthoff, U., Pross, J., De Beaulieu, J.L., Drescher Schneider, R., Vanniere,  
1630 B., Magny, M. Holocene seasonality changes in the central Mediterranean region reconstructed from the pollen  
1631 sequences of Lake Accesa (Italy) and Tenaghi Philippon (Greece). *Holocene* 21, 131–146,  
1632 <https://doi.org/10.1177/0959683610384162>, 2011.

1633 Peyron, O., Magny, M., Goring, S., Joannin, S., De Beaulieu, J.L., Brugiapaglia, E., Sadori, L., Garfi, G., Kouli,  
1634 K., Ioakim, C. and Combourieu Nebout, N. Contrasting patterns of climatic changes during the Holocene  
1635 across the Italian Peninsula reconstructed from pollen data. *Clim. Past*, 9(3), pp.1233–1252, 2013.

1636 Pol, K., Masson Delmotte, V., Johnsen, S., Bigler, M., Cattani, O., Durand, G., Falourd, S., Jouzel, J., Minster,  
1637 B., Parrenin, F., Ritz, C., Steen Larsen C. H., Stenni, B. New MIS 19 EPICA Dome C high resolution  
1638 deuterium data: hints for a problematic preservation of climate variability at sub-millennial scale in the “oldest  
1639 ice”. *Earth Planet Sci. Lett.* 298, 95–103, 2010.

1640 Pons, A. and Reille, M. The Holocene and Upper Pleistocene pollen record from Padul (Granada, Spain): a new  
1641 study, *Palaeogeogr. Palaeoclimatol. Palaeoecol.*, 66, 243–263, 1988.

1642 Pross, J., Christanis, K., Fischer, T., Fletcher, W.J., Hardiman, M., Kalaitzidis, S., Knipping, M., Kotthoff, U.,  
1643 Milner, A.M., Muller, U.C. and Schmiedl, G. The 1.35 Ma long terrestrial climate archive of Tenaghi  
1644 Philippon, northeastern Greece: Evolution, exploration, and perspectives for future research. *Newsletters on*  
1645 *Stratigraphy*, 48(3), 253–276, 2015.

1646 Pross, J., Kotthoff, U., Müller, U. C., Peyron, O., Dormoy, I., Schmiedl, G., Kalaitzidis, S., and Smith, A. M.  
1647 Massive perturbation in terrestrial ecosystems of the Eastern Mediterranean region associated with the 8.2 kyr  
1648 B.P. climatic event, *Geology*, 37, 887–890, 2009.

1649 Quézel, P. and Médail, F. *Ecologie et biogéographie des forêts du bassin méditerranéen*, Elsevier-Lavoisier eds,  
1650 Paris, France, 571 pp., 2003.

1651 Ramos Román, M.J., Jiménez Moreno, G., Camuera, J., García Alix, A., Anderson, R.S., Jiménez Espejo, F.J.  
1652 and Carrión, J.S. Holocene climate aridification trend and human impact interrupted by millennial and  
1653 centennial scale climate fluctuations from a new sedimentary record from Padul (Sierra Nevada, southern  
1654 Iberian Peninsula). *Clim. Past*, 14(1), 117–137, 2018.

1655 Raymo, M.E. and Mitrovica, J.X. Collapse of polar ice sheets during the stage-11 interglacial. *Nature*, 483(7390),  
1656 453–456, 2012.

1657 Regattieri, E., Giaccio, B., Galli, P., Nomade, S., Peronace, E., Messina, P., Sposato, A., Boschi, C., Gemelli, M.  
1658 A multi-proxy record of MIS 11–12 deglaciation and glacial MIS 12 instability from the Sulmona Basin  
1659 (central Italy). *Quat Sci Rev* 132, 12–145, 2016.

1660 Reille, M., and de Beaulieu, J. L. Long Pleistocene pollen records from the Praclaux crater, south central France.  
1661 *Quat. Res.*, 44(2), 205–215. <https://doi.org/10.1006/qres.1995.1065>, 1995.

1662 Rivas Martínez, S. Bioclimatic stages, chorological sectors and series of vegetation in Mediterranean Spain. *Ecol.*  
1663 *mediterr.*, 8(1), 275–288, 1982.

1664 Robles M., Peyron O., Ménot G., Brugiapaglia E., Wulf S., Appelt O., Blache M., Vannièrè B., Dugerdil L., Paura  
1665 B., Ansanay Alex S., Cromartie A., Charlet L., Guédrón S., de Beaulieu JL, and Joannin, S. Climate changes  
1666 during the Lateglacial in South Europe: new insights based on pollen and brGDGTs of Lake Matese in Italy;  
1667 *Clim. Past*, 19, 493–515, <https://doi.org/10.5194/cp-19-493-2023>, 2023.

1668 Rodrigo Gámiz, M., García Alix, A., Jiménez Moreno, G., Ramos Román, M.J., Camuera, J., Toney, J.L.,  
1669 Sachse, D., Anderson, R.S. and Damsté, J.S.S. Paleoclimate reconstruction of the last 36 kyr based on  
1670 branched glycerol dialkyl glycerol tetraethers in the Padul palaeolake record (Sierra Nevada, southern Iberian  
1671 Peninsula). *Quat Sci Rev*, 281, p.107434, 2022.

1672 Rodrigues, T., Voelker, A.H.L., Grimalt, J.O., Abrantes, F., Naughton, F. Iberian Margin sea surface temperature  
1673 during MIS 15 to 9 (580–300 ka): glacial sub-orbital variability versus interglacial stability. *Paleoceanography*  
1674 26, 1e16, <https://doi.org/10.1029/2010PA001927>, 2011.

1675 Rohling, E.J., Fenton, M., Jorissen, F.J., Bertrand, P., Ganssen, G., Caulet, J.P. Magnitudes of sea level lowstands  
1676 of the past 500,000 years. *Nature* 394, 162e165, <https://doi.org/10.1038/28134>, 1998.

1677 Rossignol Strick, M. The Holocene climatic optimum and pollen records of sapropel 1 in the Eastern  
1678 Mediterranean, 9000–6000 BP. *Quat. Sci. Rev.* 18, 515–530, 1999.

1679 Ruddiman, W.F. The anthropogenic greenhouse era began thousands of years ago. *Climatic change*, 61(3), 261–  
1680 293, 2003.

1681 Ruddiman, W.F. The early anthropogenic hypothesis: Challenges and responses. *Rev Geophys*, 45(4), 2007.

1682 Ruddiman, W.F., Fuller, D.Q., Kutzbach, J.E., Tzedakis, P.C., Kaplan, J.O., Ellis, E.C., Vavrus, S.J., Roberts,  
1683 C.N., Fyfe, R., He, F. and Lemmen, C. Late Holocene climate: Natural or anthropogenic? *Rev Geophys*, 54(1),  
1684 93–118, 2016.

1685 Sadori, L., Ortu, E., Peyron, O., Zanchetta, G., Vannièrè, B., Desmet, M. and Magny, M. The last 7 millennia of  
1686 vegetation and climate changes at Lago di Pergusa (central Sicily, Italy). *Clim. Past*, 9(4), pp.1969–1984, 2013.

1687 Sadori, L., Koutsodendris, A., Panagiotopoulos, K., Masi, A., Bertini, A., Combourieu-Nebout, N., Francke, A.,  
1688 Kouli, K., Joannin, S., Mercuri, A.M. and Peyron, O. Pollen-based paleoenvironmental and paleoclimatic  
1689 change at Lake Ohrid (south-eastern Europe) during the past 500 ka. *Biogeosciences*, 13(5), pp.1423–1437,  
1690 2016.

1691 Salonen, J.S., Korpela, M., Williams, J.W., Luoto, M. Machine learning-based reconstructions of primary and  
1692 secondary climate variables from North American and European fossil pollen data. *Sci. Rep.* 9, 1–13,  
1693 <https://doi.org/10.1038/s41598-019-52293-4>, 2019.

1694 Salonen, J.S., Luoto, M., Alenius, T., Heikkilä, M., Seppä, H., Telford, R.J. and Birks, H.J.B. Reconstructing  
1695 palaeoclimatic variables from fossil pollen using boosted regression trees: comparison and synthesis with other  
1696 quantitative reconstruction methods. *Quat Sci Rev*, 88, 69–81, 2014.

1697 Sánchez Goñi, M. F., Llave, E., Oliveira, D., Naughton, F., Desprat, S., Ducassou, E., Hodell, D. A., and  
1698 Hernández Molina, F. J. Climate changes in southwestern Iberia and Mediterranean Outflow variations during  
1699 two contrasting cycles of the last 1 Myrs: MIS 31–MIS 30 and MIS 12–MIS 11. *Glob. Planet. Change*, 136,  
1700 18–29, <https://doi.org/10.1016/j.gloplacha.2015.11.006>, 2016.

1701 Sánchez Goñi, M., Eynaud, F., Turon, J. L., and Shackleton, N. J. High resolution palynological record off the  
1702 Iberian margin: direct land-sea correlation for the Last Interglacial complex. *Earth Planet Sci Lett*, 171(1),  
1703 123–137, 1999.

1704 Sánchez-Goñi, M.F., Bakker, P., Desprat, S., Carlson, A.E., Van Meerbeeck, C.J., Peyron, O., Naughton, F.,  
1705 Fletcher, W.J., Eynaud, F., Rossignol, L. and Renssen, H. European climate optimum and enhanced Greenland  
1706 melt during the Last Interglacial. *Geology*, 40(7), pp.627–630, 2012.

1707 Sassoon, D., Lebreton, V., Combourieu-Nebout, N., Peyron, O. and Moncel, M.H. Palaeoenvironmental Changes  
1708 in the Southwest Mediterranean (ODP Site 976, Alboran Sea) During the MIS 12/11 Transition and the MIS  
1709 11 Interglacial. *Quat Sci Rev*, 304: 108010.

1710 Shackleton, N.J., Sánchez-Goñi, M.F., Pailler, D. and Lancelot, Y. Marine isotope substage 5e and the Eemian  
1711 interglacial. *Glob. Planet. Change*, 36(3), 151–155, 2003.

1712 Shipboard Scientific Party. Site 976. In: Comas, M.C., Zahn, R., Klaus, A., et al. (Eds.), *Proc. ODP, Init. Repts.,*  
1713 *vol. 161. Ocean Drilling Program*, College Station, TX, pp. 179–297, 1996.

1714 Siani, G., Michel, E., De Pol-Holz, R., DeVries, T., Lamy, F., Carel, M., Isguder, G., Dewilde, F. and Laurantou,  
1715 A. Carbon isotope records reveal precise timing of enhanced Southern Ocean upwelling during the last  
1716 deglaciation. *Nat. Commun.*, 4(1), p.2758, 2013.

1717 Sinopoli, G., Peyron, O., Masi, A., Holtvoeth, J., Francke, A., Wagner, B. and Sadori, L. Pollen-based temperature  
1718 and precipitation changes in the Ohrid Basin (western Balkans) between 160 and 70 ka. *Clim. Past*, 15(1), 53–  
1719 71, 2019.

1720 ter Braak, C.J.F., Juggins, S. Weighted averaging partial least squares regression (WA-PLS): an improved method  
1721 for reconstructing environmental variables from species assemblages. *Hydrobiologia* 269–270, 485–502,  
1722 <https://doi.org/10.1007/BF00028046>, 1993.

1723 Toti, F., Bertini, A., Girone, A., Marino, M., Maiorano, P., Bassinot, F., Combourieu-Nebout, N., Nomade, S.,  
1724 and Buccianti, A. Marine and terrestrial climate variability in the western Mediterranean Sea during marine  
1725 isotope stages 20 and 19. *Quat Sci Rev*, 243, <https://doi.org/10.1016/j.quascirev.2020.106486>, 2020.

1726 Turner, C. The Middle Pleistocene deposits at Marks Tey, Essex. *Philosophical Transactions of the Royal Society*  
1727 *of London, Series B* 257, 373–440, 1970.

1728 Turon, J.-L., Lézine, A. M., and Denèfle, M. Land–sea correlations for the last deglaciation inferred from a pollen  
1729 and dinocyst record from the Portuguese margin, *Quat. Res.*, 59, 88–96, 2003.

1730 Tye, G.J., Sherriff, J., Candy, I., Coxon, P., Palmer, A., Meelymont, E.L., Schreve, D.C. The  $\delta^{18}\text{O}$  stratigraphy  
1731 of the Hoxnian lacustrine sequence at Marks Tey, Essex, UK: implications for the climatic structure of MIS  
1732 11 in Britain. *J. Quat. Sci.* 31, 75–92, <https://doi.org/10.1002/jqs.2840>, 2016.

1733 Tzedakis, P. C., Hodell, D. A., Nehrbass-Ahles, C., Mitsui, T., and Wolff, E. W. Marine Isotope Stage 11c: An  
1734 unusual interglacial. *Quat Sci Rev*, 284, 107493, <https://doi.org/10.1016/j.quascirev.2022.107493>, 2022.

1735 Tzedakis, P. C., Hooghiemstra, H., and Pälike, H. The last 1.35 million years at Tenaghi Philippon: revised  
1736 chronostratigraphy and long term vegetation trends. *Quat Sci Rev*, 25(23–24), 3416–3430,  
1737 <https://doi.org/10.1016/j.quascirev.2006.09.002>, 2006.

1738 Tzedakis, P.C. The MIS 11–MIS 1 analogy, southern European vegetation, atmospheric methane and the “early  
1739 anthropogenic hypothesis”. *Clim. Past*, 6(2), 131–144, 2010.

1740 Tzedakis, P.C., Channell, J.E.T., Hodell, D.A., Kleiven, H.F. and Skinner, L.C. Determining the natural length of  
1741 the current interglacial. *Nat Geosci*, 5(2), 138–141, 2012.

1742 Vavrus, S.J., He, F., Kutzbach, J.E. et al. Glacial Inception in Marine Isotope Stage 19: An Orbital Analog for a  
1743 Natural Holocene Climate. *Sci. Rep.*, 8, 10213, <https://doi.org/10.1038/s41598-018-28419-5>, 2018.

1744 Vázquez-Riveiros, N., Waelbroeck, C., Skinner, L., Duplessy, J. C., McManus, J. F., Kandiano, E. S., and Bauch,  
1745 H. A. The “MIS 11 paradox” and ocean circulation: Role of millennial-scale events. *Earth Planet Sci Lett*,  
1746 371–372, 258–268, <https://doi.org/10.1016/j.epsl.2013.03.036>, 2013.

1747 Voelker, A. H. L., Rodrigues, T., Billups, K., Oppo, D., McManus, J., Stein, R., Hefter, J., and Grimalt, J. O.  
1748 Variations in mid-latitude North Atlantic surface water properties during the mid-Brunhes (MIS 9–14) and  
1749 their implications for the thermohaline circulation. *Clim. Past*, 6(4), 531–552, <https://doi.org/10.5194/cp-6-531-2010>, 2010.

1750 Wang, Y., Yang, X., Wang, Y., Wang, Q., and Edwards, R. L. The structure of marine isotope Stage 11 and its  
1751 alignment with the Holocene. *Palaeogeogr. Palaeoclimatol. Palaeoecol.*, 609, 111311,  
1752 <https://doi.org/10.1016/j.palaeo.2022.111311>, 2023.

1753 Watts, W. A., Allen, J. R. M., Huntley, B., and Fritz, S. C. Vegetation history and climate of the last 15 000 years  
1754 at Laghi di Monticchio, Southern Italy, *Quaternary Sci. Rev.*, 15, 113–132, 1996.

1755 West, R. The Quaternary deposits at Hoxne, Suffolk. *Philosophical Transactions of the Royal Society London.*  
1756 *Series B* 239, 265–356, 1956.

1757 Wijmstra, T. A. and Smit, A. Palynology of the middle part (30–78 metres) of the 120 m deep section in Northern  
1758 Greece (Macedonia). *Acta Bot. Neerl.* 25, 297–312, 1976.

1759 Yin, Q., and Berger, A. Interglacial analogues of the Holocene and its natural near future. *Quat Sci Rev*, 120, 28–  
1760 46, <https://doi.org/10.1016/j.quascirev.2015.04.008>, 2015.

1762 ~~Zhuravleva, A. *Paleoceanographic and climatic teleconnections between the subarctic and subtropical North*~~  
1763 ~~*Atlantic during the last interglacial (MIS 5e). Doctoral dissertation.*~~  
1764 ~~<https://doi.org/10.13140/RG.2.2.26501.86242>, 2018.~~  
1765 ~~Zonneveld, K.A. Palaeoclimatic reconstruction of the last deglaciation (18–8 ka BP) in the Adriatic Sea region; a~~  
1766 ~~land-sea correlation based on palynological evidence. *Palaeogeogr. Palaeoclimatol. Palaeoecol.*, 122(1–4),~~  
1767 ~~89–106.~~